63-3-2

402393

DEVELOPMENT OF NONDESTRUCTIVE TESTING TECHNIQUES FOR LARGE SOLID-PROPELLANT ROCKET MOTORS

402 393

United Technology Center

U
A
DIVISION OF UNITED AIRCRAFT CORPORATION

P.O. BOX 358, SUNNYVALE, CALIFORNIA

FINAL REPORT
UNDER CONTRACT No. AF 04(611)8018
1 JUNE 1962 THROUGH 31 JANUARY 1963

ASTIA

APR 2 9 1963

TISIA   A

$12.00

United Technology Center

SUNNYVALE, CALIFORNIA   739-4880

DIVISION OF UNITED AIRCRAFT CORPORATION

19 April 1963
MC 178-63

Rocket Research Laboratories
Edwards Air Force Base
California

Attention: DGSCP

Subject: Final Report
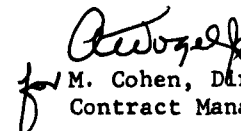
Reference: Contract AF 04(611)8018

Gentlemen:

United Technology Center submits the Final Report 2015-FR in accordance with
referenced contract. Distribution of subject report was made as of this date,
as directed by the referenced contract.

Very truly yours,

UNITED TECHNOLOGY CENTER

M. Cohen, Director
Contract Management

MC:wdj

Enclosures

cc: AFSC CMO (w/encl)
     USAF, Director of Procurement
       Headquarters, AFFTC
       Edwards AFB, California
       Attn: Contracting Officer (K. A. Stengel) (w/encl)

⑥ DEVELOPMENT OF NONDESTRUCTIVE TESTING TECHNIQUES
FOR
LARGE SOLID-PROPELLANT ROCKET MOTORS,

Research and Advanced Technology
UNITED TECHNOLOGY CENTER
Sunnyvale, California

⑦ FINAL REPORT.

1 JUNE 62 THROUGH 31 JAN 63,

Headquarters, Air Force Flight Test Center
Edwards Air Force Base, California

---

⑤ Prepared by:

Charles Harris
Project Engineer

Approved by:

C. M. Frey
Solids and Advanced Materials
Branch
United Technology Center

TABLE OF CONTENTS

LIST OF ILLUSTRATIONS

LIST OF ILLUSTRATIONS (Continued)

LIST OF ILLUSTRATIONS (Continued)

LIST OF ILLUSTRATIONS (Continued)

LIST OF TABLES

1.0 INTRODUCTION AND SUMMARY

~~The objective of this program was to~~ A study ~~and define~~ the capabilities of nondestructive test methods best suited to the detection of critical defects in large solid-propellant motors.

A critical defect may be defined as an imperfection in a motor which will impair the success of an assigned mission. Two general types of defects are classified as critical regardless of their size. These are (a) a case-insulation unbond exposed to propellant gases, and (b) any defect which tends to propagate without limit. Analytical studies ~~made under this contract~~ suggested that certain configurations of propellant-liner unbonds and cracks may propagate. Experimental studies conducted with a PBAN propellant showed no evidence of defect propagation.

2.0 TECHNICAL DISCUSSION

The program is divided into five items of work. These are discussed separately in this section.

2.1 DEFECT ANALYSIS

This item of work is comprised of an analytical study of the various critical defects which could occur in a large solid-propellant motor. Solid motors in the range of interest are presented in Table I.

A critical defect may be defined as any imperfection which would result in a lowered probability of successful completion of a mission. A defect leading to structural failure of the case is an obvious example. Some defects may be classed as critical or noncritical, depending on the mission. For example, if one booster in a multimotor stage produces other than design thrust, the capabilities of the thrust vector control system may be exhausted prior to stage burnout. Therefore, only after a careful review of the system capabilities and of the mission can a defect be conclusively classified as critical or noncritical.

In general, the effects of propellant defects are more severe in small motors than large ones; consequently, defects critical in small motors affect the operation of the large motors to a lesser degree.

The defects encountered in solid-propellant rocket motors are cracks, unbonds, voids, porous propellant (here taken to denote connected pores), and variations in chemical composition or cure. The study of these defects

TABLE I

PARAMETERS OF TYPICAL LARGE
SOLID-PROPELLANT MOTORS

Motor Diameter in.	Burning Time sec	Thrust lb	Propellant Weight lb	Burning Area in.^{2}
120	120	785,000	384,000	160,000
156	120	3,500,000	1,710,000	710,000
240	150	6,280,000	3,850,000	1,280,000

is outlined in Figure 1. It will be noted that many of the defects have common failure modes. Owing to the universal nature of two of the failure modes, excessive pressure and case overheating, these modes of failure will be discussed in a general manner.

2.1.1 Mission Failure Because of Excessive Chamber Pressure

The mission failure may occur from either a catastrophic failure of the motor case caused by overpressure or excessive thrust brought about by the overpressure. These types of failures will be discussed separately.

2.1.1.1 Catastrophic Overpressures

Catastrophic overpressures may result from three causes: a single large defect, a multiplicity of smaller defects, or a single small defect which propagates into a large defect.

A. Single Large Grain Defect

A single large grain defect is critical if its surface area represents an increase in chamber pressure sufficient to cause
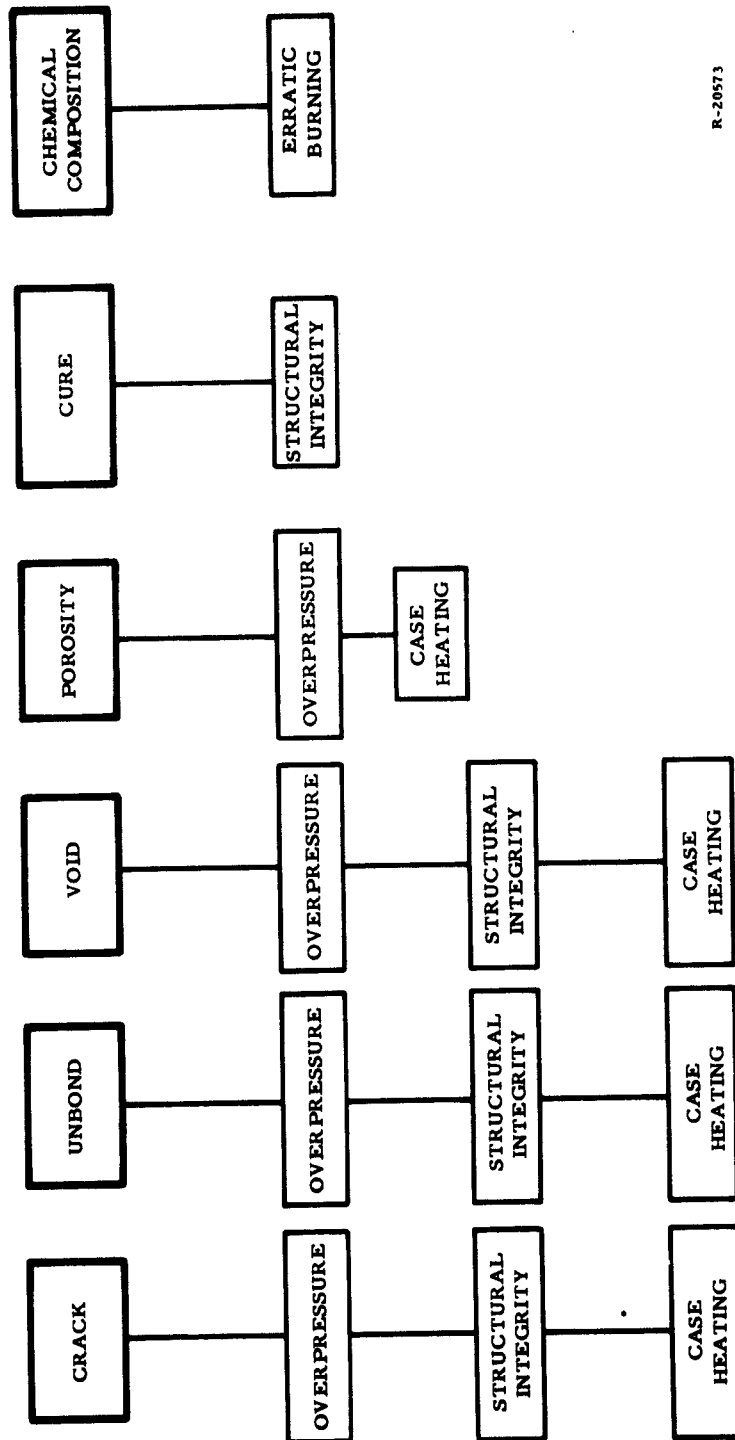
Figure 1. Modes of Failure for Various Defects in Solid-Propellant Motors

case failure. A defect of this type may be evaluated from the information presented in Figure 2. The factors required to class the defect as critical are the propellant burning rate exponent, percent of increase in burning area (actual over design), design chamber pressure, and case pressure failure criteria.

Assuming a case burst pressure of 120 percent of design pressure, and a PBAN propellant with burning ratio of 0.26, a burning area increase of 14.2 percent will result in a catastrophic overpressure.

The sizes of single defects required for catastrophic overpressures are summarized below in Table II.

TABLE II

SIZE OF SINGLE CRITICAL DEFECT FOR
CATASTROPHIC OVERPRESSURE

Motor Diameter in.	Diameter of Spherical Void in.	Length of Crack 12 in. Deep ft	Circumferential Length of Propellant Liner Unbond 12 in. Wide ft
120	85.6	80	160
156	181	356	712
240	242	640	1280

B. Multiplicity of Defects

It is possible that a critical overpressure can be caused by a number of smaller defects, any one of which is not sufficiently large enough to be classified critical. The evaluation procedure is similar to that for a single defect except that the burning area

The graph shows:

$$\frac{A_s}{A_{so}} = \left(\frac{P_c}{P_{co}}\right)^{1-n}$$

P_c - Chamber Pressure

A_s - Burning Propellant Surface Area

n - Burning Rate Exponent

n = 0.20
n = 0.25
n = 0.30
n = 0.35
n = 0.40
n = 0.45

Vertical axis: A_s/A_{so} (1.00, 1.05, 1.10, 1.15, 1.20, 1.25)

Horizontal axis: P_c/P_{co} (1.00, 1.05, 1.10, 1.15, 1.20, 1.25, 1.30)

R-20884
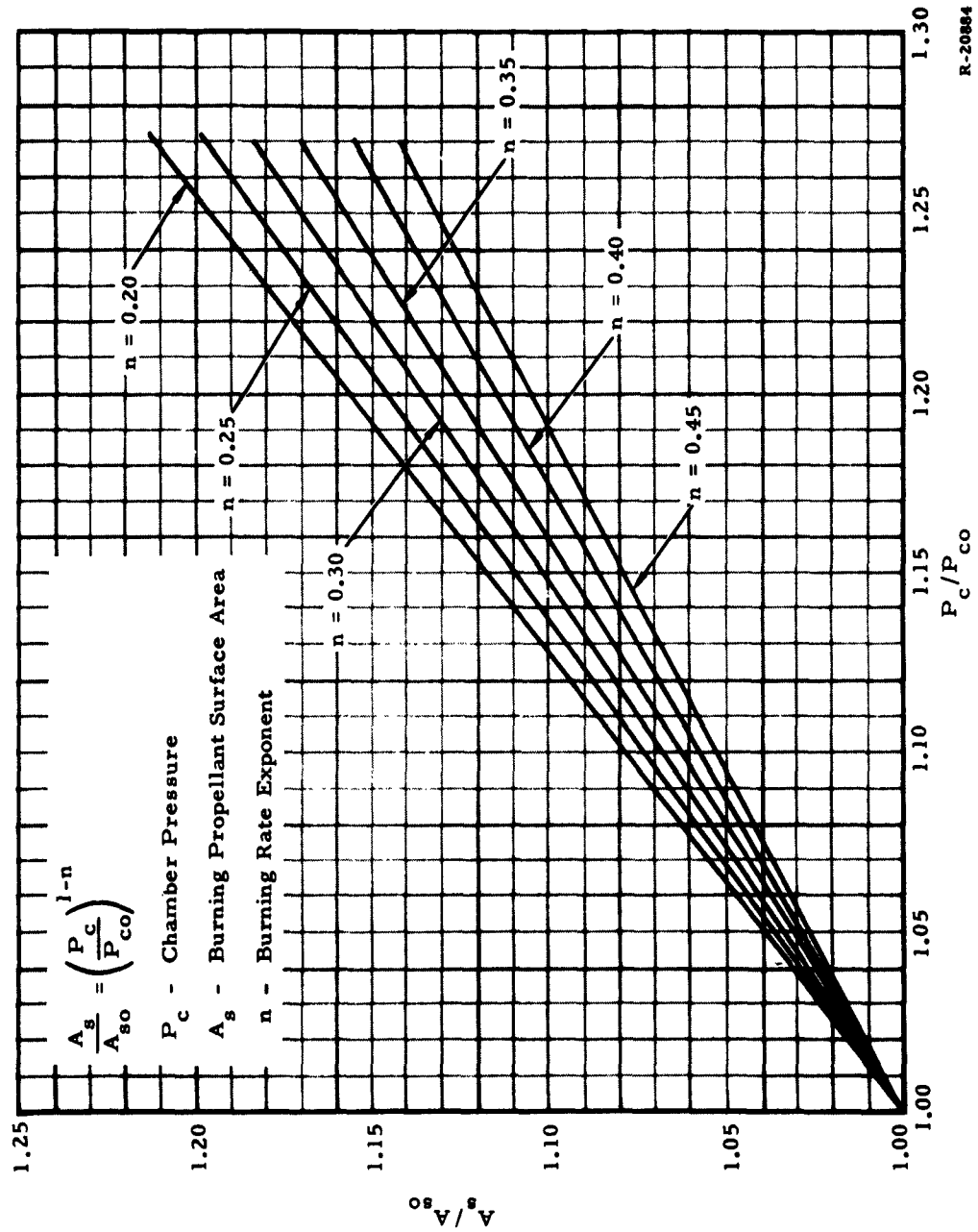
Figure 2. Variations of Propellant Burning Rate Versus Chamber Pressure

percentage increase must be evaluated over the grain burning time in order to arrive at the maximum percentage area increase. In the event of a progressive or regressive pressure-time design, both case design pressure level and burning area increases, plotted as a function of time, are required to judge criticality.

C. Propagation of Defects

The assumption of fixed dimension of grain defects is implicit in the considerations given above. In the study of cracks and propellant-liner unbonds, it was determined that the possibility of spontaneous enlargement of these defects existed under conditions of motor operation.

1. Cracks

The nature of crack formation would lead to the assumption that the edges of the crack are highly stressed. The possibility of any additional stress causing the crack to enlarge poses a potential danger that cannot be overlooked. Such an enlargement would lead to the exposure of more burning area to the advancing flame front, and could conceivably result in structural failure of the grain.

The enlargement of a crack owing to motor pressurization and to the attendant strains imposed on the propellant case structure has been investigated with a small scale model motor (Figure 3).

Propellant cracks and unbonds were incorporated in three motors as shown in Figure 4. The cracks and unbonds were cut in the live propellant and filled with a blue dye. The motors were assembled and pressurized to 800 psig at the

Figure 3.   Scale Model Motor
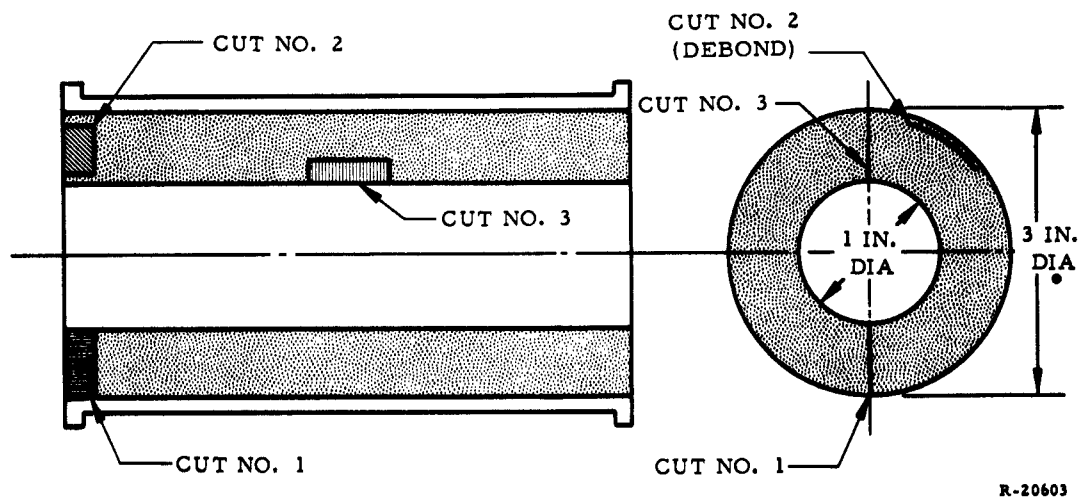
Figure 4.   Propellant Cracks and Unbonds - Motor Defects

at the following pressurization rates: 25,000 psi/sec, 10,000 psi/sec, and 5000 psi/sec. The test temperature was ambient (80°F). The pressurizing medium was a transparent silicone oil.

All test results were negative inasmuch as the built-in cracks did not propagate, the debonded areas did not increase, and no new grain ruptures were observed. Dissection of two of these grains substantiates these conclusions.

Of course, the artifically induced cracks do not perfectly simulate the stress field of a crack naturally formed. However, the extremely sharp edges of a crack formed by slitting should result in a high stress concentration factor on pressurization.

• The case of burning in the crack was investigated and reported in detail in the First Technical Note under this contract. It was demonstrated that if burning exists on the interior surface of a long, thin crack, severe pressure gradients can result which might easily cause propagation in the crack. The conditions under which this phenomenon may appear involve flame-front advancement into the crack fast enough so as to engulf the entire area before the burning at the mouth of the crack has significantly altered the geometry.

An attempt was made to ascertain the rate of flame propagation down certain defects with a Plexiglas motor (Figure 5). Holes of varying diameter were incorporated

R-20610

FORWARD CLOSURE PLATE (MILD STEEL)

PROPELLANT GRAIN

ALUMINUM PLUG

RETAINING NUT (STOCK LOCK)

TRANSPARENT MOTOR CASE (PLEXIGLAS STOCK)

CYLINDRICAL FLAWS

O-RING

PRESSURE TAP (AN-FITTING WELDED IN PLACE)

RETAINING ROD (4 REQ) (STEEL 140,000 psi YIELD)

PLATE

NOZZLE INSERT ATJ GRAPHITE

O-RING
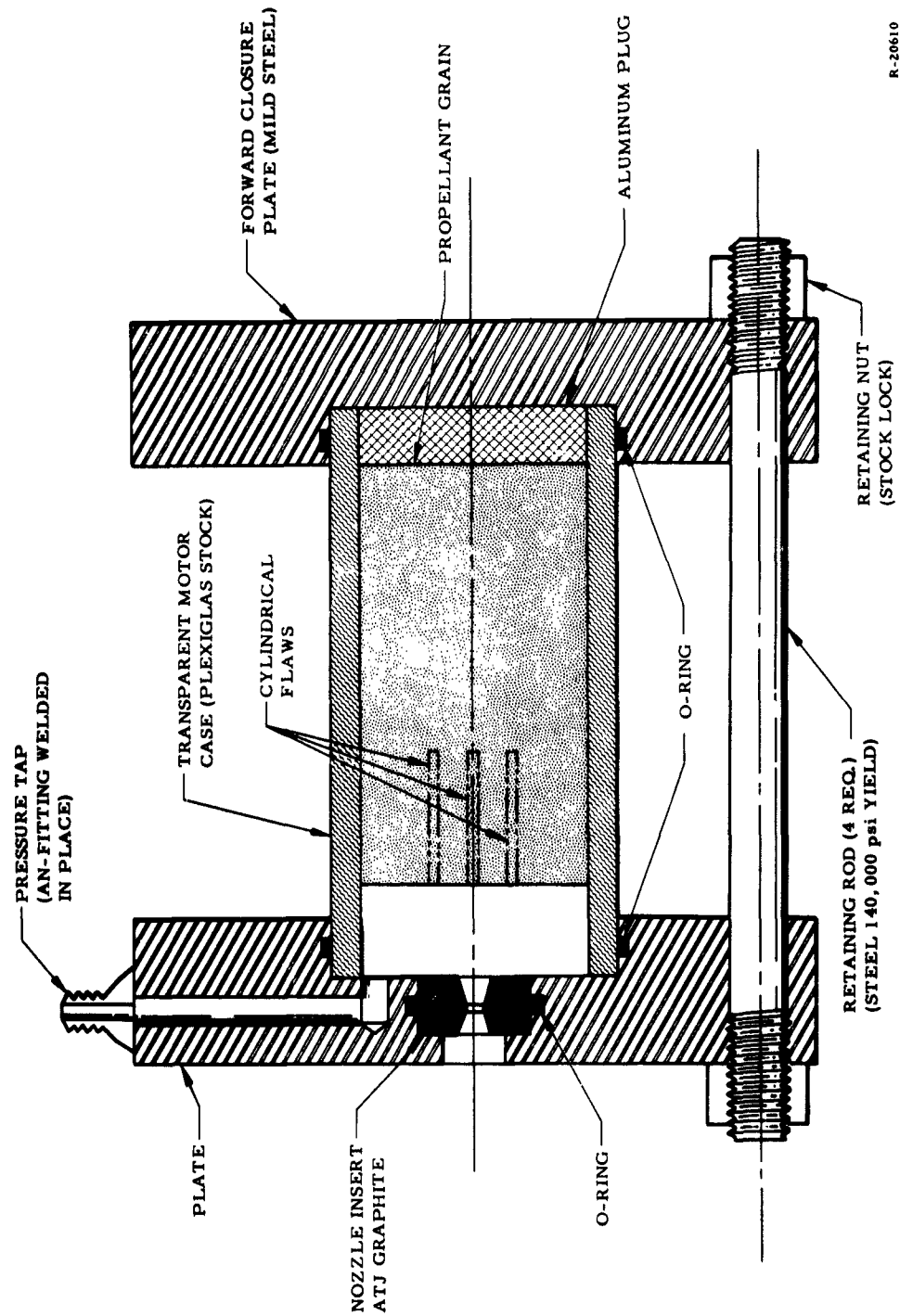
Figure 5. Transparent Motor Assembly

into the grain adjacent to the case wall and high speed photography was used to determine the rate of flame propagation down these defects.

Ignition of the first two motors resulted in catastrophic increase of the burning area. This was traced to an insufficient liner thickness (the liner had originally been designed about 0.005-inch thick to give minimum interference for good photography). A third motor incorporating a thicker liner was successfully fired on 24 August 1962.

The flaws incorporated in this motor consisted of three cylindrical defects, four inches long, with diameters of 0.0155, 0.0255, and 0.033 inch. Upon motor ignition, burning propagated down all three defects at the same rate. From photographic coverage, the rate of flame propagation into the defects was found to be 4.66 inches per second. The normal burning rate of the propellant at the pressures encountered is 0.38 inch per second.

These data appear inconsistent with the propagation rate of about 500 inches per second observed in the breakup of the second motor in this series. No explanation of this variance in rate can be offered at this time.

Experimental studies with PBAN propellant (discussed in Section 2.2 of this report) disclosed no tendency of cracks to propagate during motor operation. This mode of failure has not been encountered in the processing of PBAN propellant at UTC.

2. Propellant - Liner Unbonds

Propellant liner unbonds are also suspected to have the ability to propagate. The burning phenomenon for a propellant-liner unbond is mathematically similar to that for cracks, and much of the experimental work is valid for both. For this reason, the experimental program carried out in Task II of this contract was oriented to survey a large number of configurations of propellant-liner unbonds in a deliberate attempt to induce defect propagation. No defect propagation was observed over a wide range of differing unbond geometries.

2. 1. 1. 2 Noncatastrophic Overpressures

As discussed previously, the restrictions on variations from the design thrust time curve of a solid motor used in a multimotored stage are likely to be quite severe. Consequently, the defects present in the motor must be evaluated to determine the possibility of causing mission failure. Although it is possible that a single defect will cause a chamber pressure rise sufficient to cause a catastrophic failure, it is much more likely that the defect will cause but a slight perturbation in the expected thrust-time curve. However, the cumulative effects of all anomalies present must be evaluated, rather than the individual effects. A typical mission involving a multimotored stage requires that the motor thrust vary no more than two percent from the design thrust-time curve. A corollary of this statement requires that the difference in burning time vary by not more than two percent. It is obvious that this criterion is much more severe than a case-structural failure criterion.

For the purpose of plotting this deviation it is assumed that the thrust, given by $F = C_F A_t P_c$, may vary by ± 2.0 percent, and that A_t and C_F variations are negligible. Thus the chamber pressure must be within ± 2.0 percent of design throughout the burning time, and from the relationship

$$K_n \approx \left(\frac{P_c}{1000}\right)^{1-n}$$

where
$$K_n = \frac{A_b}{A_t}$$

where   n   is the burning rate exponent

P_c is the chamber pressure

A_b is burning area

A_t is nozzle throat area

the consequent maximum deviations of burning area with time can be determined. This relationship is plotted in nondimensional form in Figure 2.

The acceptability of a given motor can be evaluated by predicting the actual burning area as a function of time. This function would be identical to the design function if no defects were present. If the relationship is reduced to a percentage increase in burning area, the effects on chamber pressure may be readily found from Figure 2. The variation in chamber pressure is then directly proportional to the variation in motor thrust if the thrust coefficient and throat area are assumed to be constant.

The techniques involved in arriving at the burning area as a function of time will be reviewed. Requisites for these analyses are the propellant grain configurations and dimensions, the nozzle area as a function of time, and the ballistic data for the propellant. The initial burning area is first calculated. The initial K_n is obtained and the initial chamber pressure obtained. A burning rate for this pressure is determined from the ballistic data, and a small increment of time is assumed. The burning area at the conclusion of this time interval is found by projecting the initial burning surface inward a distance equal to the product of the assumed time interval and the burning rate. A new burning area is computed and the process repeated until all burning surfaces reach the case wall. The function derived from this procedure is the designed burning area as a function of time, and normally it is carried out by high speed computing machines.

To arrive at the actual burning area as a function of time, the number, type, size, orientation, and location of the various propellant defects must be determined. All grain defects will show up as increases in burning area when first touched by the flame front. Their effect will diminish in time owing to the geometry of the phenomena. It may easily be seen that the maximum effect of a given number of defects will occur when all are located an equal distance from the initial burning surface. Conversely, the minimum effect will occur when all defects are located at different distances from the initial burning surface.

A brief discussion on the behavior of the various types of defects is given in the following subsections.

A. Voids

For purposes of this discussion, any cavity in the propellant grain which has no dimension less than 10 percent of its largest dimension is classified as a void.

The excess burning area presented by this type of defect is simply the surface area of the defect itself. Experimental investigations[1]* have shown that the void actually ignites shortly before the flame front reaches it because of the collapse of the roof of the void. Typical flame front separations are given as 19 to 25 percent of the void dimension at 700 psi chamber pressure.

In large solid rocket motors, the pressure rise due to the inclusion of voids in the propellant grain is not very serious. A 1.00-inch diameter void represents the upper limit of voids normally encountered in PBAN type propellant. The number of 1.00-inch voids burning simultaneously and required to raise chamber pressure by two percent is given as follows:

Motor Diameter in.	Number of 1.00-in. Voids Required for 2 Percent Rise in P_c
120	747
156	3320
240	5980

The probability of occurrence of these numbers of such large voids is very low with modern vacuum casting techniques, and the probability of all lying at the same distance from the propellant surface (in order for all to burn simultaneously) is

* Refer to List of References on page 160 for index to superscript numbers.

extremely remote. In short, the likelihood of this type of defect causing a pressure rise of two percent or more is negligible.

Cracks or fissures in the propellant grain must be investigated for two modes of failure, overpressure and premature case burnthrough. It has been shown in experiments performed that cracks do not tend to propagate in PBAN type propellant (Section 2.2).

C. Propellant-Liner Unbonds

The area of a propellant-liner unbond becomes a potential burning area when touched by the advancing flame front. The rate flame propagation into the defect is almost certainly faster than the normal burning rate of the propellant, and very high propagation rates have been experimentally observed. A conservative method of evaluating the excess area is recommended in that the total area is assumed instantaneously ignited. This would have the effect of instantaneously increasing the burning area by the amount of the unbonded area. Further information on flame propagation rates is presented in Section 2.2.

D. Porous Propellant

Porous propellant is here taken to denote small interconnected voids contained in an area of the propellant. The flame front encounters a large surface area, and excessive amounts of propulsive gases are generated.

The incidence of porous propellant varies with the type of propellant and the processing techniques. No known instances of this phenomenon have been encountered at UTC with PBAN-type propellant.

The chief difficulty in predicting the amount of excess area involved is in characterizing the geometry of the pores. The surface-to-volume relationships of some typical geometries are presented in Figure 6. In the absence of experimental data it is recommended that a high surface-to-volume ratio (about 4000) be assigned. To arrive at the burning area of the defect the total volume of the block of porous propellant may be evaluated from radiographs, and this evaluation multiplied by the assumed surface/volume ratio. Conservative appraisal again suggests that this be considered an instantaneous area addition.

2.1.2 Case Failure Caused by Premature Web Burnthrough
Premature web burnthrough, caused by the flame front jumping across a propellant defect, results in excessive heating of the case wall, which may lead to a temperature-induced pressure failure.

2.1.2.1 Defects in the Propellant Grain
The procedure for classification of a defect in the propellant grain as to critical or noncritical may be described as follows:

A. The location of the premature burnout on the case wall is determined by a vector perpendicular to the flame front passing through the defect;

B. The insulation thickness at this point is obtained and the temperature of the case as a function of time is determined from a heat transfer analysis;
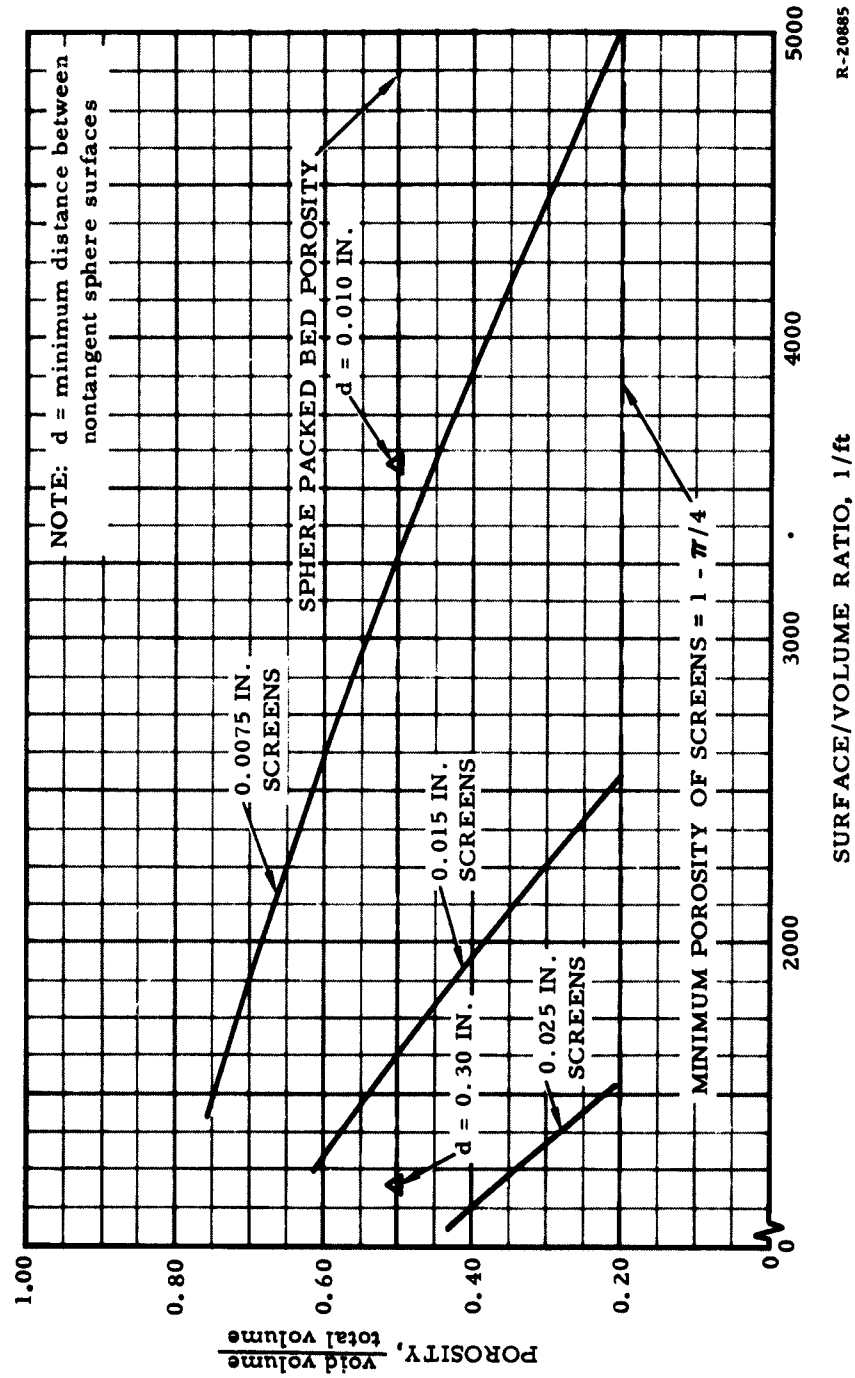
Figure 6. Surface-to-Volume Relationships of Some Typical
Geometries of Propellant Pores

(d = Minimum distance between non-tangent sphere surfaces)

C. The above function is reviewed and safety factors applied
    in the light of the original assumptions of the study and pre-
    vious experience;

D. A failure criterion of the case is derived in terms of time lapse;

E. The time of exposure of the case wall directly under the de-
    fect is determined by consideration of the maximum dimension
    of the defect in the direction of flame propagation, the rate of
    flame propagation through the defect, and the burning rate of
    the propellant;

F. The defect is classified critical if, on premature web burn-
    through, the case reaches the critical temperature.

It will be instructive to illustrate this procedure in finding the
approximate maximum allowable radial dimension of a defect for
large motors. Analytical studies of the relationship between time
of exposure and temperature for various insulation thicknesses
have been reported in the First Technical Note. The results of
this study are given in Figure 7.

The assumptions made include thermal properties of the case and
insulation invarient with temperature* and uniform thermal film
resistance on the surface of the insulation.

An analysis has been made of the expected case temperature rise
when protected by a minimum liner thickness at a point at which
premature burnout of the propellant is caused by a void defect.
The prediction as derived from this analysis is that the motor liner
itself serves as adequate protection from the premature burnout

---

* The insulation thickness includes the liner thickness.
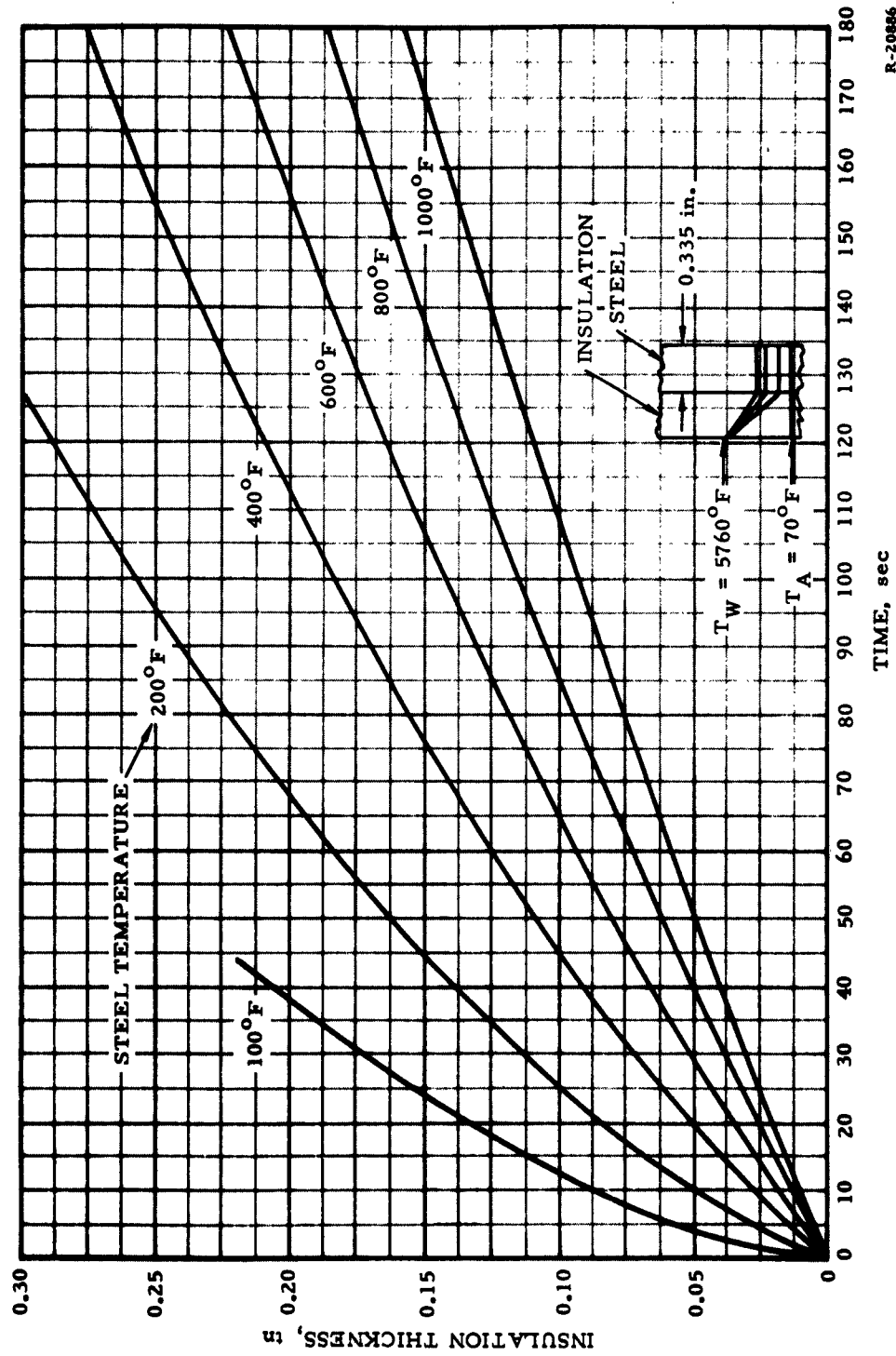
Figure 7. Insulation Thickness Required Versus Time for Various Steel Temperatures

for times up to and greater than a minute. However, there are
a number of difficulties in the conventional analysis in this complex
situation that arise from the lack of knowledge of phenomena
of heat transfer and the high temperature behavior of rubbers and
plastics. The most important of these are (1) lack of
knowledge of the character of the secondary flow in a burning cavity
arriving at the insulation face, (2) lack of ability to define boundary
layer behavior on the cold wall, and (3) lack of information on the
properties of the material itself.

The third area of difficulty refers to the fact that liner materials
char as they reach pyrolysis temperatures. The charred material,
carbon, has basically a higher conductivity than the parent
material; however, the char is porous and the precise nature of
the radiative transfer across the pores at high temperatures has
not yet been determined or measured. Furthermore, the effective
conductivity of the char and the parent material generally decreases
with rising temperature although sufficient data are not available
in support of this hypothesis. Specific heat and density also change.
At UTC, therefore, the design procedure is to consider the best
available analytical data and to apply safety factors based upon
past experience in similar situations. In this case a factor of
four to five times should be applied to the expected exposure
time to determine required thickness.

The critical case temperature is assumed to be 400 $^\circ$F. A typical
minimum thickness of liner and insulation (120-in. dia motor) is
0.2 inch. From Figure 7, an allowable exposure time of 110 sec-
onds is obtained and in consideration of the limitations of the
analysis detailed above, this time is reduced by a factor of five.

Assuming a burning rate of 0.33 in./sec, and taking note of the phenomenon of void roof collapse noted earlier, the diameter of the critical size void is computed. A similar procedure illustrates the case for the larger motors.

Motor Diameter in.	Critical Void Size in.
120	5.8
156	7.5
240	11.6

It is apparant that the risk of encountering this mode of failure from nonpropagating grain defects is negligible.

2.1.2.2 Defects in the Bond Structures

Defects in the case-insulation bond that allow combustion gases to come into direct contact with the case are critical. Case heating would be very severe in this area and would probably lead to a failure early in the burning time. Defects in the propellant-liner bond allow the flame to propagate in the direction normal to the flame front faster than anticipated and thus lead to a longer flame exposure time on the insulation structure. The evaluation of criticality is carried out in a manner similar to that described in Section 2.1.2.1 .

The maximum allowable time for exposure is 22 seconds. The maximum allowable depth of the unbond, assuming a burning rate of 0.33 in./sec, is then 7.3 inches. This consideration is, of course, independent of the overpressure limitations which were discussed in Section 2.1.1.2 .

2. 1. 3 Miscellaneous Failure Modes

The grain is normally supported by a bond between the propellant and insulation and by another bond between the insulation and case. The structural strength of these bonds holds the grain in place and resists pressure and flight loads. Motors have been successfully fired with as little as 35 percent of the bond intact, and it may be seen that this particular mode of failure is not ordinarily encountered.

A. Variations in Chemical Composition

Local variations in propellant burning rates, caused by variations in chemical compositions may result in off-design motor thrust. In the study on probability of defect study presented in the next section, it is shown that the likelihood of this type of defect is very low. Moreover, the effects on the ballistic parameters of propellant having small local variations in composition is likewise small. The strict quality control measures performed before committing a propellant batch to casting reduce the effects of this type of defect to a negligible level.

B. Variations in Propellant Cure

Variations in propellant cure are normally evaluated from the physical properties of samples cast and cured along with the propellant grain and are not therefore considered a part of the nondestructive testing reported here.

2. 1. 4 Probability of Defect Occurrence and Location

The purpose of the study described here was to conduct a statistical investigation of the above types of defects with regard to both frequency of occurrence and location within the rocket motor. In addition, there was interest in determining what differences exist among the various

combinations of propellant grain (PBAN and polyurethane) and core geometries (cylindrical and star). The conclusions of the study are of particular interest for the large diameter motors now under construction.

For purposes of the investigation, propellant defects were classified into five main categories. They are defined by the following physical descriptions.

A. Voids are bubbles or spherical cavities which occur within the propellant mainly as a result of the pouring and casting technique. While they may occur anywhere in the propellant configuration, there seems to be a tendency for them to accumulate near the top of the rocket motor.

B. A dense collection of connected voids of moderate size is considered to be a separate defect and is called a porosity. If a collection of voids are not connected, such a defect is not considered to be a porosity but rather a concentration of individual voids.

C. Cracks are tears or splits in the propellant and may be further classified by length/diameter ratios. Notable causes for these defects are excessive pressure and volume changes during cooldown.

D. Separations between liner and propellant as well as between liner and motor casing may occur. Such separations are referred to as unbonds and both types of unbonds are considered of importance in studying defects, although liner-casing unbonds are less important than the liner-propellant unbonds.

E. The final type of defect studies is called nonhomogeneity and is defined as a departure from the intended chemical properties of the propellant resulting from incomplete mixing. Such defects are a definite function of the production process used to produce the propellant. These variations are not common in modern processing techniques and may be closely associated with porosity. This type of defect may occur anywhere in the propellant grain.

Complete information of a form suitable for the study was restricted to 16 motors of eight-inch diameter with star configuration and PBAN propellant.

Accepting the basic premise that a statistical study depends critically upon the available data, it is clear that the limitations imposed by the lack of data previously described are significant. Hence, the reader is cautioned to note the reservations that must accompany statistical conclusions when data are not available to strongly support them. An attempt is made to point these out at the appropriate locations in the ensuing sections. In some cases, the conclusions are, of necessity, based upon the best engineering judgment that could be determined within the time limitation and are not based on supporting data because the latter do not exist.

Of primary concern is the matter of estimating the probability of occurence for each defect mode at various locations. For each defect mode, the rocket motor was divided into regions

that should be investigated. As to the frequency of occurrence of a given type of defect, several statistical models were examined and evaluated on their appropriateness to the underlying physical conditions. In this way, the statistical models adopted have the feature of being both reasonable and practical.

Other problem areas appear well defined through extrapolation techniques. First there is the extrapolation of the estimates from eight-inch motors to very large motors. Secondly, it is desirable to extrapolate the information obtained on PBAN-star motors to the other three geometry grain combinations that are possible. The latter extrapolation is primarily necessitated by the lack of data on any combination other than the PBAN star.

In an effort to determine underlying relationships to assist in all the problem areas, particularly for extrapolations, a brief literature survey was conducted. Notably, SPIA abstracts were surveyed for appropriate titles and the corresponding articles were in turn examined. Generally speaking, the available literature on the subject is concerned with either technical discussions of techniques for observing defects or the effect of various defect modes on the successful operation of the motor. But this study is not directly concerned with either of these points; moreover, the methods of gathering observations were essentially predetermined by the availability of data. Consequently, the literature has been of little direct assistance.

.2. 1. 4. 1 Voids

Voids were first divided into three separate categories: diameters less than 1/4 inch, between 1/4 inch and 3/4 inch, and greater than 3/4 inch. It is always assumed that one of the above categories is fixed so that the discussion that follows will always be relative to that particular category.

In order to establish location, it was necessary to divide the propellant configuration into separate regions. In Figure 8, this division is shown schematically. First, the cross-section was divided into two regions by drawing an imaginary circle from the center of the configuration using the distance to a star point as a radius. In this way, an inner region consisting of the configuration contained within the circle just drawn and the outer region consisting of the annular region contained between the two circles is obtained. For a cylindrical core, it is assumed that the same inner circle is drawn to define an inner and outer region. Next, the configuration was divided longitudinally into three equal parts starting from the top of the motor.

In the manner prescribed by the preceding paragraph and Figure 8, six regions were defined for locating voids. These were labeled R_1, R_2, and R_3 for the three inner regions starting from the top of the motor and R_4, R_5 and R_6 for the corresponding outer regions beginning at the top of the motor. Finally, the volumes for these regions have been entered in Table III for both eight-inch and the 120-inch motors. The ratios of the volumes for the various regions were also entered and are useful in the problem of extrapolating the results which appear at the end of this section.

VOID REGIONS

L = MOTOR LENGTH

R-20887
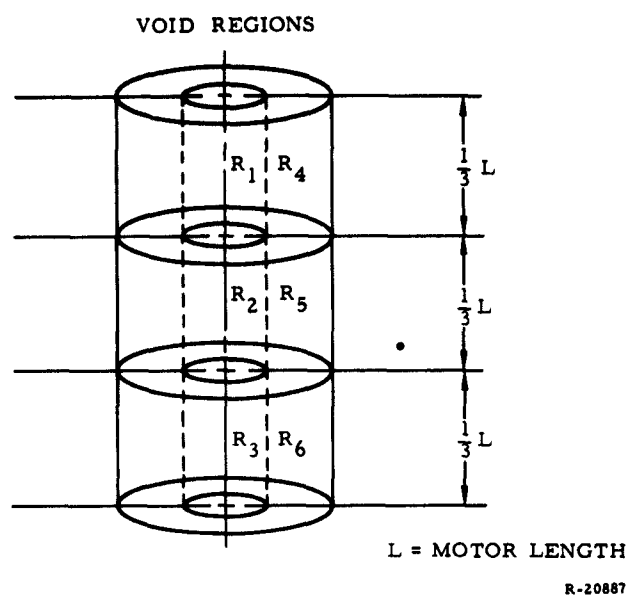
Figure 8. Schematic of Division of Propellant Configuration
into Separate Regions

TABLE III

REGION VOLUMES

	R_1	R_2	R_3	R_4	R_5	R_6
V_i, in.^{3}	5462	15,932	25,699	375,394	375,394	375,394
v_i, in.^{3}	36	45	51	255	259	243
$k_i = \dfrac{V_i}{v_i}$	152	354	504	1472	1449	1545

v_i = volume of propellant in Region R_i (8-inch motor, star core), i = 1, ..., 6

V_i = volume of propellant in Region R_i (120-inch motor, tapered cylindrical core), i = 1, ..., 6

2.1.4.2 Statistical Model

Given a particular void size, the following quantities for the eight-inch motor are defined:

X_i = number of voids in region

   R_i, $i = 1, 2, \ldots, 6$

λ_i = average number of voids in region

   R_i, $i = 1, 2, \ldots, 6$

x_{ij} = observed number of voids in region

   R_i of the jth observed motor,

   $i = 1, 2, \ldots, 6$; $j = 1, 2, \ldots, 16$ (1)

With the above quantities defined, it is assumed that the random variable X_i is distributed according to a Poisson probability law with parameter λ_i. Accordingly, the probability that X_i will assume a particular integer value k, $P[X_i = k]$, is given by

$$P[X_i = k] = e^{-\lambda_i} \frac{\lambda_i^{k}}{k!} \quad \text{for } k = 0, 1, 2, \ldots \quad (2)$$

The assumption of the Poisson probability law for the statistical model seems quite suitable in terms of the problem at hand. First, the distribution of points in space are considered. To determine the spatial distribution it is assumed that voids of a given size are distributed in a given region at random and that the probability of finding k voids in any specified domain of the region depends only on the volume of the domain and not its shape. Moreover, it is assumed that if the volume v of a specified domain is small, then the probability of finding more than one void is small as compared to v.

Having established the model, it is of interest to estimate λ_i, the mean or average number of voids in each region R_i. To estimate λ_i, it is computed that the maximum likelihood estimate $\hat{\lambda}_i$, is given by

$$\hat{\lambda}_i = \frac{1}{16} \sum_{j=1}^{16} x_{ij} \tag{3}$$

Again, it is emphasized that the subscript i fixes the region to be considered and it is always assumed that a given void size has been previously selected for purposes of discussion.

So far only the problem of estimating averages for various regions of the eight-inch motors has been discussed. To extrapolate the data of the statistical model to the 120-inch and larger motors the propellant must be divided into six regions similar to those of the eight-inch motor discussed in Section 2.1.4.1. It is then assumed that a given region in the larger motor consists of several of the corresponding regions of the smaller motor with regard to statistical behavior. The factor k_i, entered in Table III, determines the number of such regions for a given and corresponding region of the large motor. Once this is established, it follows that the number of voids (of a specified size and course) in the ith region of the 120-inch motor is distributed according to a Poisson law with parameter $\mu_i = k_i \lambda_i$ and the best estimate of μ_i is given by

$$\hat{\mu}_i = k_i \hat{\lambda}_i \tag{4}$$

Again the magnitude of μ_i as an estimate of the average number of voids in the ith region of the large motor is of interest.

The above assumptions, by means of which a distribution on the number of voids in the 120-inch motor is induced, are equivalent to assuming a direct scaling in extrapolating from eight-inch to 120-inch motors. This assumption may or may not be valid. However, it is felt that it is a good approximation to the real situation, although there is a general feeling that the actual number of voids should be slightly less in the 120-inch motor. This is partly because of the pouring process wherein several batches are used to pour a single 120-inch motor so that the time between pourings allows for a certain amount of dissipation before curing begins. However, in the absence of verification of this point, it is suggested that whenever this assumption can be made more definitive by producing a scale factor, then the estimates given here may be accordingly adjusted by such a factor.

2. 1. 4. 3 Experimental Results

The frequency of occurrence of the various voids in each of the regions, obtained from radiographs of the 16 small motors available for study, have been entered in Table IV. The resulting sums and corresponding values of the maximum likelihood estimates of the averages are also tabulated.

From Table IV, several conclusions can be drawn concerning the nature and behavior of voids. One outstanding fact is that large voids, that is, voids where diameters exceed 3/4 inch, appear to present no problem since none was observed in any region. For all practical purposes, the same remarks might be made concerning voids where diameters are between 1/4 inch and 3/4 inch.

TABLE IV

VOID FREQUENCY

Motor Number	Region 1 (R_1) S_1*	S_2	S_3	Region 2 (R_2) S_1	S_2	S_3	Region 3 (R_3) S_1	S_2	S_3	Region 4 (R_4) S_1	S_2	S_3	Region 5 (R_5) S_1	S_2	S_3	Region 6 (R_6) S_1	S_2	S_3
1	0	0	0	0	0	0	0	0	0	0	0	0	0	0	0	0	0	0
2	0	0	0	0	0	0	0	0	0	24	0	0	0	0	0	1	0	0
3	0	0	0	0	0	0	0	0	0	40	0	0	0	0	0	0	0	0
4	0	0	0	0	0	0	1	0	0	0	0	0	1	0	0	0	0	0
5	0	0	0	1	0	0	0	1	0	0	0	0	1	0	0	0	0	0
6	4	0	0	0	0	0	0	0	0	4	0	0	15	0	0	44	0	0
7	0	0	0	0	0	0	0	0	0	0	0	0	1	0	0	0	0	0
8	0	0	0	0	0	0	0	0	0	12	0	0	0	0	0	0	0	0
9	0	0	0	0	0	0	0	0	0	50	0	0	2	0	0	0	0	0
10	0	0	0	0	0	0	3	0	0	38	0	0	0	0	0	0	0	0
11	0	0	0	0	0	0	0	0	0	27	0	0	1	0	0	0	0	0
12	0	0	0	0	0	0	0	1	0	108	0	0	0	0	0	0	0	0
13	0	0	0	0	0	0	0	0	0	124	0	0	95	0	0	6	0	0
14	0	0	0	0	0	0	0	0	0	182	0	0	25	0	0	7	0	0
15	0	1	0	0	2	0	1	0	0	69	0	0	94	0	0	18	0	0
16	0	0	0	0	0	0	0	0	0	195	0	0	29	0	0	13	0	0
Σx_{ij}	4	1	0	1	2	0	5	2	0	873	0	0	264	0	0	89	0	0
$\hat{\lambda}_i$	0.25	0.06	0	0.06	0.12	0	0.31	0.12	0	54.6	0	0	16.5	0	0	5.6	0	0
$\hat{\mu}_i$	38	9.5	0	22	44	0	158	63	0	80316	0	0	23908	0	0	8594	0	0

*S_1 = void diameter less than 1/4 in.; S_2 = void diameter between 1/4 in. and 3/4 in.; S_3 = void diameter greater than 3/4 in.

The tendency for small voids (diameters less than 1/4 inch) to
occur more often in the outer regions rather than the inner regions
is quite striking. There is a noticeable difference in the average
number of voids in regions R_4, R_5, and R_6 as compared with
regions R_1, R_2, and R_3. Also noticeable is the fact that there is
a tendency for voids to migrate toward the top of the motor con-
figuration. This was explained as a phenomenon resulting from
the gravity forces in the viscous propellant.

In contrast to the small voids it is observed that the few moderate
size voids (between 1/4 inch and 3/4 inch) that do occur tend to
appear in the inner regions rather than the outer regions, though
the frequency of occurrence is relatively minor.

2. 1. 4. 4 Nonhomogeneity

A nonhomogeneity defect results when the mixing process fails
to blend the individual propellant ingredients uniformly.

A long mixing period will reduce the probability of a nonhomogeneity
defect, while a short period will increase this probability. However,
long mixing periods reduce production and hence there exists a trade-
off between production rates and the probability of nonhomogeneity.
The mix will represent a period which could result in a nonhomo-
geneous batch but only with a small acceptable probability,   p.
For the present process the probability of nonhomogeneity occurr-
ing is between 0. 0001 and 0. 00001.

Large motors will be composed of several batches of propellant
each manufactured under the same specifications and conditions
and each manufactured independently of the others. Thus if N

batches of propellant are used in a single segment the probability of the final segment being nonhomogeneous (i. e. , at least one batch of propellant being nonhomogeneous) is denoted P_N and is given by

$$P_N = 1 - (1 - p)^N \tag{5}$$

where p is the probability of an individual batch being nonhomogeneous.

Propellant batches are to be mixed in quantities of either 2600 lb or 6500 lb depending upon the capacity of the mixing unit. The weight of a single 120-inch segment is 70,000 lb. Thus, in round numbers, the number of batches in a single 120-inch segment will be between 11 and 27.

In view of the above remarks, the expressions

$$P_{27} = 1 - (1 - p)^{27}$$

$$P_{11} = 1 - (1 - p)^{11} \tag{6}$$

for $0 \le p \le 1$ are derived. The results are shown in Table V. If both mixers are operating simultaneously, the numbers of batches required for a 70,000 lb motor would be about 16. The resulting values for P_{16} are also given in Table V.

Thus it is estimated that the probability of a nonhomogeneity based on a motor consisting of 16 batches is between 0.0002 and 0.0016.

TABLE V

PROBABILITY OF A NONHOMOGENEITY IN 11, 16, OR 27 BATCH SEGMENTS VERSUS THE PROBABILITY OF THE NONHOMOGENEITY OF A SINGLE BATCH

P	P_{11}	P_{16}	P_{27}
0.05	0.4312	0.5599	0.7497
0.035	0.3242	0.4344	0.6178
0.025	0.2432	0.3332	0.4953
0.020	0.1992	0.2761	0.4203
0.015	0.1531	0.2147	0.3349
0.010	0.1046	0.1474	0.2374
0.005	0.0537	0.0772	0.1267
0.001	0.0108	0.0157	0.0264
0.0001	0.0011	0.0016	0.0027
0.00001	0.0001	0.0002	0.0003

2.1.4.5 Unbonds

By their very nature, unbonds occur at the surface of the grain configuration. This is true of both types of separations, namely, liner-casing and liner-propellant. Replacing the notion of volume by area, it is possible to set up a Poisson model for unbonds similar to that established for voids.

First the motor is divided longitudinally into three equal parts as before, thereby defining three surfaces. Assume that the unbonds in a given surface are distributed at random throughout that sur-face in such a way that the probability of finding k of them in a specified domain of the surface depends on the area of that domain.

The number of unbonds will thus be a random variable distributed according to a Poisson law with some parameter which determines the average of such unbonds in the surface.

As before, once the Poisson law is established, estimates for various probabilities as functions of the parameter estimates may be obtained. It may also be of interest to further classify unbonds by size as in the case of voids. This would mean assuming a separate distribution for a given type of unbond and a given size in a given region.

Before any estimates can be obtained for the above quantities, however, it is necessary to secure data in the form of counts of the number of unbonds for several motors. First it was thought that the radiographs for the 16 small motors which were used for voids would also yield a count on the number of unbonds. As it developed, however, the photographic techniques of direct shooting which were used for counting voids would not reveal unbonds. A special technique involving tangential photographs is necessary and these are available for only one complete motor. Obviously such data are entirely inadequate for estimating the quantities of interest.

It should be mentioned that no unbonds were discovered in the single motor which was examined. Even if several motors were available for study there is still the problem of extrapolation as in the case of voids. It is believed that, in contrast to voids, the frequency of unbonds should increase slightly when extending to the larger motor.

2.1.4.6 Cracks and Porosity

No crack defects have ever been observed in the various motors produced under the present production process. Although it has not been mathematically demonstrated, there is a strong probability that any crack in a propellant grain would either start at, or propagate to, a free surface, and thus be discovered by visual inspection.

Similarly, no porous propellant has ever been detected at UTC. Indeed, in this case, the lack of radiographic inspection has prohibited detection if porosity were present. It would, therefore, be dangerous to formulate conclusions about random occurrence of crack and porosity defects from the zero observations.

2.1.4.7 Extrapolation to Other Grain - Geometry Combinations

The danger of drawing conclusions without some sort of supporting data mentioned in preceding sections is perhaps even more critical in the problem of extrapolating to different grain - geometry combinations. The motors available for this study were of the PBAN-star type although interest lies in the other three combinations of grain and core geometry. However, no motors of any of the other three combinations were available for study.

Consequently, any statements made at this point regarding the other combinations cannot be based on statistical evidence. Significant changes in the frequency of occurrence of various defects in combinations other than the PBAN-star types are not likely. This is particularly true of the change from a star core to a cylindrical core. Of course another factor to be considered is the relative importance of such changes, if

indeed they exist, in the other combinations. Also to be considered are the effects on the end product of the various defects.

2.2 EXPERIMENTAL STUDY OF DEFECT-FAILURE RELATIONSHIP

The purpose of this item of work is to study the effects of propellant grain defects under simulated operating conditions. The technique originally proposed (and written into the contract) incorporated a closed bomb in which slabs of defective propellant could be observed while burning. The contractor believes that actual operating conditions would be simulated more closely in small-scale rocket motor firings than in a window bomb. The window bomb has been studied extensively elsewhere and it is unlikely that any breakthroughs can be expected from further study under this contract.

To obtain true simulations of structural interaction between case and grain, model studies under actual firing conditions are required. Thin wall cases duplicating case strains during firing are essential for simulation of grain strains. Grain strains are amplified by case dilation; consequently, previous tests employing heavy wall cases which minimize case dilation have been misleading.

No previous tests of flightweight model motors for study of the effects of grain defects on performance have been reported.

An experimental study was undertaken to determine the sizes and configurations of typical grain defects which would cause malfunctions in large solid-propellant rocket motors. This study provided experimental verification of the analytical study regarding the defect-failure relationship.

The small-scale rocket motor used in this study (Enclosure 1 - Drawing 3001-964) represented a 1/20 size model of a 120-inch diameter motor. The thin case (0.016-inch thick in the model) allows the propellant grain to undergo strains closely simulating the actual operation of the full size item.

Grain defects simulated in the program are listed in Table VI. Twenty-five firings were carried out in this program. Chamber pressure was monitored during the firings. In addition, X-ray movies were employed on ten of the firings to aid in visualizing flame propagation into a propellant-liner unbond. The data were correlated with the site and configuration of the defect built into the motor, thus forming a basis for the prediction of defects in large motors as to critical or noncritical.

TABLE VI
2015 PROGRAM 1/20th SCALE MOTOR

Motors	Defects
No. 1 through 5	None (Checkout Firings)
6, 7, and 8	1/4-in. dia void (not loaded)
9, 10, and 11	Propellant-liner unbond, 2-in. deep; 0, 0.030, 0.060 in. separation
12, 13, and 14	Propellant-liner unbond, 3-in. deep, 0, 0.030, 0.060 in. separation
15, 16, and 17	Propellant-liner unbond, 4-in. deep, 0, 0.030, 0.060 in. separation
18, 19, and 20	Propellant-liner unbond, 5-in. deep, 0, 0.030, 0.060 in. separation
21 and 22	Porosity
23, 24, and 25	Propellant grain cracks

2. 2. 1 Firing Results - Checkout Firings
Checkout firings of the first five subscale motors were completed
25 October 1962. All rounds successfully ignited, and the pressure-
time curves conformed closely to predicted values (a typical pressure-
time curve is given in Figure 9,

A motor case burnthrough was experienced in one firing (See
Figure 10). This occurred at 5. 4 seconds of the six-second burning
time. The burnthrough occurred on the insulated wall of the aft end
of the motor. The affected section was exposed to the hot propellant
gases for the entire length of burning time. Postfiring examination
of another motor revealed small areas of excessive case heating in
the same location.

The case insulation in the affected areas consists of 0. 10 inch of
liner. Corrective action on 11 September 1963 was taken to increase
this thickness to 0. 130 inch and no further difficulties were encountered
in subsequent firings.

2. 2. 2 Test Firings of Defective Motors
The preparation of motor defects and the test results will be dis-
cussed. All motors were case separately for each class of defects
with UTP-3001 (an aluminized PBAN propellant). In addition, all
motors were radiographed prior to firing to insure that no other
defects were present.

2. 2. 2. 1 Void Defects (Motor No. 7 and No. 8)
Two motors were processed containing 0. 50-in. diameter cylin-
drical voids oriented as shown in Figure 11. These defects were
prepared by coring out a piece of propellant with a length of
sharpened tube and cementing a plug in the top of the cavity to
form a buried void.
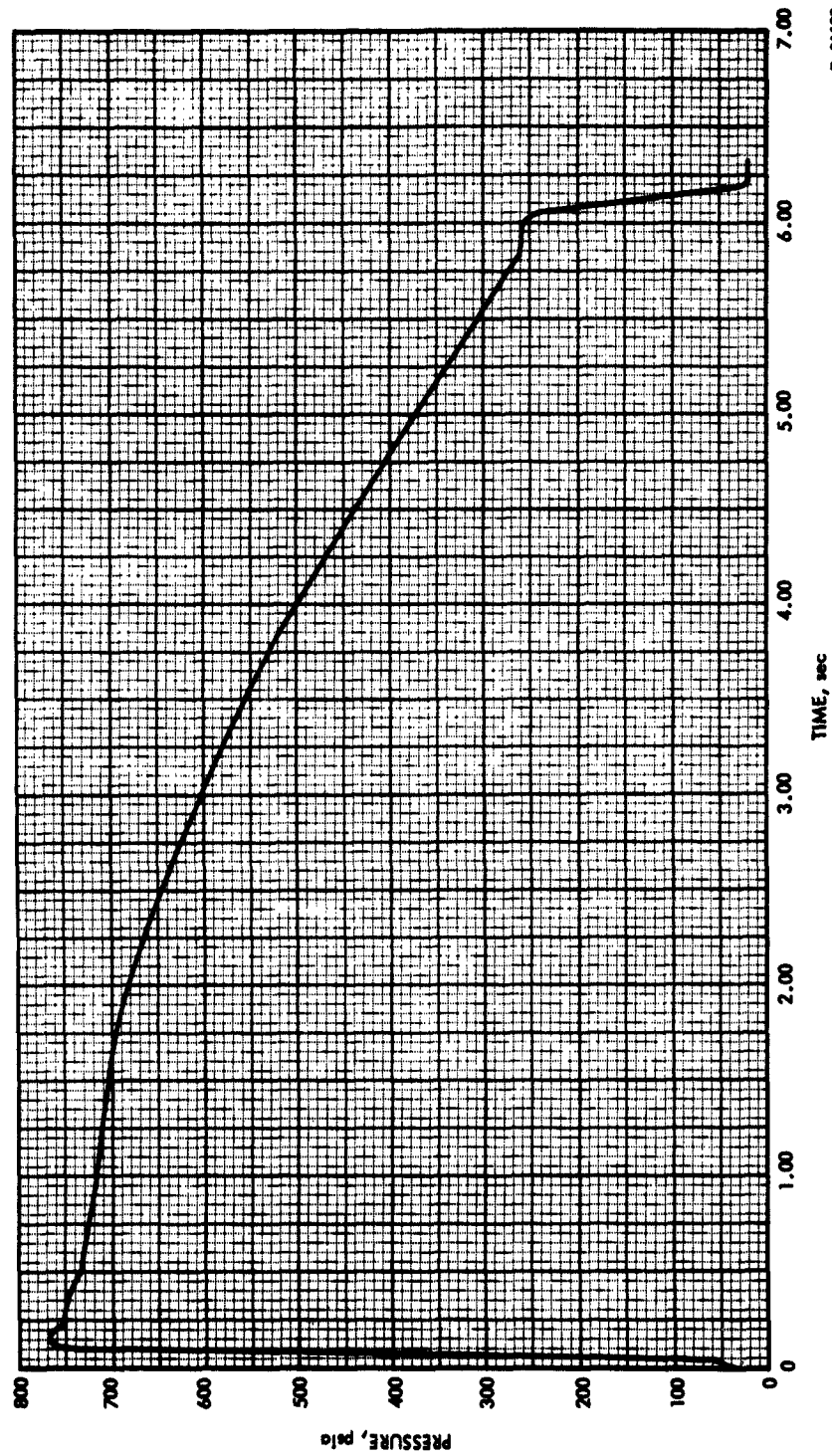
Figure 9. Pressure versus Time for Typical Subscale Motor
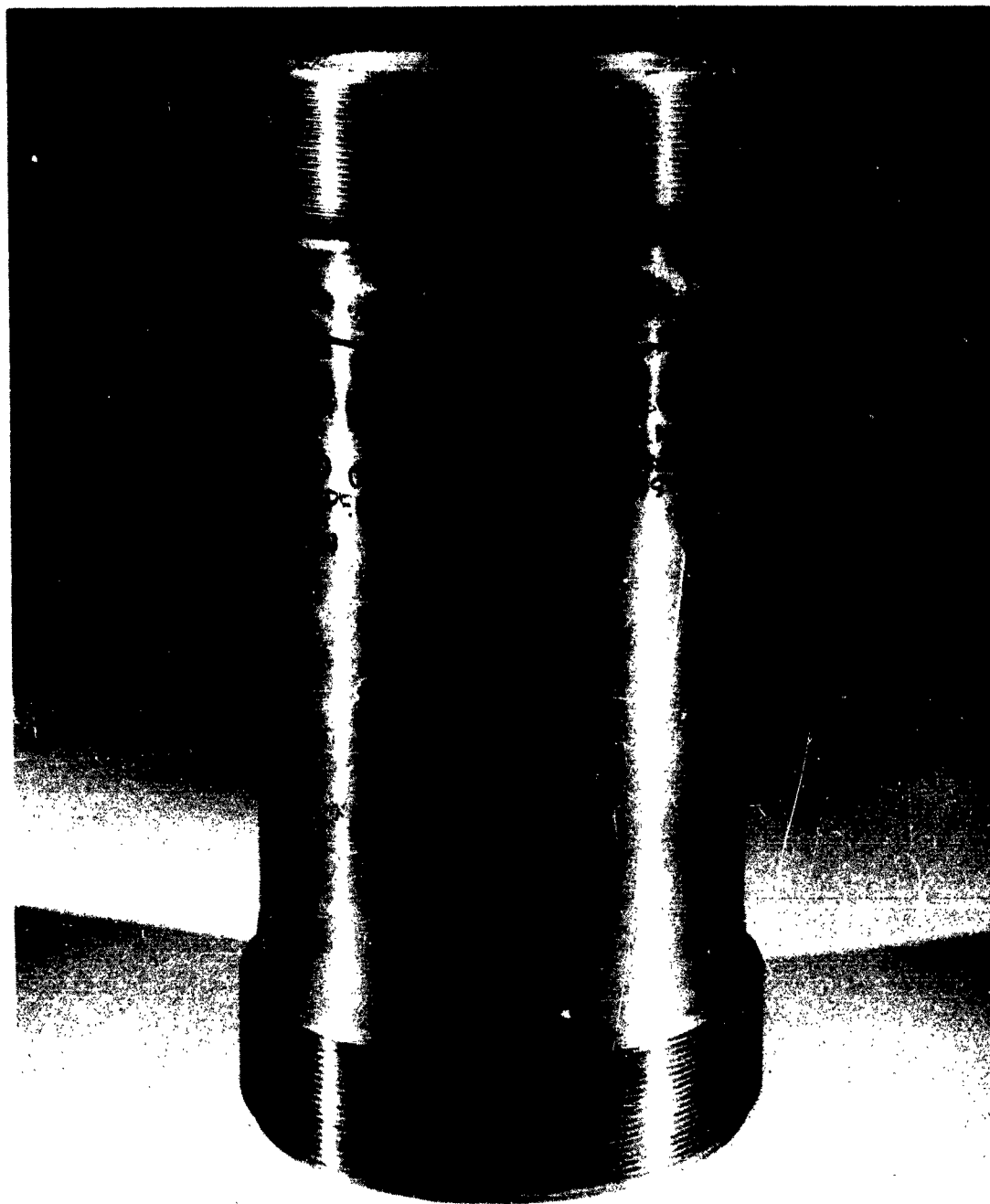
R-21107

Figure 10.   Burnthrough in Subscale Motor

R.-30181

LINER — CASE

PROPELLANT GRAIN

0.5 in. DIA VOID

3.0 in. ± 0.5 in.

1.0 in.

FWD
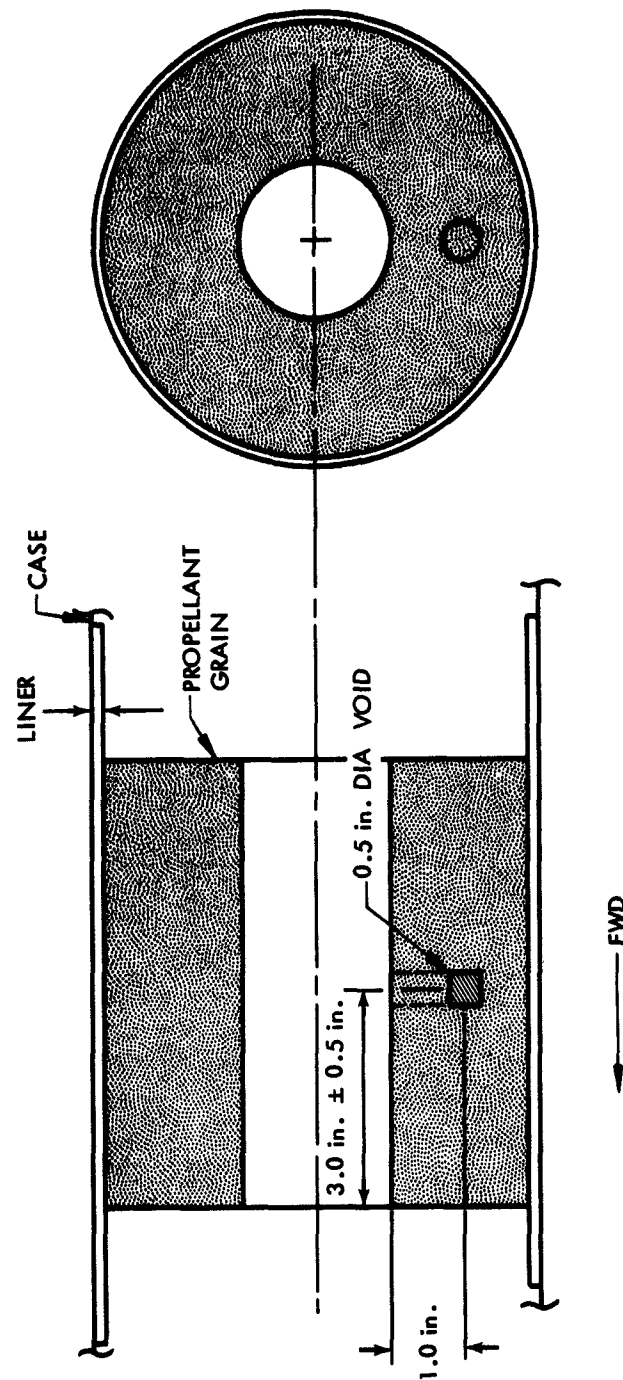
NOTE: Maximum Pressure Rise Expected is 10 psi 2 sec After Ignition.

Figure 11. Propellant Grain Defects for Motors No. 6 and 7

The pressure-time trace of Motor No. 7 is shown in Figure 12, and the curve for the defect-free motor in Figure 9. Motor No. 7 burned as expected. The void in Motor No. 8 apparently collapsed on ignition by shearing out the plug used to form the void. Even under these conditions, it is to be noted that the over-all pressure rise is very moderate.

2.2.2.2 Propellant-Liner Unbonded (Motor No. 9 thru 20)

Experimental firings of twelve motors were specifically oriented to permit exploration of the possibility of propellant-liner unbond propagation. These motors had unbonds varying in nominal thickness from zero to 0.060 inch and in length from two to five inches (Figure 13). The zero thickness unbond was prepared by coating the liner with RTV-60. In the others, a shim of the appropriate thickness coated with RTV-60 was used to form the unbond. X-ray films were taken in ten of the twelve firings. The frame speed of the X-ray film was 100 frames per second. The complete unbonded surface was lit in less than one frame which corresponds to 10 milliseconds for all unbonded surfaces. Although a finite time interval must elapse for the flame to propagate along the unbond surface this time was not measureable. All X-ray movie-graphs are represented by the depth of the unbond and the length of the unbond measured from a arbitrary data plane.

2.2.2.2.1 Zero Thickness Unbonds (Motor No. 9, 12, 15, and 18)

Two of these motors were prepared with unbonds that did not extend to a free surface (the unbond began 0.10 to 0.12 in. below the surface of the grain). Postfiring examination of the liner surface showed no evidence of burning in the unbond, a conclusion verified by the pressure time traces (Motor No. 9 and 12, Figure 14). Motor No. 15 and 18 had unbonds extending to a free surface. After curing and cooling to ambient temperatures these unbonds had opened up to about 0.008-in. thickness.
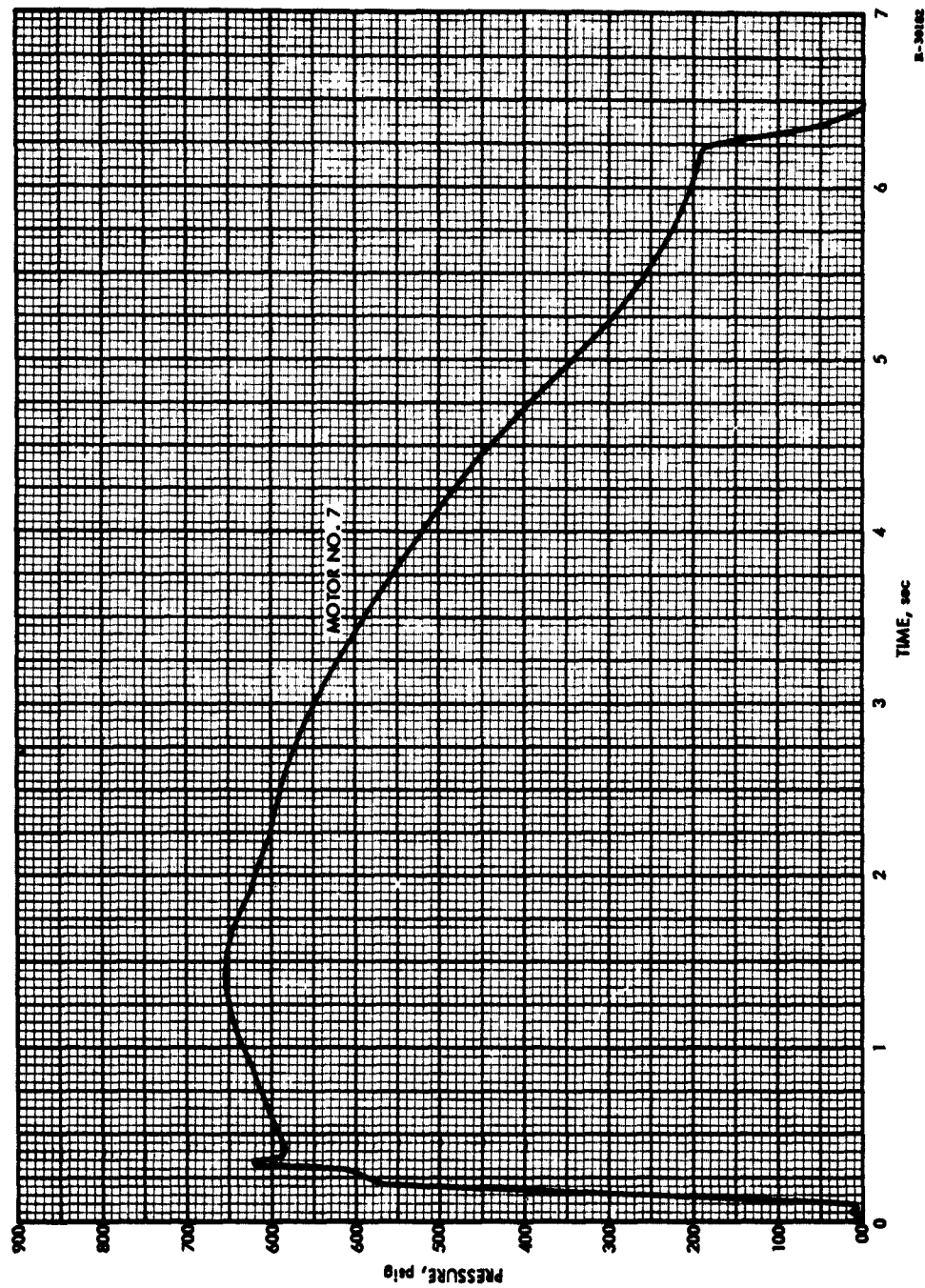
Figure 12. Pressure versus Time trace for Subscale Motor No. 7

R-30183

CASE

LINER

PROPELLANT GRAIN

PROPELLANT-TO-LINER UNBOND

L

t

FWD

60°
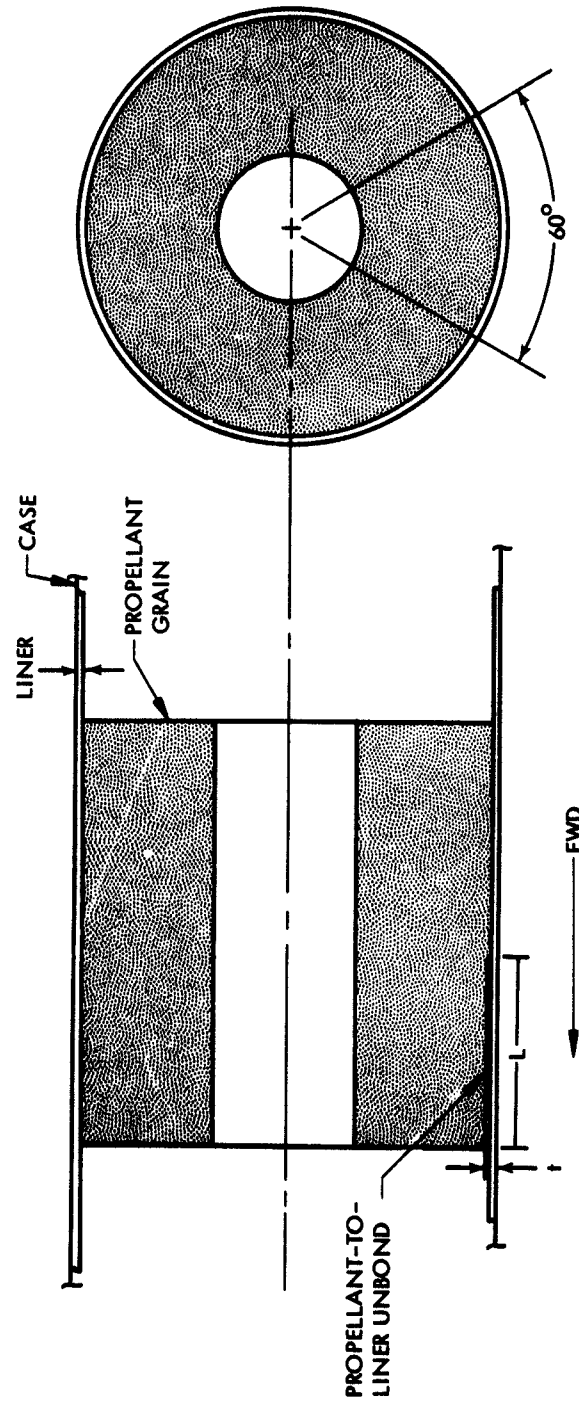
MOTOR NO.	9	10	11	12	13	14	15	16	17	18	19	20
L	2.0	2.0	2.0	3.0	3.0	3.0	4.0	4.0	4.0	5.0	5.0	5.0
t	0	.030	.060	0	.030	.060	0	.030	.060	0	.030	.060

NOTE: Zero Thick Unbond Formed with Release Agent Only.

Figure 13.   Propellant Grain Defects for Motor No. 9 through 20
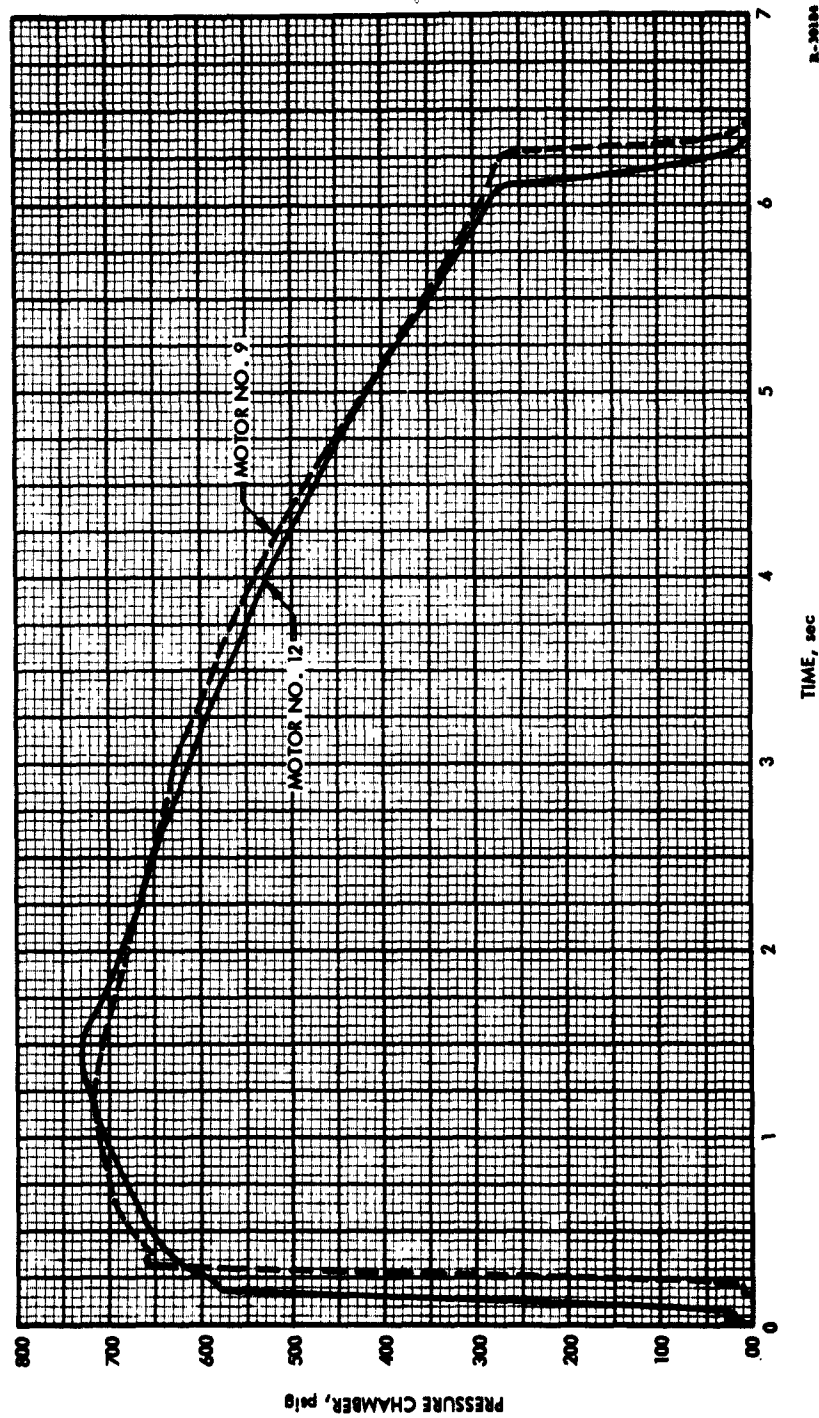
Figure 14. Pressure versus Time Trace for Subscale Motors No. 9 and 12

None of these unbonds was detectable with the radiographic techniques employed. The pressure-time traces of these firings are shown in Figure 15. Motor No. 15 and 18 failed by case burnthrough which in turn was caused by burning in the propellant-liner unbond. Figure 15A and 15B illustrate the length and depth of burning surfaces during the firing duration. In Figure 15A the whole unbond surface is seen to be higher in the 57th frame which corresponds to 570 milliseconds after ignition.

2.2.2.2.2 0.030-in. Thickness Unbonds Motor No. 10, 13, 16, and 19
Actual inbond thicknesses are reported in Table VI. These 0.030-inch unbonds were confirmed by radiographs. The pressure-time curves for these motors are shown in Figure 16. All four motors failed by motor case burnthrough. X-ray movies again revealed the unbond area to ignite in less than 10 milliseconds. Figure 16A and 16B show the length of burning unbond and depth of unbond thickness as a function of firing time for Motors No. 10 and 13 respectively.

2.2.2.2.3 0.060-in. Thickness Unbonds (Motor No. 11, 14, 17, and 20)
The actual unbond thicknesses are reported in Table VI. These unbonds were confirmed by radiography. The pressure-time traces for these motors is shown in Figure 17. All four cases failed by motor case burnthrough at the unbond area. Figure 17A and 17B show the burning surfaces as a function of burning time for Motors No. 11 and 14. From these figures we can see the 0.060-in. unbond surface is ignited in less than 10 milliseconds.

2.2.2.3 Porosity Defects (Motor No. 21 and 22)
The porosity defects were simulated by producing a cavity into the propellant grain in a manner similar to that for the void defects. This cavity was filled with particles of UTP-3001 propellant, with particle sizes of 0.025 to 0.030 inch. The cavity was located as shown in Figure 18. The pressure-time traces for Motor No. 21 are shown in Figure 19.
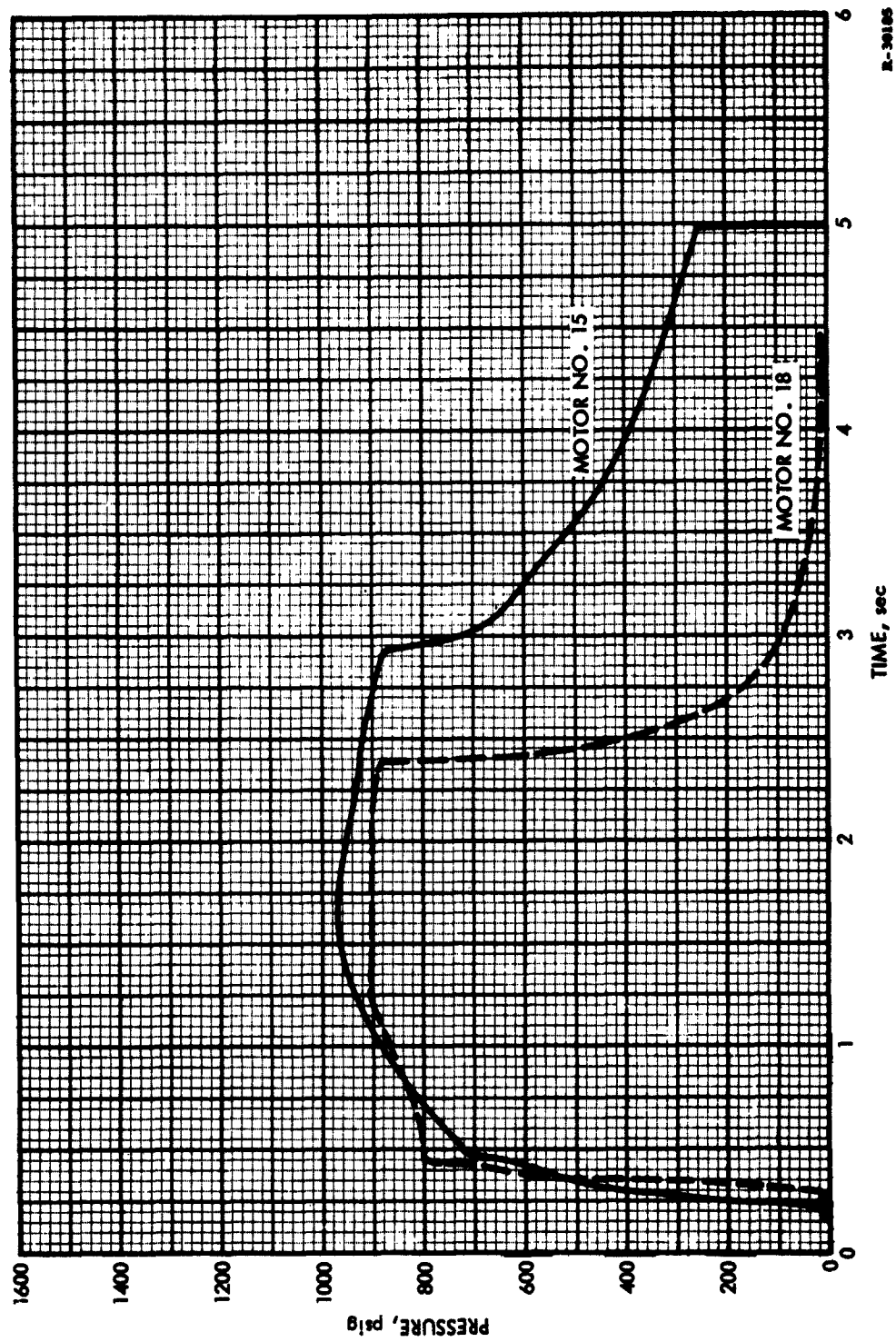
Figure 15. Pressure versus Time Trace for Subscale Motors No. 15 and 18
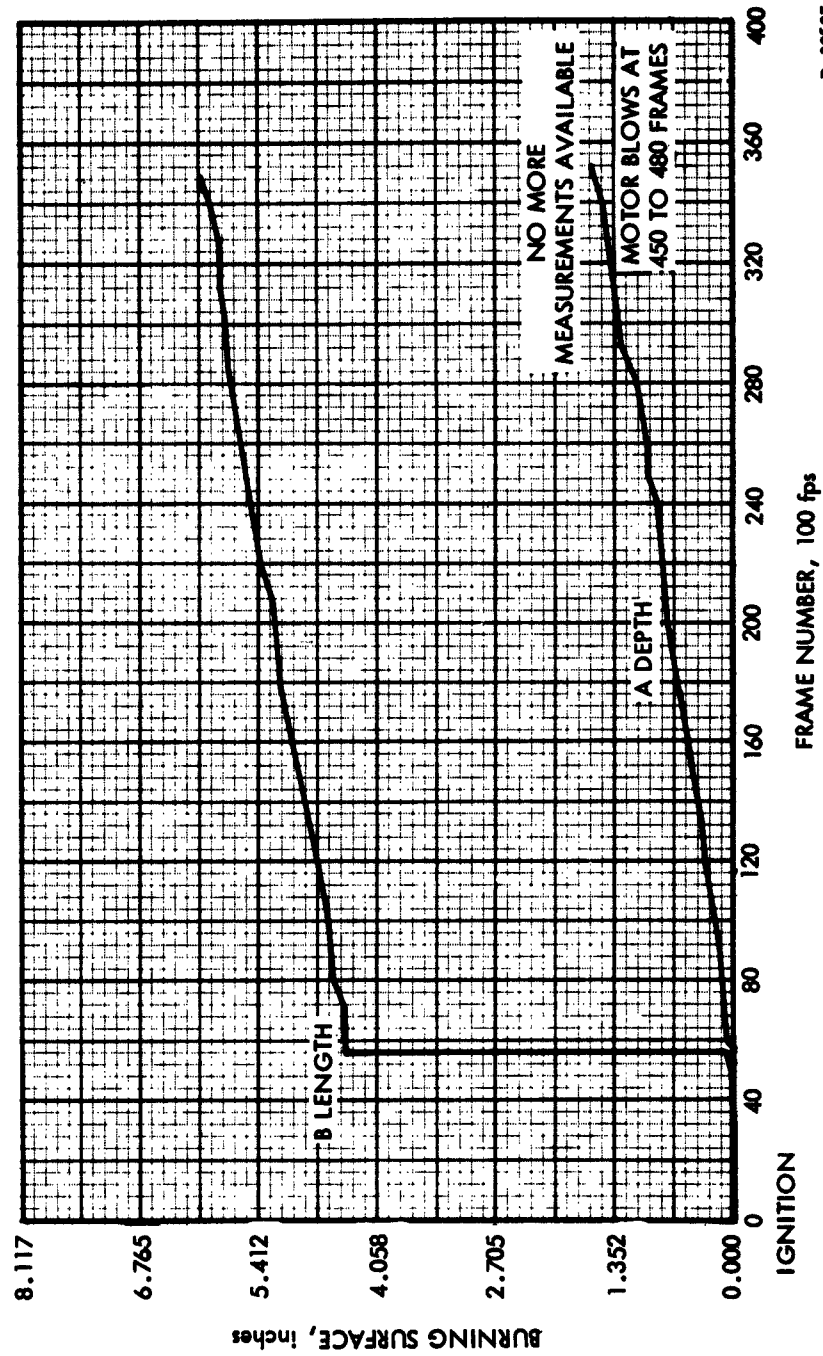
Figure 15a. Length of Burning Unbond and Depth of Unbond Thickness
as a Function of Burning Time (Motor No. 15)

R-30507
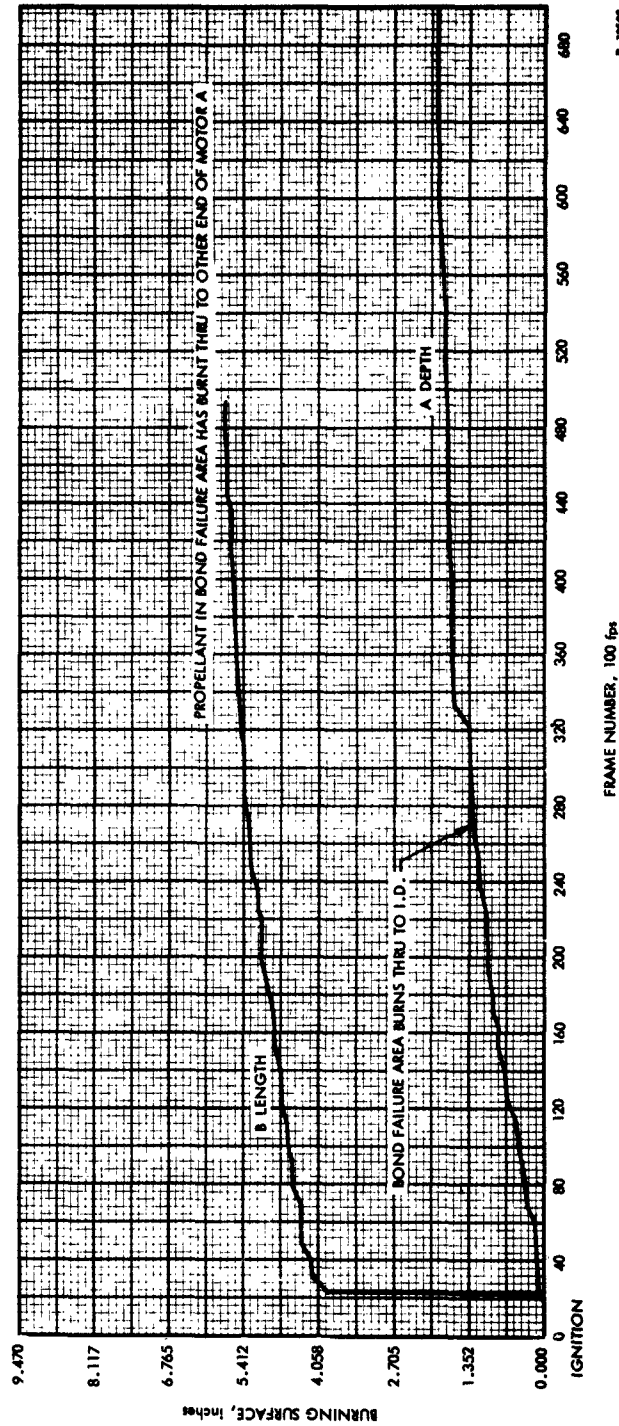
Figure 15b. Length of Burning Unbond and Depth of Unbond Thickness
as a Function of Burning Time (Motor No. 18)
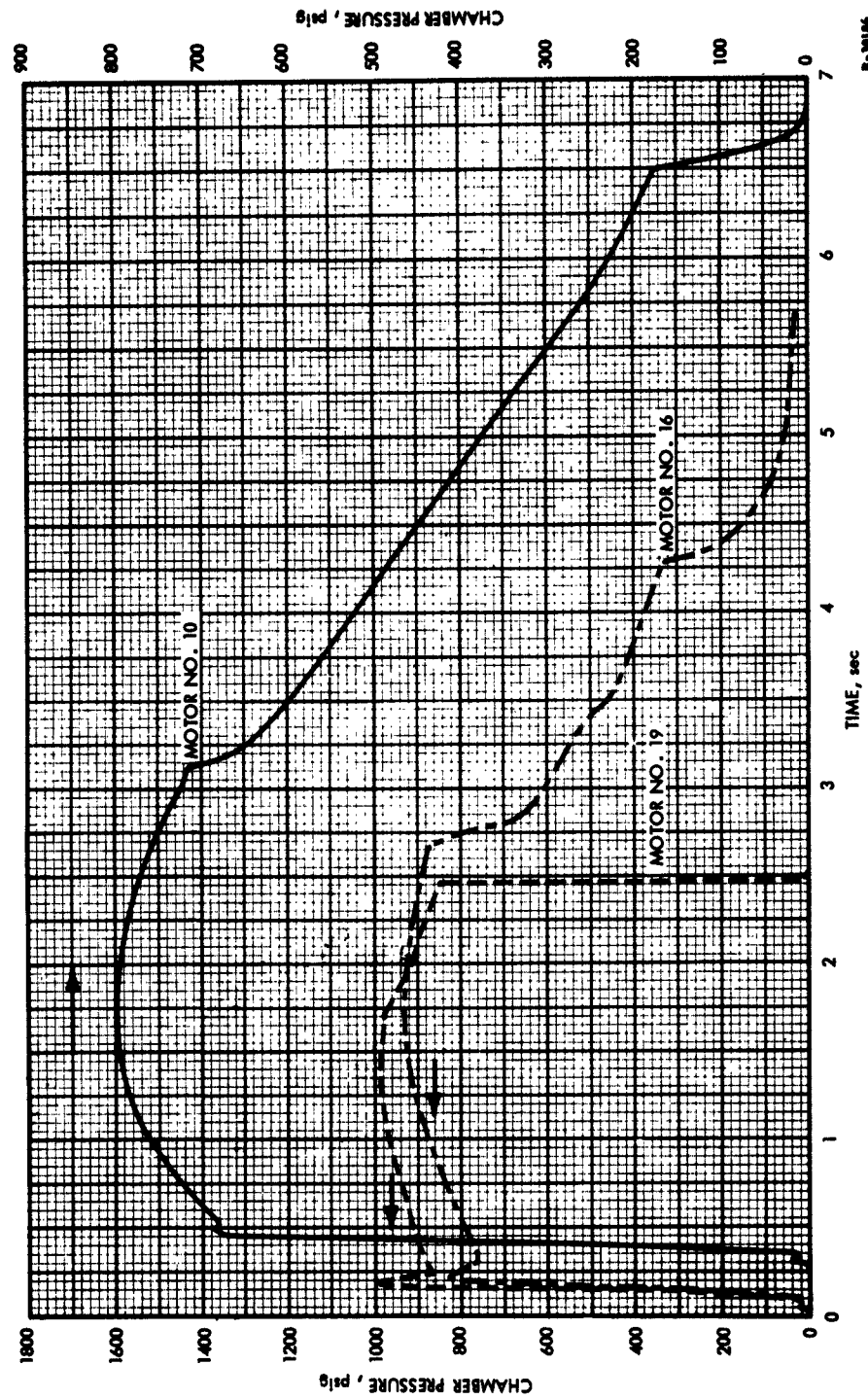
Figure 16. Pressure versus Time Traces for Subscale Motors No. 10, 16, and 19
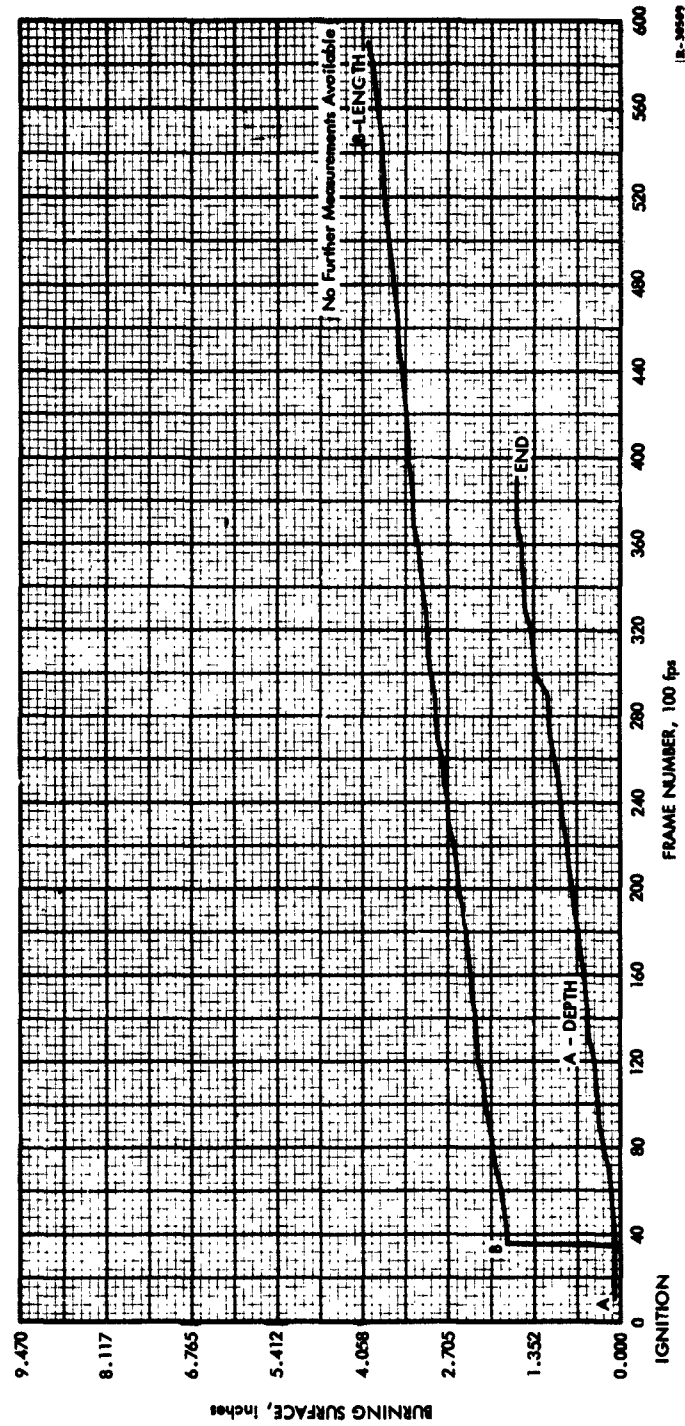
Figure 16a. Length of Burning Unbond and Depth of Unbond Thickness as a Function of Burning Time (Motor No. 10)
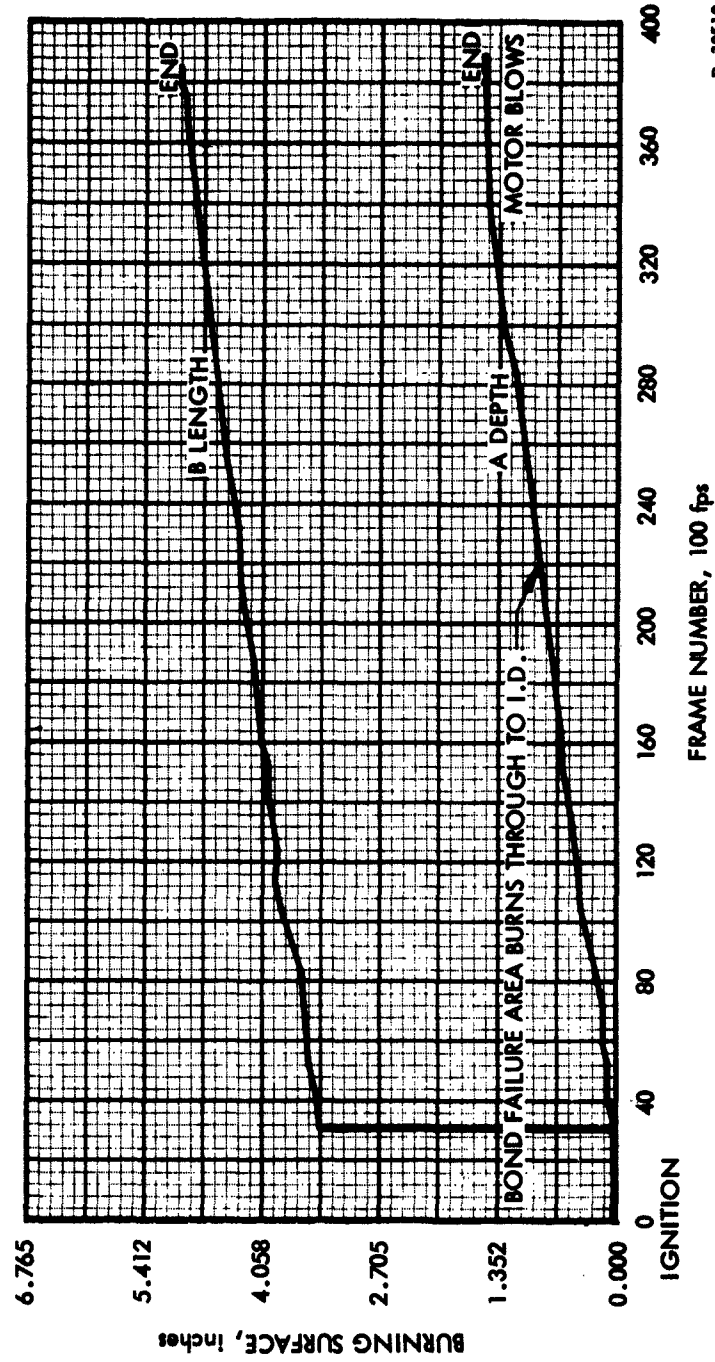
Figure 16b. Length of Burning Unbond and Depth of Unbond Thickness as a Function of Burning Time (Motor No. 13)
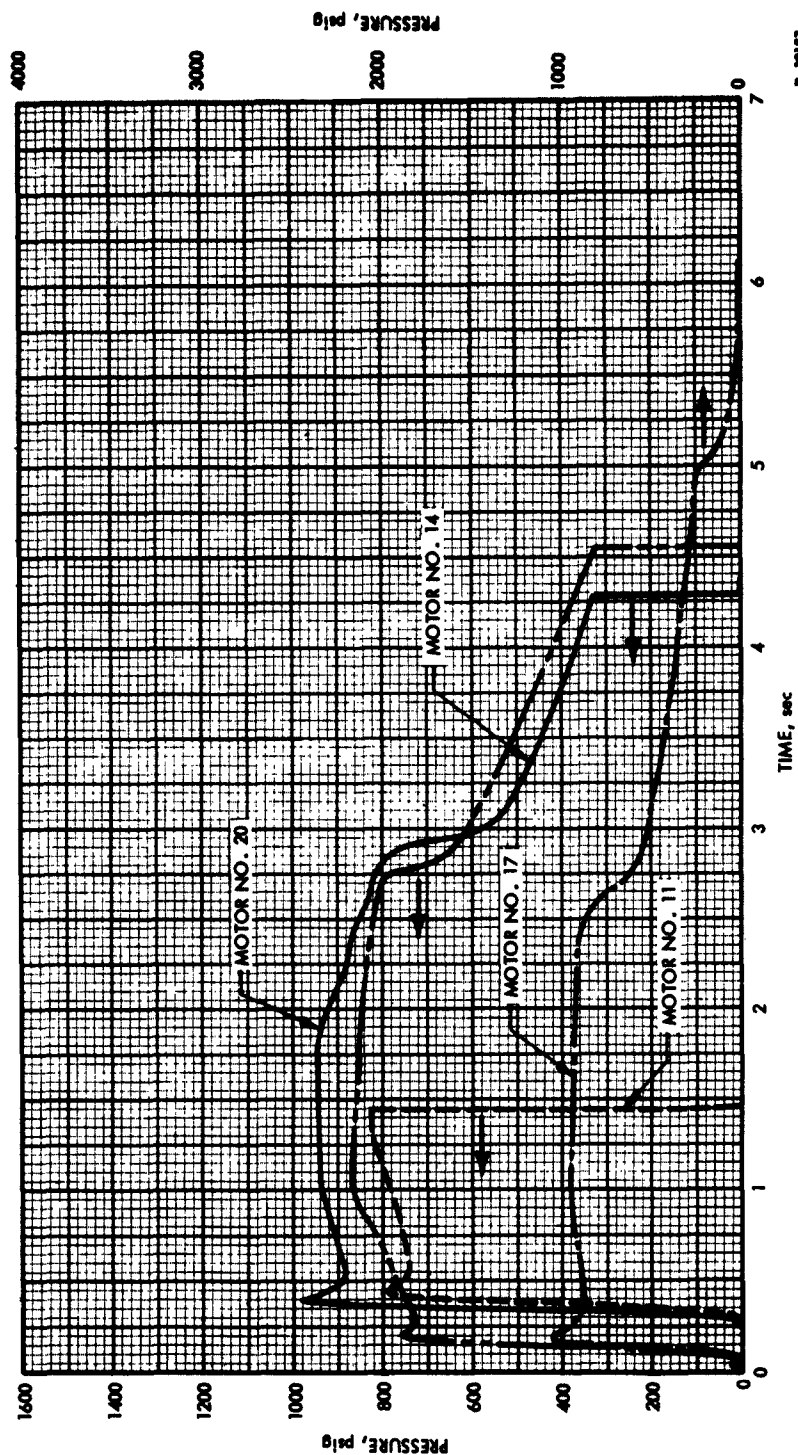
R-30510

Figure 17. Pressure versus Time Trace for Subscale Motors No. 11, 14, 17, and 20
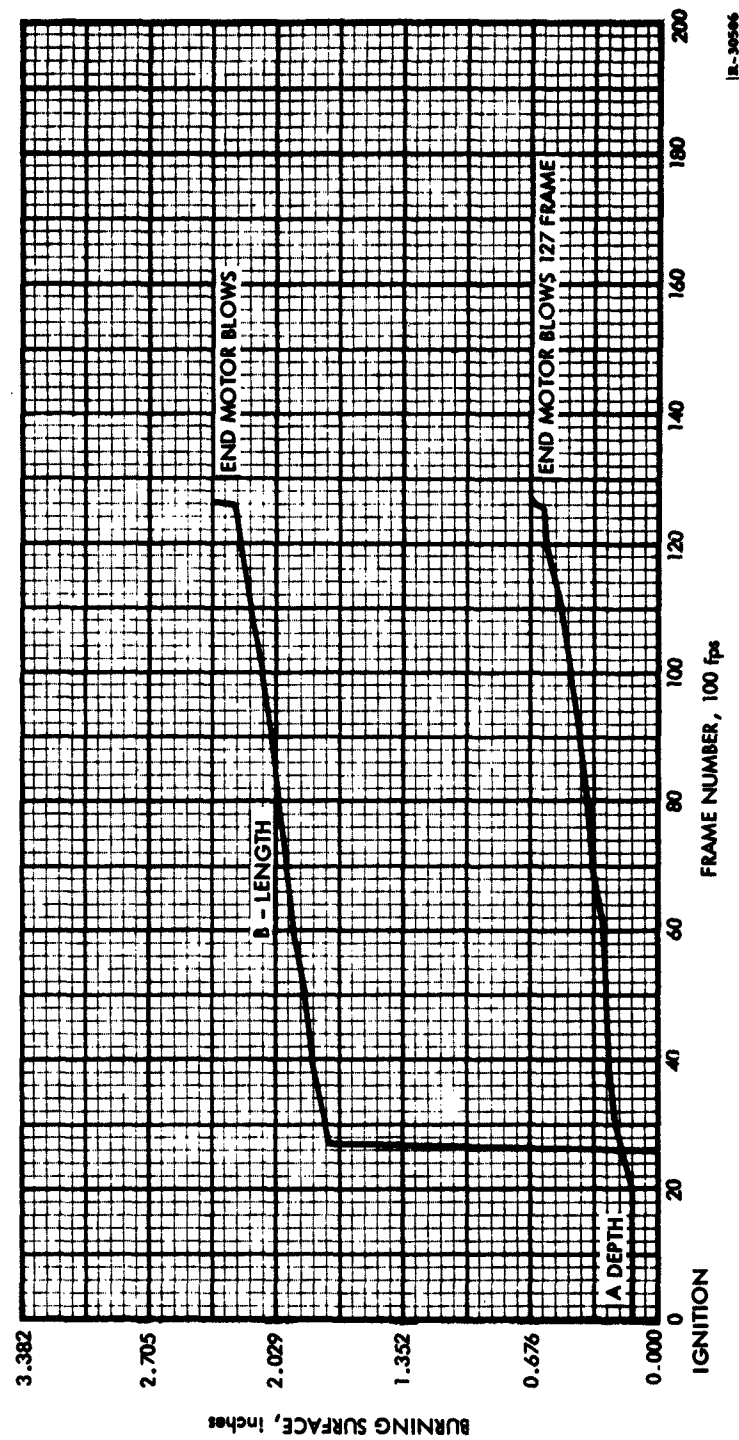
Figure 17a. Length of Burning Unbond and Depth of Unbond Thickness as a Function of Burning Time (Motor No. 11)
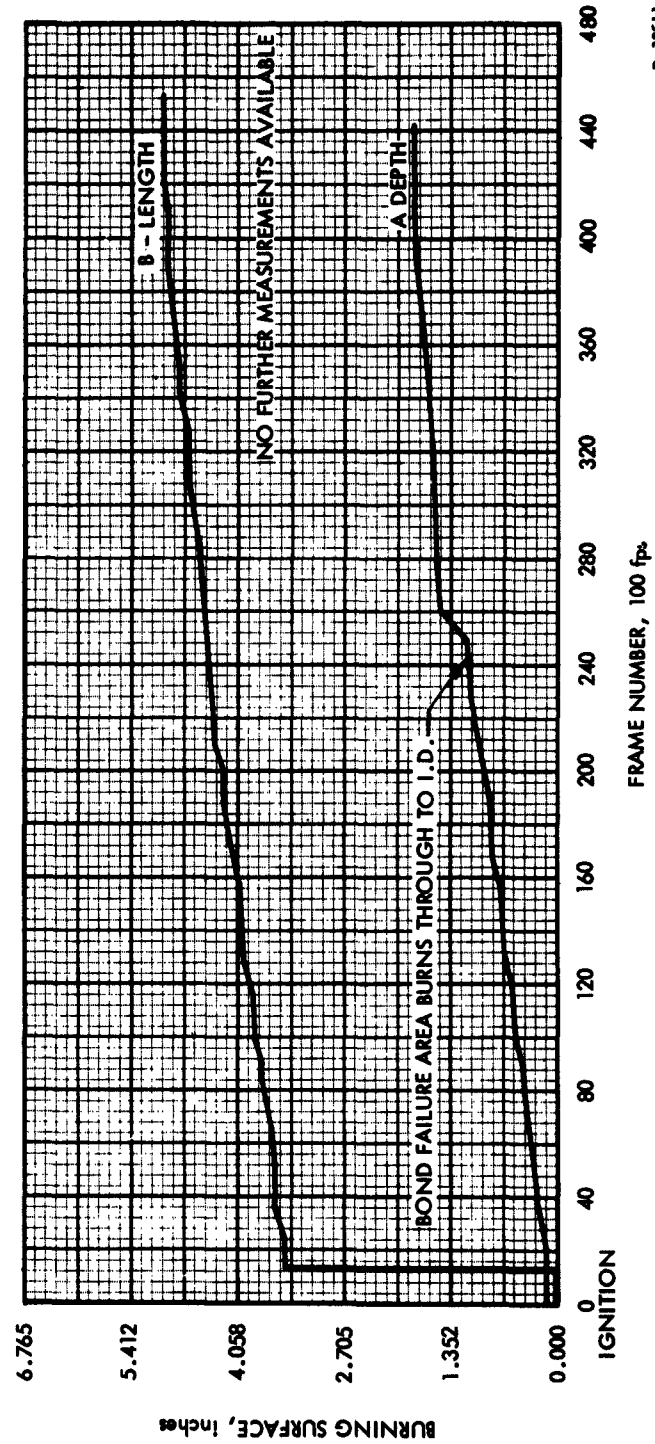
Figure 17b. Length of Burning Unbond and Depth of Unbond Thickness as a Function of Burning Time (Motor No. 14)
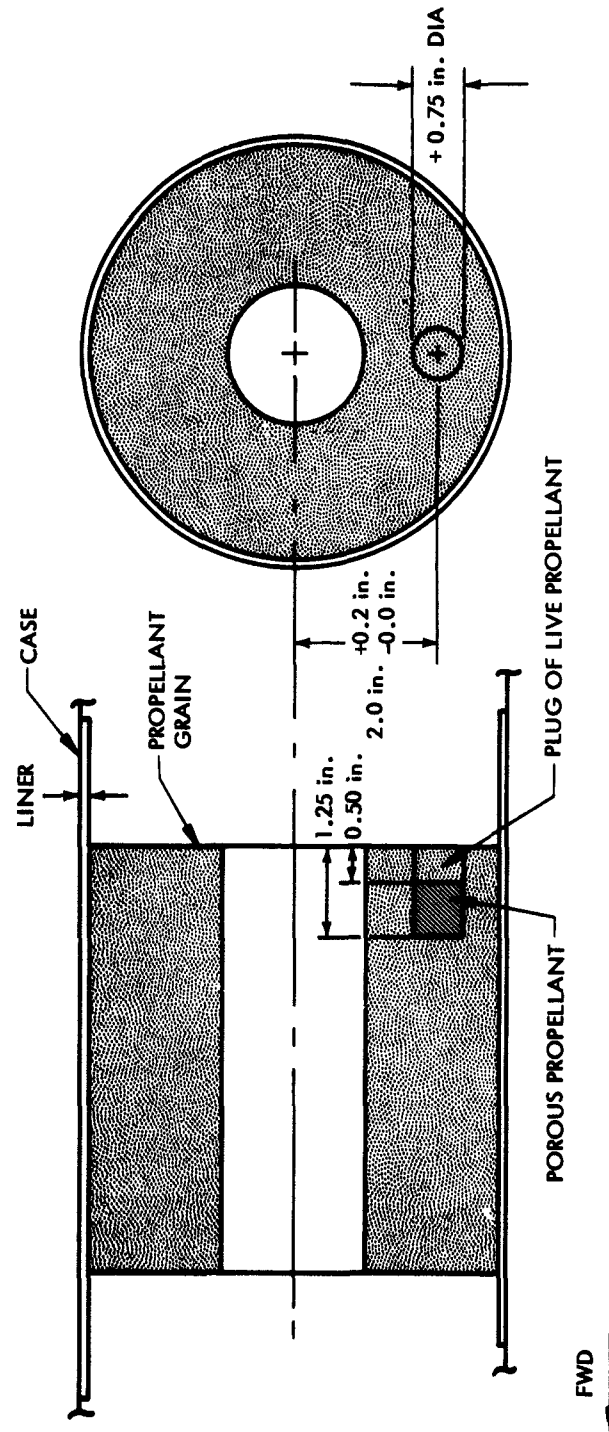
NOTE: 1. Porous Propellant to be Made of Propellant Particles with Maximum Dimension of 0.060 in.

2. Cement Plug in Place with Liner

3. Catastrophic Overpressure Expected 1.5 sec After Ignition

Figure 18. Propellant Grain Defects for Motors No. 21 and 22

R-30188
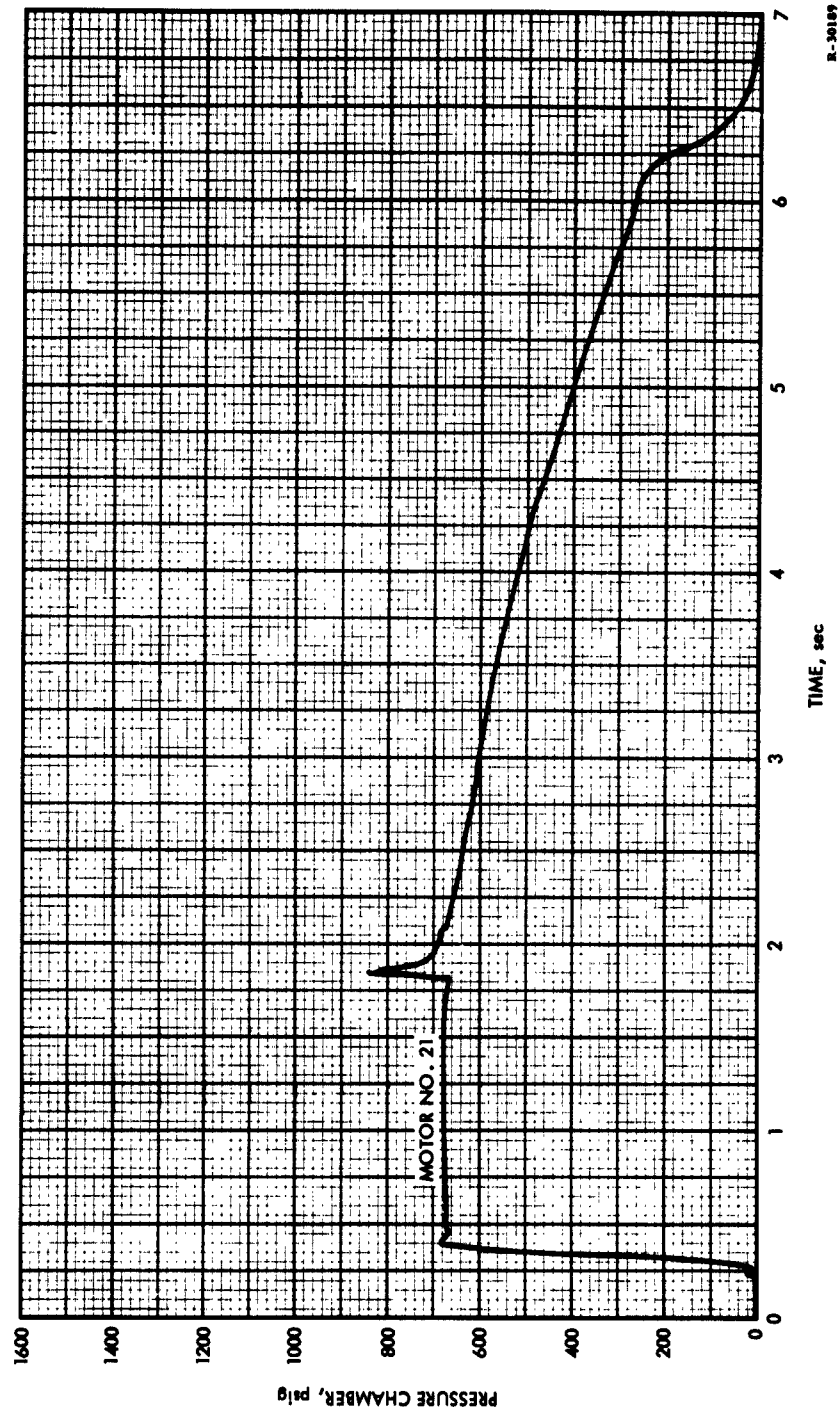
Figure 19. Pressure versus Time Trace for Subscale Motor No. 21

Motor No. 21 burned as predicted, showing a spike in the pressure trace and indicating where the burning front first reached the porous propellant. Motor No. 22, however, exploded on ignition. The malfunction was apparently due to the initial propagation of the flame front into the porous propellant. This could happen if the plug sheared loose on initial pressurization, as occurred during the firing of the motor containing the void defect (Motor No. 6). Several pieces of unburned propellant were recovered showing fracture lines which were indicative of a rapid pressure rise in the cavity containing the propellant particles. The mere presence of unconsumed propellant is proof that detonation did not occur.

2.2.2.4 Crack Defects (Motor No. 23, 24, and 25)
Motors No. 23, 24, and 25 were prepared with cracks in the tubular section of the grain with thicknesses between 0.005 and 0.010 inch. (See Figure 20). The cracks were expected to produce an initial pressure somewhat higher than that registered in uncut grain.

The pressure trace for Motor No. 23 (Figure 21) indicates that ignition was normal and the crack began burning about 0.25 seconds after full pressure was reached. At approximately 3.1 seconds, the end of the crack and the end surface of the grain burned together producing a definite stepped decrease in the pressure. A slight increased steepness of the trace indicates that the bottom of the crack began to burn through to the case at about four seconds.

Motor No. 24 (Figure 21) produced a pressure trace which indicates the crack ignited erratically causing minor peaks in the pressure. In contrast to Motor No. 23 no distinct burnout of the crack was observed but the maximum pressure indicates that the crack did burn.

In addition to the artificially produced crack in Motor No. 25 (Figure 21) a circumferential crack developed around the periphery

R-30190

CASE

LINER

PROPELLANT
GRAIN

+.000
0.010 in. -.005

0.75 in.

1.0 in.

1.00 in.

CUT IN PROPELLANT GRAIN

FWD
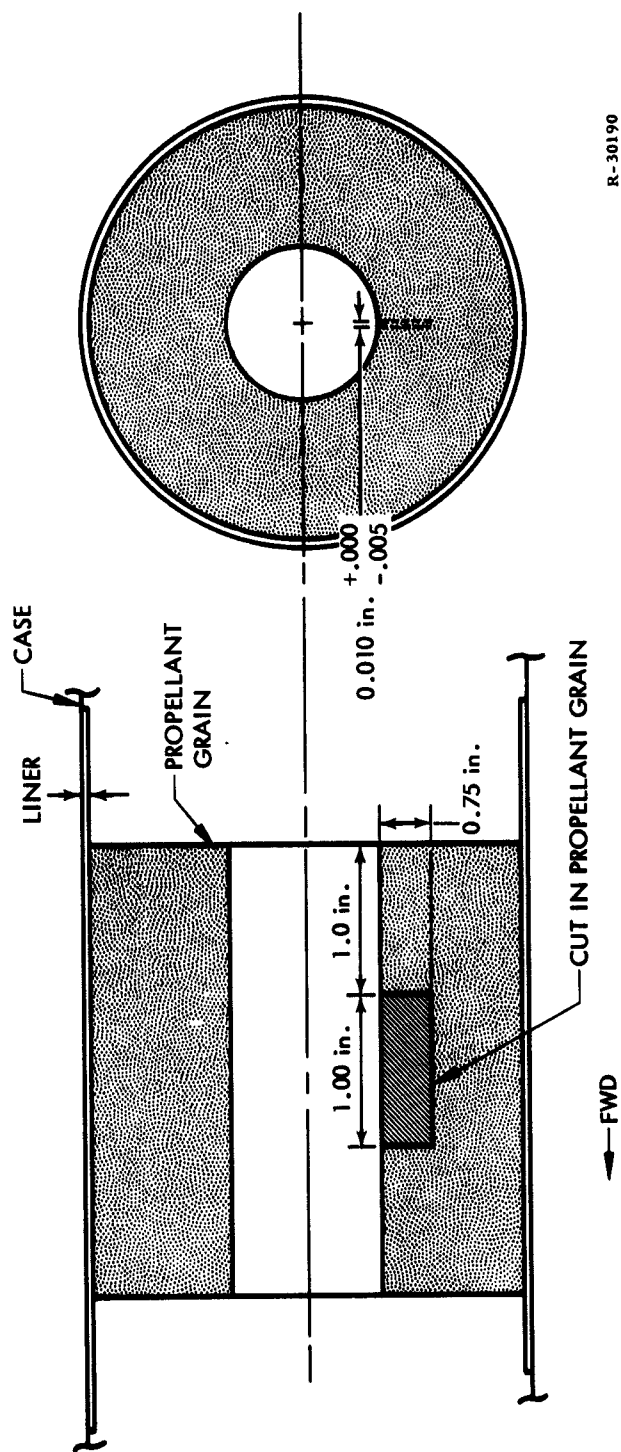
Figure 20. Propellant Grain Defects for Motors No. 23, 24, and 25
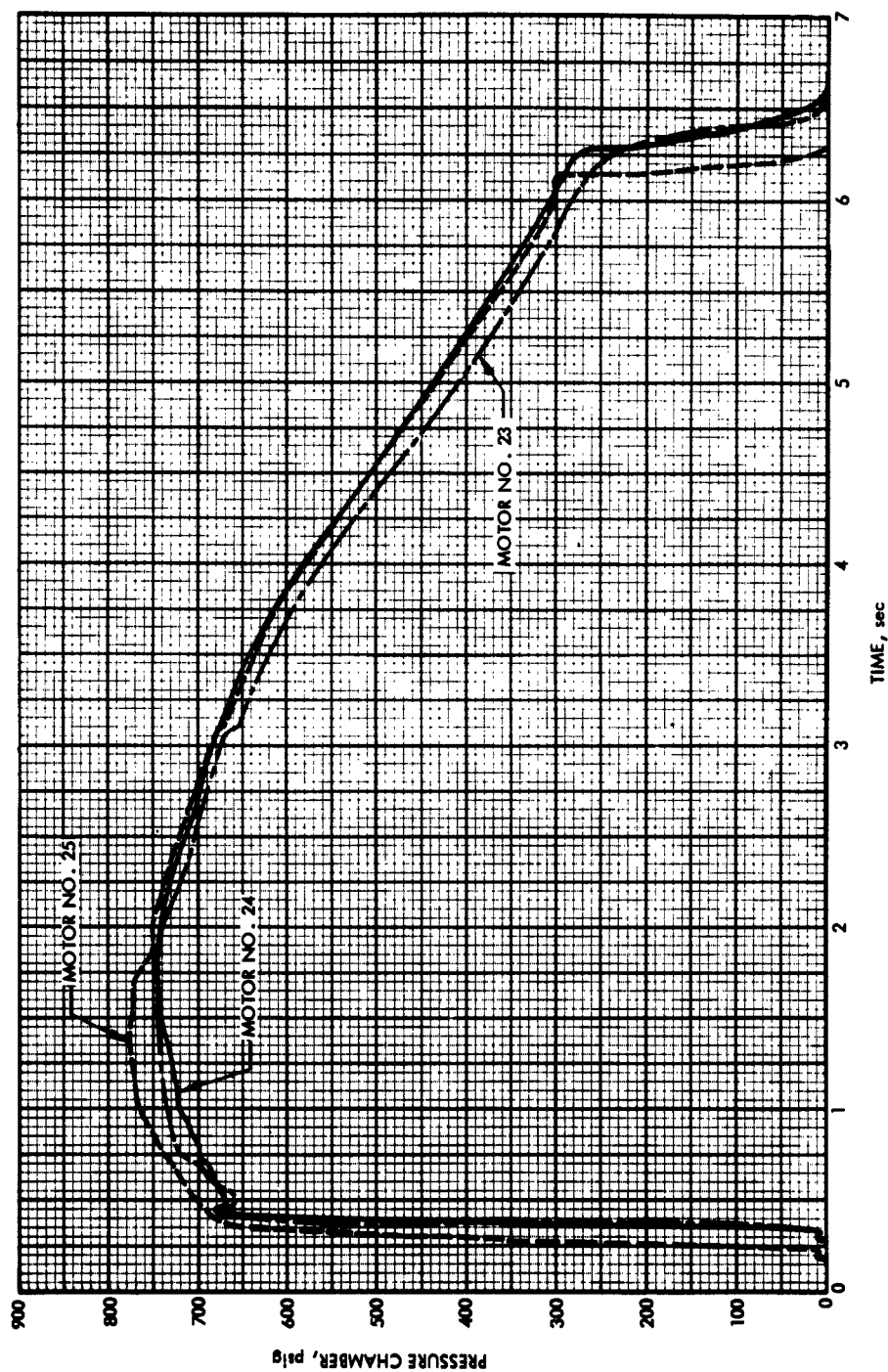
Figure 21. Pressure versus Time Trace for Subscale Motors No. 23, 24 and 25

of the grain extending about 200° around the grain. This crack was about 0.6 inch in from the forward end of the grain and connected to the surface by a small void. Part of this area along with the artificial crack began burning on ignition as indicated by the pressure reached. The circumferential crack and the end surface burned together at about 1.75 seconds and the artificial crack and end surface burned together at about three seconds each, thus producing a definite decreasing pressure step. The remainder of the trace was slightly above normal which was caused by increased burning area within the crack.

2.3 EVALUATION ON NDT TECHNIQUES

A number of NDT techniques were surveyed for possible use with large solid propellant motors. These techniques may be conveniently divided into operational methods and experimental methods.

2.3.1 Operational Techniques

Visual, ultrasonic, radiographic, and profilometry are the principal methods in use at this time for routine inspection of solid-propellant rocket motors. These are discussed separately below. A brief summary of the pertinent factors involved is given in Table VII.

2.3.1.1 Visual

For assurance of general integrity and an over-all surface condition free of defects (defects which in many instances are indicative of an internal, obscured condition) no substitute has yet been found for visual inspection. Visual inspection of propellant grain surfaces readily reveals surface voids, cracks, and porosity. In some instances the presence of gross internal defects can be deduced by bulging and waviness in the grain surface (these phenomena formed the basis of inspection by profilimetry, which will be discussed in later sections). In addition, unbonds which are present at the edge of the grain are also detectable.

TABLE VII

SUMMARY OF ROUTINE NDT TECHNIQUES

	Visual	METHOD Ultrasonic	Radiographic
Type of defect detectable	Cracks, unbonds, voids and porosity (all occurring at grain surface)	Case-liner or case-insulation unbonds	Cracks, unbonds, voids, porosity, variations in propellant density
Sensitivity	Defects greater than 0.030 inch in any direction; cracks over 0.005 inch width	Unbonds larger than 0.25-inch diameter	1/2% of propellant web thickness
Approximate capital investment required (production-line inspection)	Negligible	$8,000	$1,000,000
Approximate direct labor	4 manhours	8 manhours	36 manhours radiography 12 manhours photographic processing 180 manhours film interpretation
Approximate time required	4 hours	8 hours	Radial and tangential Radiography: 152 hrs (NAD Concord) (120-inch segment) 12 hrs (minimum estimated time in production facility) Interpretation: 180 hrs
Level of personnel training required	Moderate	Moderate	High
Advantages	Inexpensive and quick	Inexpensive -- relatively quick	Excellent definition of internal grain defects and permanent record
Disadvantages	Applicable for surface defects only	Applicable for first-layer unbonds only	1. Large capital investment in equipment and facilities 2. Considerable length of time required to interpret radiographs

From consideration of grain stresses caused by curing and cooling, grain cracks should begin on the surface of the core and propagate in a radial direction. This theory has been confirmed by experience thus leading to the conclusion that visual inspection of the grain core can be relied upon to detect grain cracks. The use of specialized instruments such as boroscopes and direct viewing television systems normally is not required for the inspection of large segmented solid propellant boosters. The excellent access to all portions of the grain interior renders such instruments desirable only if a permanent record is required.

2.3.1.2 Ultrasonic

Ultrasonic bond integrity measuring devices have been in use for several years and have reached a high degree of effectiveness in the detection of case-liner unbonds as demonstrated in the subscale NDT studies of this contract. Case-liner unbonds 1/4-inch in width were repeatedly discovered with this instrument. Consequently, the continued use of this technique to detect these defects reliably is indicated.

Efforts to extend the use of ultrasonic inspection techniques to the detection of propellant-liner unbonds have met with little success. Several organizations are active in this field, among them the Naval Ammunition Depot, Concord, California. A demonstration of this technique was investigated, but the experimenters are not confident of success at the present time.

2.3.1.3 Radiographic

Radiographic techniques are the only methods available at this time for inspecting the interior of the propellant grain for defects. The commonly used technique for large solid-propellant motors employs a linear accelerator and conventional X-ray film. The sensitivity which is normally obtainable, 0.5 percent, is the outstanding feature of this method. (Sensitivity in this context denotes detection of variations in absorption equivalent to 0.5 percent of the thickness of the propellant.) The radiographs provide a permanent record of the inspection process.

The chief disadvantages attending the use of this technique are the high initial cost of the high-energy machine and its shielded building, personnel protection, the time required to completely radiograph large motors, the photographic processing required, and the time-consuming interpretation of the radiographs.

Radiographs are commonly taken in two orientations, radial and tangential (Figure 22).

Radial

The radial orientation allows the detection of voids, cracks parallel to the path of the high energy beam, and areas of propellant differing significantly in density (such as porosity, oxidizer-and/or fuel-rich areas). One-half percent sensitivity is routine, and sensitivities of 0.3 percent have been achieved. The motor is normally rotated to obtain 100 percent coverage of the entire grain. Triangulation techniques allow the precise location of any defect discovered.

Tangential

Tangential radiography is used for inspection of the bond structure. Any bond separation, when oriented parallel to the high energy beam, results in a readily detectable darker area on the radiograph. The minimum separation detectable is a function of the thickness and absorbtivity case, liner, propellant, radius of the case, and the placement of the detection device.[*] The minimum detectable separation as a function of radiographic sensitivity for a 120-inch diameter segment is given in Table VIII.

If the separation is not aligned parallel to the high-energy rays, the ability to detect it is markedly decreased. The closer the circumferential

---

[*] NAD Concord Presentation at 16th Meeting of Polaris Minuteman NDT Committee 28 March 1961.

VACUUM CASSETTE

CASSETTE CARRIER

BACK SCATTER SHIELD

TANGENTIAL SET-UP

MOTOR SEGMENT

LINAC

MOTOR DOLLY
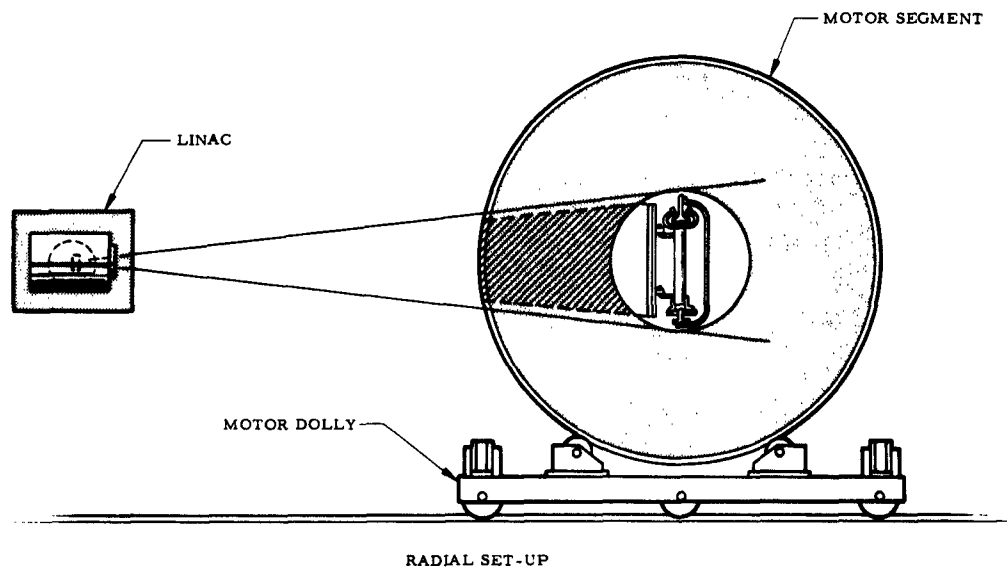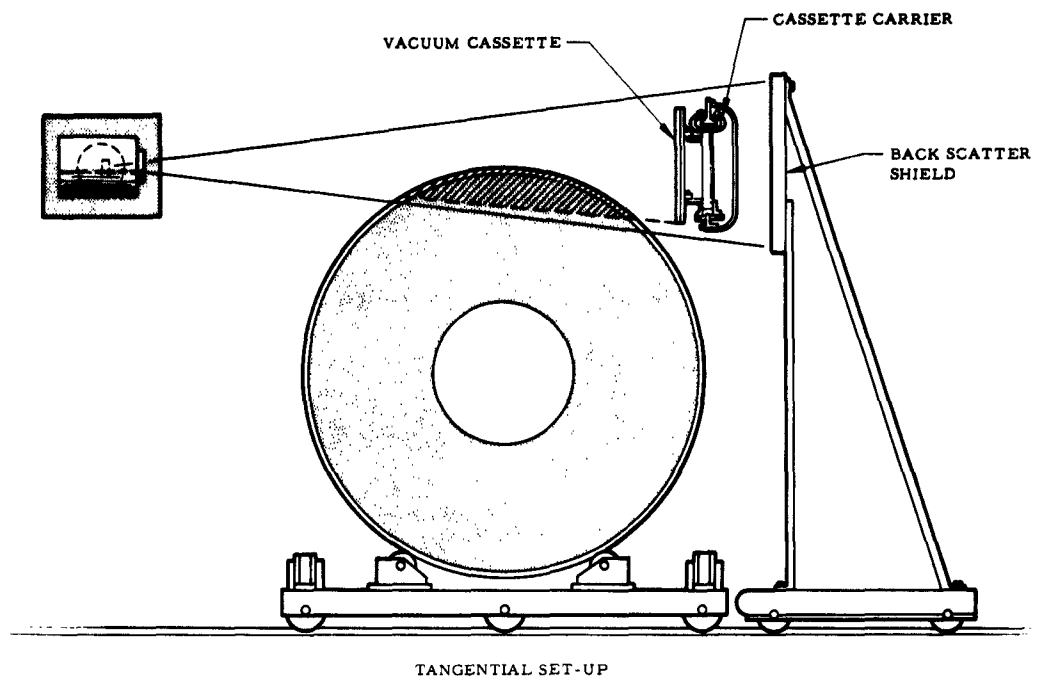
RADIAL SET-UP

R-20851

Figure 22. Tangential and Radial Set Ups for Large Motor Segment

TABLE VIII

SENSITIVITY REQUIRED TO DEMONSTRATE
LINER-PROPELLANT SEPARATIONS

Tangential Radiography - 10-mev LINAC

L-P Separation (in.)	Tangential Position Cylinder, Near Aft End (percent)	Along Motor Central Cylinder (percent)
0.001	0.65	1.25
0.002	0.94	1.74
0.003	1.16	2.15
0.004	1.36	2.50
0.005	1.53	2.79
0.010	2.18	3.95
0.015	2.69	4.84
0.020	3.13	5.59
0.025	3.53	6.25
0.030	3.88	6.85
0.040	4.53	7.91
0.050	5.10	8.85
0.060	5.63	9.69
0.080	6.59	11.19
0.100	7.44	12.51

spacing of the radiographs, the greater the probability of detecting a given unbond. These relationships for a 120-inch diameter motor are shown in Figure 23. The reconciliation of these conflicting factors calls for a high degree of engineering judgment. A choice of 20 exposures equally spaced about the circumference of a 120-inch diameter motor yields a 35 percent probability of not detecting a 12-inch long liner-propellant separation. This figure is comparable to those obtained in Polaris and Minuteman programs. The fact that this probability must be accepted is a further disadvantage of the radiographic technique.

High Energy Particle Sources

The primary sources of high energy particles in use are isotope sources, linear accelerators, and betatrons. Parameters of interest in evaluating the capabilities of these sources are emission energy level, emission intensity, minimum focal spot size, and the half-intensity emission cone included angle. The level of emission energy, usually specified in million electron volts (mev) is a measure of the penetrating power of the high energy particles. The emission intensity, usually denoted by rads/minute at 1 meter, denotes the output of the machine. The relationship of the first two of these parameters to radiograph exposure time at the center of the emission cone of several machines is shown in Figure 24. The size of the focal spot limits the sharpness of the radiograph. A small focal spot leads to a sharp radiograph. A focal spot of 1-2 mm has proven satisfacotry in current practice. The half-intensity cone indicates the useful coverage at a given focus-film distance. Approximate figures on the cost of these systems are given in Table IX.

Isotope Sources

Five years ago, when conventional industrial X-ray machines had reached a maximum photo energy level of about two mev with the use of electron beams of that level bombarding a target, the principal competition for the inspection of heavy metal castings and thick propellant
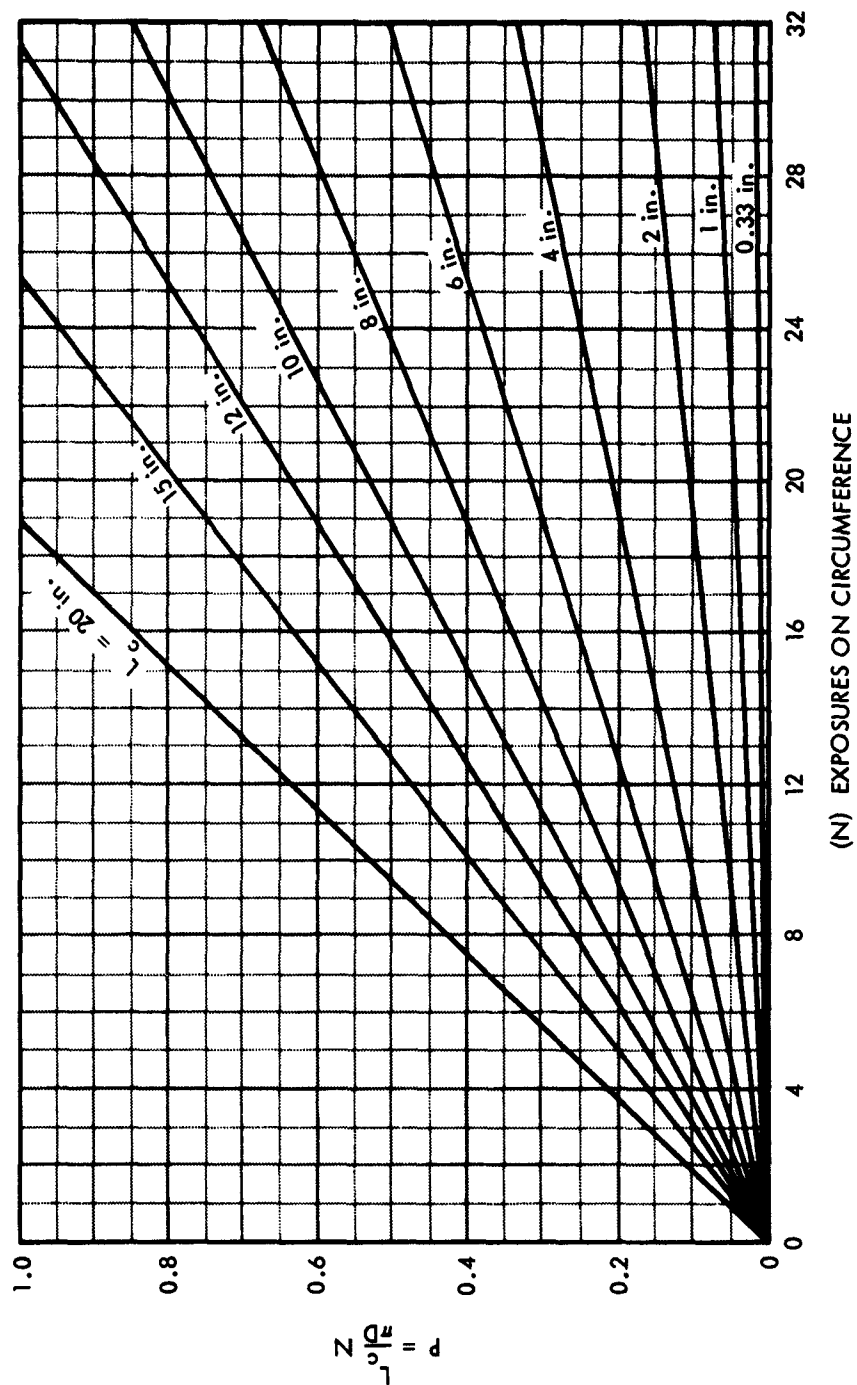
R-30192

L_c = Circumferential Length of Separation

Figure 23. Probability of Demonstrating Liner/Propellant
Separations in Tangential Radiography
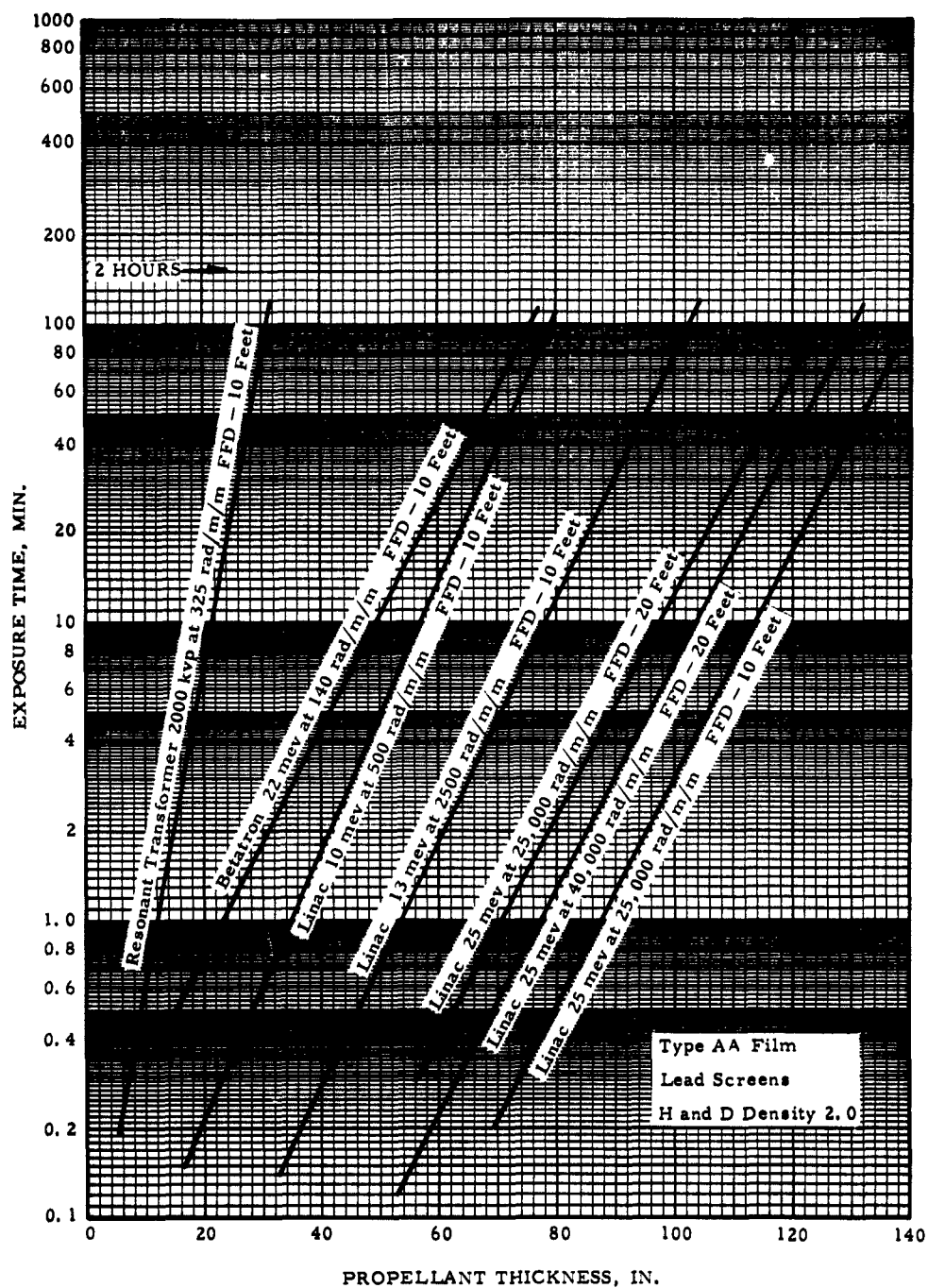
Figure 24. Typical Exposure Curves for Propellant

R-20456

TABLE IX

EQUIPMENT COST SUMMARY

Equipment Type	Equipment Base Cost	Total Cont. Operation at 40 Hour/Week	Equipment Down for Maintenance	Replacement Cost of Parts	Replacement Cost Per Year
Cobalt 60 Source 1.35 Roentgen Curie/Hours	Approx. $10,000 Exclusive of Scanning and/or Handling Equipment	5880 Hours 156 Weeks	12% of Total/Hour 735 Hours 18.3 Weeks	$7,500.-- Cobalt 60 Source	$2,500.
Betatron 25 mev 150 Roentgen P/min. at 1 meter	Information not available on a non specific basis	300 Hours 7.5 Weeks	10% of Total/Hour 30 Hours 7 Weeks	$4,000.-- Doughnut Vacuum-Tube	$26,000.
Linac 1 - 17 mev 8-3000 rads/min. at 1 meter	$185,000. Eqpt. 30,000. Hnd. Eqpt. $215,000. Total Approximate Base Price	1000 Hours 25 Weeks	5% of Total/Hour 50 Hours 1.2 Weeks	$4,000.--for Magnatron Tube $13,000 - for Klystron Tube	$32,000.
25 mev up to 40,000 rads/min. at 1 meter	Approximate Base Price $385,000	Not Available	Not Available	Not Available	Not Available

webs was offered by the Cobalt 60 source. Sources of up to 1000 curies strength were squeezed into a 1/8-inch diameter and although this meant a focal spot larger than that of the X-ray machine, the exactly dichromatic gamma emission at 1.17 and 1.33 mev was felt to be an advantage in comparison with the continuous spectrum of the X-ray machines, the low cost of the gamma equipment, and its simplicity in use were also considered attractive.

Polaris motor inspection has been carried out with a 1000 curie Colbalt 60 source with satisfactory results.

High Energy Machines

The superiority of isotope sources has been challenged by the development of higher energy machines. Commercially available equipment has been developed from some of the electron-accelerating nuclear research machines that are described briefly in the following paragraphs.

1. Van De Graaf Generator

In this machine, a belt operates at high speed around two flat pulleys. A surface charge builds up and electrons are collected from the belt at a point. Up to 10 mev has been achieved in research machines and industrial machines were offered to two mev with a focal spot of 1 mm^2. These had accurate control of photon energy level, but intensity of output was low, about 100 rads/min at one meter, and higher mev was desirable for thick propellant because of the absorption characteristics of the material as a function of mev. No applications of this device to routine solid-propellant rocket motor inspection have been disclosed.

2. Betatron

To obtain higher emission energies, higher level electron beams were required. These had been obtained in nuclear research by the linear accelerator, the betatron, and the electron synchrotron. The betatron utilizes the improved cyclotron system of accelerating pulses of electrons in a circular path on the rise quarter cycle of a surrounding

magnetic field. Electrons at 0.07 mev are already travelling at 1/2 the velocity of light. At 20 mev they are approaching 0.9999 light speed, whereby mass is increasing (relativistically) rather than velocity, hence the problem of keeping the particle in phase with the accelerator. The pulses are quite short so that the net intensity is lower than X-ray machines, although the photon energy level is higher. General Electric offers industrial machines at 10 and 15 mev with focal sizes of 1 x 0.3 mm. Other machines are available from Siemens, a 15 mev at 1/2 x 1/2 mm focal spot; Allis Chalmers, a 22 mev at 0.2 mm diameter focal spot; and Brown Boveri, a 31 mev at 0.1 x 0.3 mm spot size. The Allis Chalmers betatron is used in the United States for large solid-propellant motor inspection and is rated at 140 rads/min at 1 meter.

3. Linear Accelerator

To cope with the problem of relativistic mass increase, the linear accelerator employs a straight path and a high intensity radio frequency in a travelling wave guide energized by magnetrons or klystrons. The tube length required is about 10 feet at 10 mev. Mullards offers a 5 mev machine with a focus of 2 x 2 mm. High Voltage Engineering and Varian Associates offer machines at 8 to 25 mev with intensities of 140 to 40,000 rads/min and focus size of 1 mm^2 in the smaller machines and up to 5 mm^2 in the large. In these machines transmission target emission is used instead of reflection and the target is cooled and rotated to dissipate heat.

Linear accelerators are coming into increasing usage for inspection of large solid-propellant rocket motors.

Radiographic Read-Out Techniques

The techniques to capture and evaluate the information contained
in the high energy rays comprise two basic approaches: static
systems and scanning systems.

The leading technique in the static system field is the use of
X-ray film. The X-ray film is essentially a chemical amplifier
with gains of up to 10^9. A large body of experience has been
accumulated with X-ray film, and its application to radiography
is a routine matter. It is relatively cheap, and provides both
information and a permanent record of the inspection at the
same time.

The use of film, however, has several disadvantages in large
solid-propellant rocket motor radiography. An extremely large
number of radiographs are required and a great deal of inspection
time is spent in changing film cassettes and adjusting the position
of the motor or film for the reported shots. Since personnel
must be separated from the high energy machine by several feet
of shielding, the operation is rather time-consuming. Personnel
at Naval Ammunition Depot, Concord, estimated that the ratio
of down-time to exposure-time is between five and six. From
this, it may be seen that complete radiographic coverage of a
large rocket motor is a time-consuming operation.

The processing of the photographic film alone also represents a
considerable investment in facilities, manpower, and time.
Automatic processing machines capable of producing developed
film at the rate of six inches per minute are available, however,
and may become mandatory for high motor production rates.

The evaluation of the radiographs is also a tedious task. Complete inspection of a large solid-rocket motor involves a very large number of radiographs, each of which must be carefully evaluated by experienced personnel. Eastman Kodak has expressed interest in automating this procedure, but its present efforts are at a standstill.

Attempts have been made to combat these difficulties by means of either automated digital-readout scanning systems or direct-viewing television systems. Both these attempts to replace the more conventional film techniques have suffered from equipment problems and lack of resolution. The magnitude of these problems may be judged from the fact that insofar as can be determined only the conventional film techniques are being used today for routine inspection work.

One scanning system has been in routine use as a production inspection device. It is a gamma scintillation inspection system, operated by Aerojet-General Corporation, and is used to detect propellant grain defects in the Polaris missile. An array of collimated detectors surrounds the motor chamber during inspection. Gamma photons from a Cobalt 60 source located in the central core of the motor constitute the high energy particles. The increase of photons impinging on the series of collimated detectors is directly and volumetrically correlatable with certain grain defects, voids, and cracks. The inspection process is completely automated up to and including readout. It is understood that a tangential readout of the bond system was contemplated at one time, but has never become operational. The results of the inspection are evaluated strictly on the basis of gamma-ray count. Only those areas deviating more than five percent in count are recorded.

The chief disadvantages in the use of this system are low sensitivity (five percent compared with 0.5 percent of that obtainable with conventional radiographic practices), the difficulty encountered in visualizing the nature of the defect, and the inability to detect bond separations. The scintillometers currently in use scan only a very small spot. In order to reduce the inspection time, 48 such devices are used. The maintenance of these devices in optimum operating condition is a potential source of difficulty.

4. A Radiographic Facility for Production Inspection of Large Motors
The key to effective usage of the large capital investment of a modern high energy radiographic facility lies in the reduction of film handling time.

In facilities having a moderate work-load of production-type inspection, the films are made up manually in cassettes, together with their screens, and are manually placed in the appropriate positions about the motor. All personnel then withdraw to a safe place behind the massive shielding required for high-energy machines, the exposure is taken, and the cassettes manually replaced. This procedure, while adequate for research and pilot-production quantities, is not economically feasible for large production runs.

A study of feasibility of a 13 mev LINAC facility for the one-a-day inspection of 120-inch motor segments has been made. This study revealed that the following features would be required:
1. trolly-rail-mounted cassette frames
2. vacuum cassettes for multiple film holding
3. an automatic film processing facility.

These features increase the utilization of the LINAC so that an inspection rate of one segment every 12 hours may be achieved.

A set of illustrations for this inspection has been prepared. In Figure 22 two elevations of the end view of a segment are shown. In one case, through-web shots with the mobilized cassette in the core are depicted, and in the other tangential or chordal shots are shown. Care must be taken that scattered rays from steel frames and the room walls do not affect the exposure. The cassette and its trolley frame must be designed, using aluminum or reinforced plastics wherever possible, to minimize this effect. In the tangential shots it may be required that a copper shield be positioned behind the work for this purpose, as shown in Figure 22. The segment itself will have been mounted on the track-mounted dolly as shown in Figure 25 (use is made of a set of folding jacks in the process). Motorized rollers turn the motor segment for successive shots and a remote-indicating angle position device enables this being done by the operators in the control room without their having to enter the radiography room.

Adapter rings that mate with the segment case joints serve for both handling the motor segment with a crane and providing a surface for operating on the dolly rollers, once the lifting trunnions have been removed from the rings.

It should be noted that the cassette on a trolley frame is brought to position either in the motor segment core or behind the motor by means of a tram rail. This is the same rail in both cases, and the motor segment dolly is moved towards the LINAC the required distance for the tangential setup, and the rail system is raised to
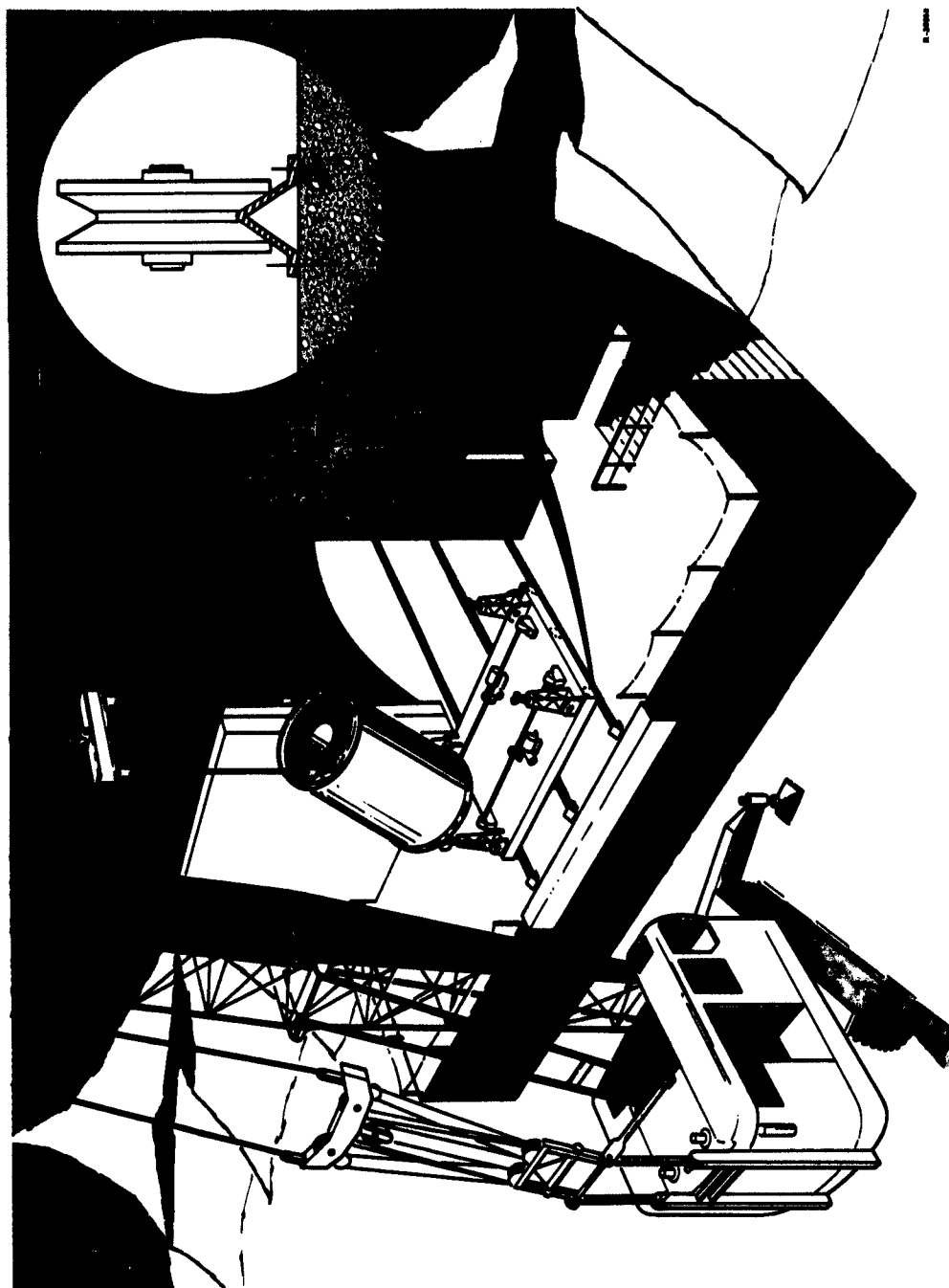
Figure 25.   Control of Segment in Radiography

the required position.   The whole facility is envisioned to handle segments up to 160-inch diameter size.

Figure 26 is a plan of the facility (not to scale).   The span required of the bridge crane of the LINAC is about 36 feet.   At the time this layout was prepared all shielding calculations had not been made.   In addition to what is shown, the shielding separating the main room from the developing and control rooms will probably have to be double wall construction with stabilized earth in between.   Also, in the front of the building, barricades may be required to protect transient personnel from the reverse rays from the LINAC head, and lights and warning horns may be required to exclude personnel from inside the barricades during this time.   Terrain is expected to act as shield in the principal shooting direction.

Figure 27 illustrates the trolley system for shuttling vacuum cassettes between the control room and the core or the back of the motor segment between shots.   It is anticipated, if the track system can be kept straight as shown, that the positioning of the frame for a shot can be done with a motorized cable reel from each end of the track system.   A section of track, with a lower track to maintain the cassette frame vertical, can be withdrawn from the motor core from each end of the motor while the initial set up is being made.   During this time, two types of penetrameters would be applied to the outside of the case: hole type for through-web shots and wires tape wrapped a r o u n d the case for the tangential shots.   It is hoped that the penetrameter images besides determining sensitivity, will serve to confirm the proper positioning of the shot on the motor longitudinally.   For the purpose of
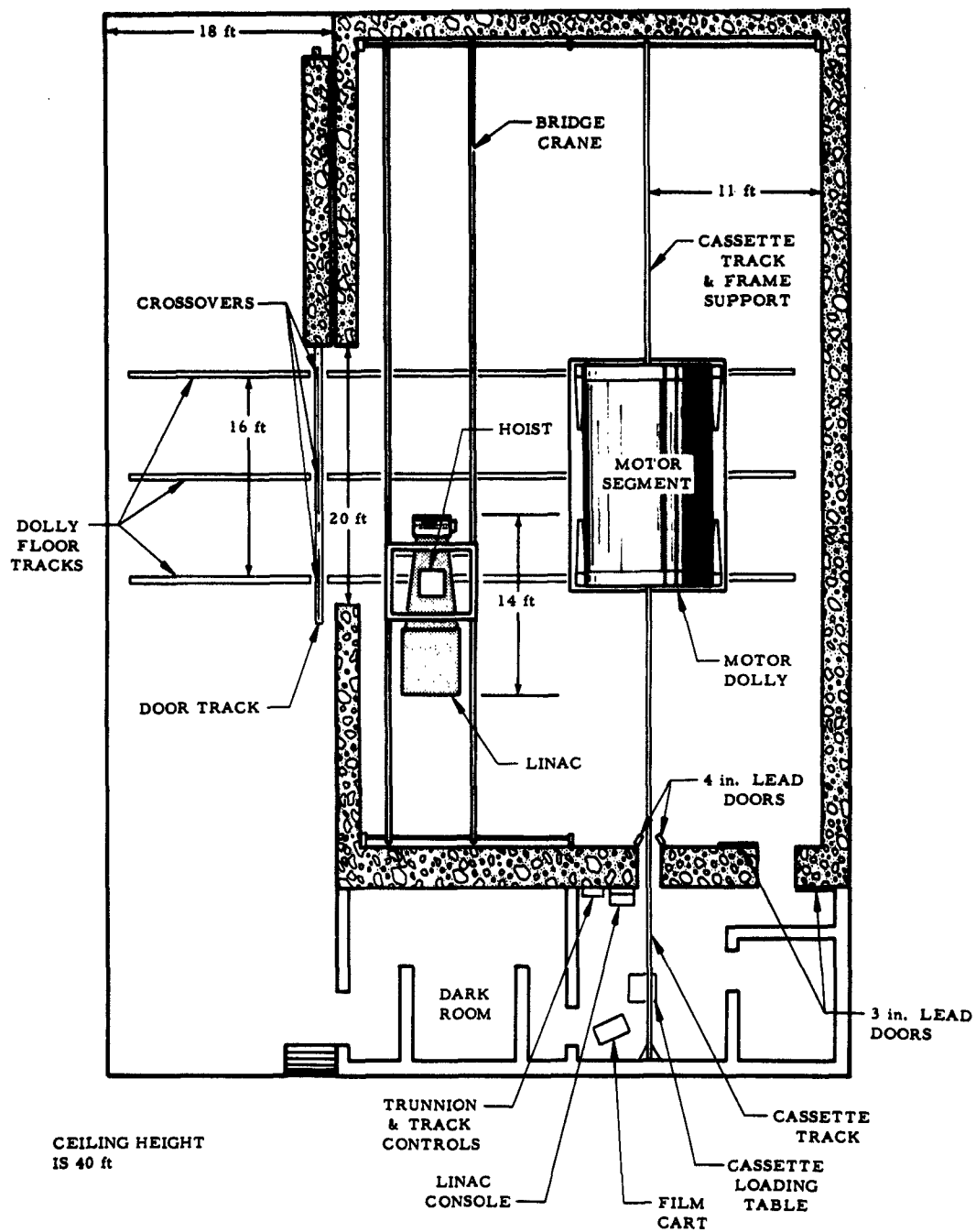
Figure 26. Plan of Facility

1

UTC 2015-FR
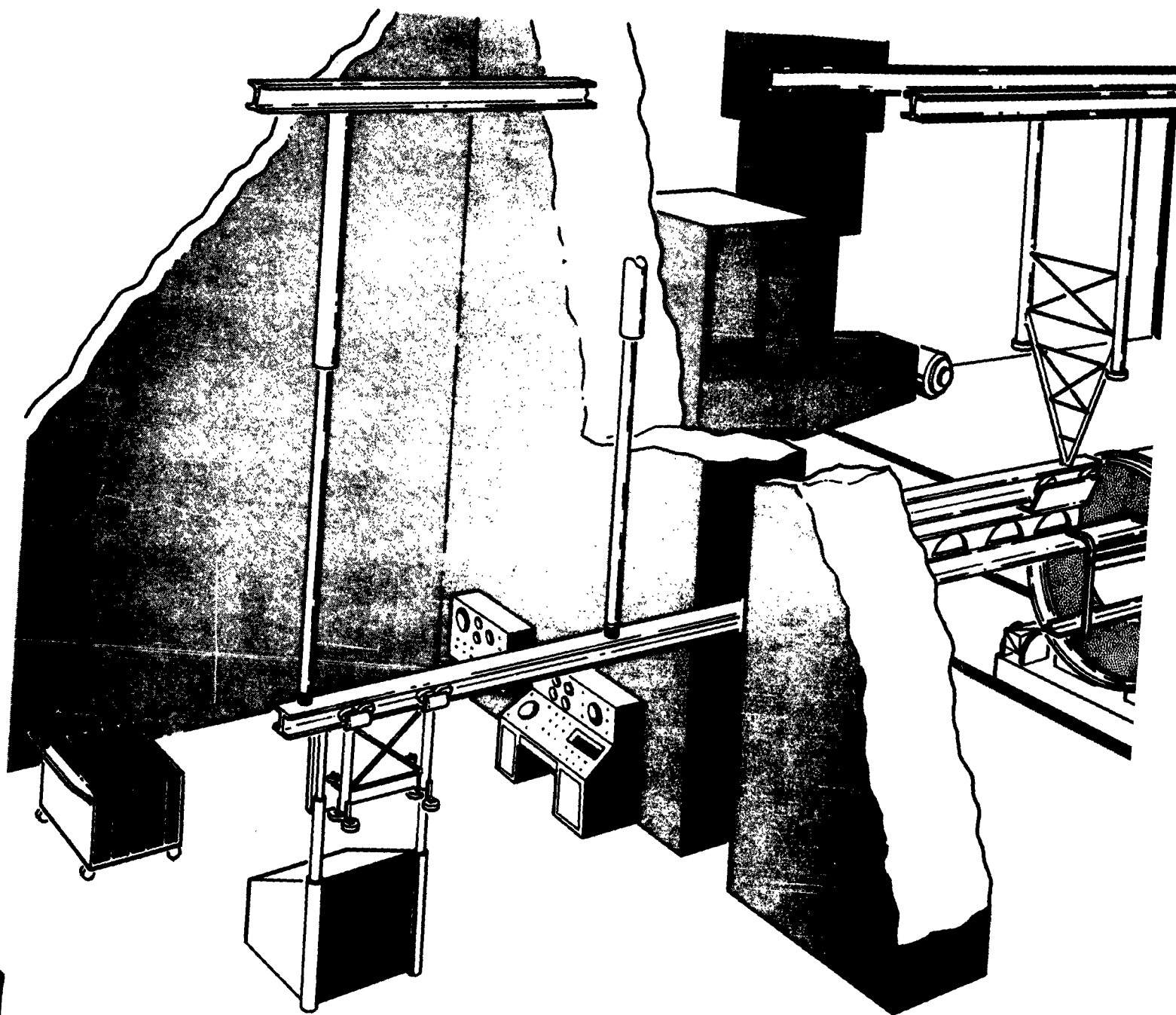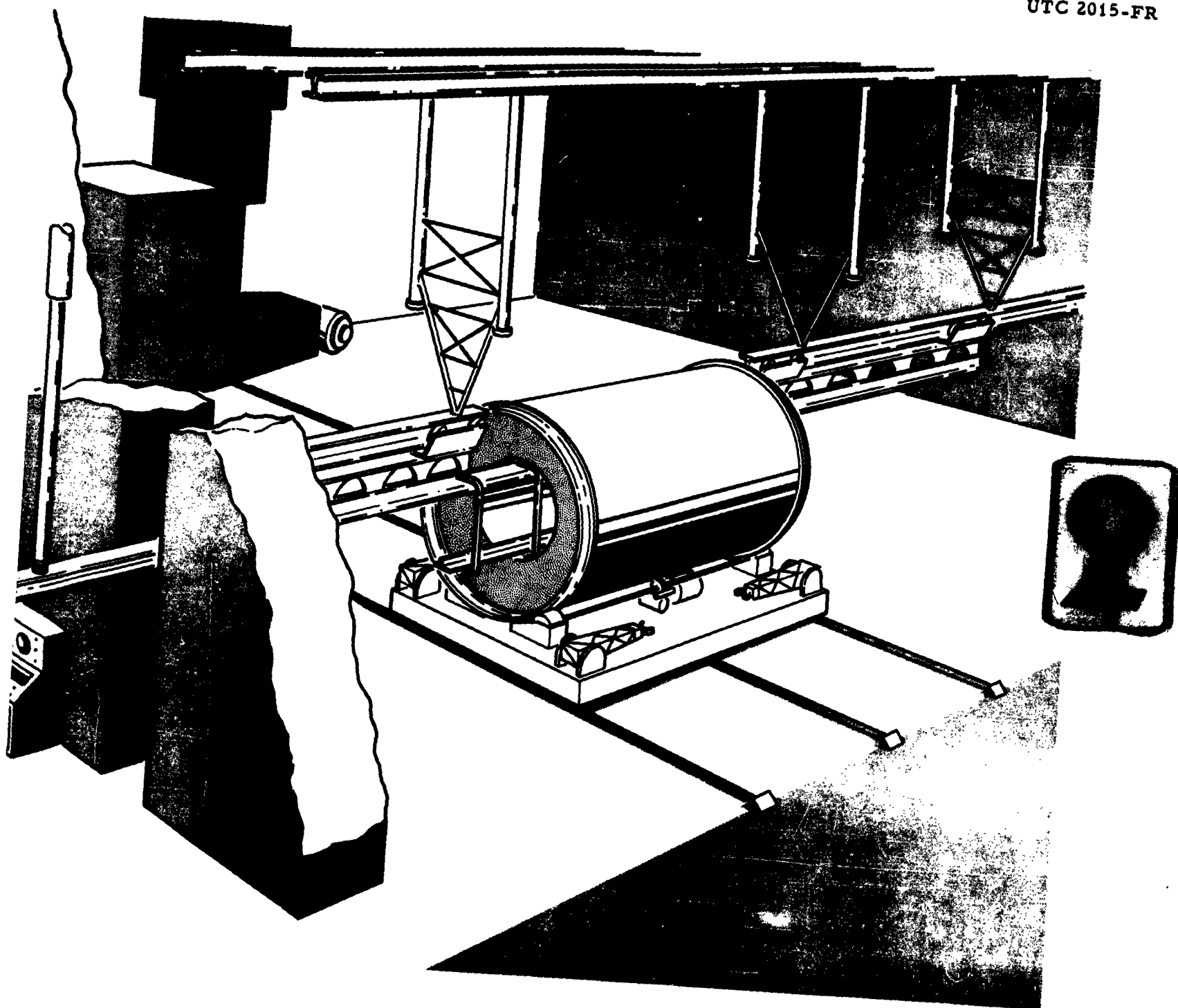
R-20852

Figure 27.   Trolley System for Shuttling
Vacuum Cassettes
Page 76

identifying the films of a motor segment set, pre-exposed numbers are applied to the films in the film loading cart when the cart is loaded in the developing room and before it is brought to the control room. The operators then apply notches to the edge of each film as it is placed in the cassette to indicate position.

A cycle is envisioned as follows:

A. Operator A loads film into a cassette on the sloping-front loading table, notching films as required and positioning films precisely as required with tape. The cassette hinged cover is closed and vacuum is applied. After vacuum and closure are confirmed as evidenced by vacuum gage and inspection, valves are closed and the vacuum line disconnected. If vacuum holds, the cassette is ready for attaching to the cassette trolley frame.

B. When the trolley frame is released by operator B from the previous shot, operator A raises the cassette to the trolley frame on the track by means of the lifting devices on his loading table (cassette weight is about 70 lbs.). Operator A then operates the trolley cables to position the frame at the motor.

C. Operator A remotely rotationally positions the motor segment at the control panel. He then operates all required interlocks, positions the LINAC remotely and makes the exposure.

D. Operator A withdraws the cassette trolley frame to his loading table and removes the cassette with the lifting devices. At this point, he releases the trolley frame to operator B.

Radial exposures utilize four 17 x 17 mm films arranged in a square. Tangential (or chordal exposures) use only two of the standard films horizontally. The conveyor system is arranged so that one cassette may be reloaded in the shielded area while another is being exposed. Remote controls allow the positioning of the motor as desired between exposures. In this manner, the entry of personnel to the working space is not required during the entire inspection time.

Rapid film handling after exposure is facilitated by the use of an automatic film processing machine, such as the Eastman Kodak X-O-MAT. Although the use of this machine is desirable to handle the number of films produced by this method, it also is desirable from the standpoint of uniformity of processing techniques available only with automatic equipment.

A summary of operating times has been prepared to illustrate the over-all effectiveness of this facility. It was assumed that the motor to be inspected is 10 feet long. A 13 mev Linear Accelerator was deemed a good compromise between exposure time and facility capital investment. The pertinent parameters of the operation are summarized in Table X . It will be noted that this facility is expected to produce 544 radiographic films with a cycle time of less than 11 hours, a significant increase in effectiveness over contemporary installations.

2. 3. 2 Nonoperational NDT Techniques

The NDT techniques discussed in this section range from basic concepts to methods under intensive development. No known routine

TABLE X

OPERATING PARAMETERS FOR RADIOGRAPHIC INSPECTION
OF 120-INCH DIAMETER MOTOR SEGMENT

Web Shots

Film-focal distance, in.	180	
Cassette (vacuum), in.	34 x 34	
Screens, in.	head 0.03 rear, 0.06 front	
Film	Ektakrone Co. AA, Four 17 x 17	
Density range	Center to corner 2.5/1	
Exposure time, sec	33	
Number longitudinal positions	4	
Longitudinal overlap, in.	4	
Number rotating positions	16	
Rotating overlap, in.	2.4	
Total shots	64	
No. of operators	1	2
Turnaround time, minutes	6 (includes exposure)	3
Total time, minutes	384	192

Chordal Shots

Same FFD, cassette, use two 14 x 17 films horizontally		
Exposure time, sec	72	
Longitudinal positions	4	
Rotational positions	36	
Total number of shots	144	
No. of operators	1	2
Turnaround time, minutes	6	3
Total time, minutes	864	432

Time Summary

No. of operators	1	2
Radiography time (including film positioning, cassette loading, etc.)	20 hr 48 min	10 hr 24 min
Time to relocate motor and equipment between web and chordal shots	1 hr	30 min
Total time	21 hr 48 min	10 hr 54 min

application of the following techniques has been made to solid propellant rockets.

2.3.2.1 Profilimetry

Based upon studies conducted at UTC and reported in this contract, the profilimetry technique has been classified operational[2]. However, further contact with Pershing representatives have disclosed that this method is not in routine use.

Profilometry consists of the mechanical measurement of propellant grain contours and the comparison of the profiles from the motor being inspected to a standard profile. A displacement of the test profile from the normal one at a standardized temperature indicates cure of compositional deviation. Anomalies in the contour allow the detection of void areas, porosity and propellant liner or liner-case separation.

This technique was employed at UTC on the five subscale motors and is discussed in detail in Section 2.4.5. These tests failed to show definite correlation between the experimentally observed profiles and known propellant defects. It is therefore the contractor's opinion that this technique is not immediately applicable for NDT purposes. This view is also held by another firm active in this area.*

---

* TCC-"Evaluation of the Profilometer as a ND Tool", C. D. Wallace presentation to the 24th Meeting of the Polaris/Pershing/Minuteman, NDT Committee.

2.3.2.2 Infrared Techniques

Infrared measurements of both steady-state and transient temperature
conditions have been investigated by several agencies for use as NDT
measures. As applied specifically to solid-propellant rockets, these
studies have been directed primarily toward the propellant-liner and
liner-case unbonds rather than the propellant itself. The methods
that are known to have been considered include measuring heat flow
patterns through the propellant from both constant and pulsed heat
sources, heat flow patterns developed during cool-down, and heat
flow patterns developed by dissipation from spot areas on the case.

In all cases except the latter one major problem stands out.
Irregularities in the pattern of heat flow through the low-conductivity
propellant and insulation are washed out by the highly conductive
case so that only the strongest evidence of near-surface flaws can be
detected. (This difficulty will disappear in applications where figerglass
motor cases are used.) Therefore, only the latter case will be reported
here in any detail. Some discussion of imaging devices will follow,
however, because it is conceivable that direct image conversion
device might be useful with other systems.

TIRI (Thermal Infrared Inspection) System
Perkin-Elmer Corporation has completed the first phase of an experi-
mental program which began in November 1960 that is directed toward
the development of a practical thermal infrared inspection technique
for application to solid-propellant rockets. The study had as
its primary goal the detection and location of flaws at the bonded
interfaces of the laminated outer structure. Ultimate application of
the system would probably be limited to such bonding flaw detection,
although there is evidence that propellant voids near the liner might

also be detected. The work is supported by ARGMA and the ORMA under Contract No. DA-19-020-ORD-5243.

The results of this first phase investigation significantly substantiate both the key principles and practicability of this technique for detection of bonding flaws between the case and insulation. Recent measurements have been extended to the second interface flaw region with most encouraging results. With experimental assemblies composed of layers about 1/8-inch thick, the system demonstrated the capability to define first interface-void type defects 0.250 square inch or larger in area with 90 percent detection probability. More subtle flaws were synthesized by placing cellophane adhesive tape between casing and liner. No observable void is detected when this tape area is one square inch or larger. Synthesized gross second interface voids of one-inch diameter in the test specimens have been routinely defined. It is predicted that the usefulness of the system will not be limited to specimens of that thickness but can be extended to half-inch layers by suitable selection of heat energy input and measurement times.

The system employs conventional induction heater apparatus and a concentrator coil assembly for continuous injection of heat energy into elemental adjoining areas of the specimen with subsequent measurement of the emission from the heated region. (See Figure 28) The departure of the surface emission characteristic from norm in the vicinity of flaw regions is a dynamic effect which varies with the structure and thermal properties of the material under test. An intrinsic property of the technique permits segregation of the defects by interface location or depth through application of an exposure delay time technique. Exposure delay time in this case refers to the delay or lag between the instant of injection of heat energy and the moment when thermal emission from the exposed area is observed.

Page 82

R-26575

RECORDING
SYSTEM

ELECTRONICS

INFRARED
RADIOMETER

FOLDING
MIRROR

DIRECTION OF
ROTATION
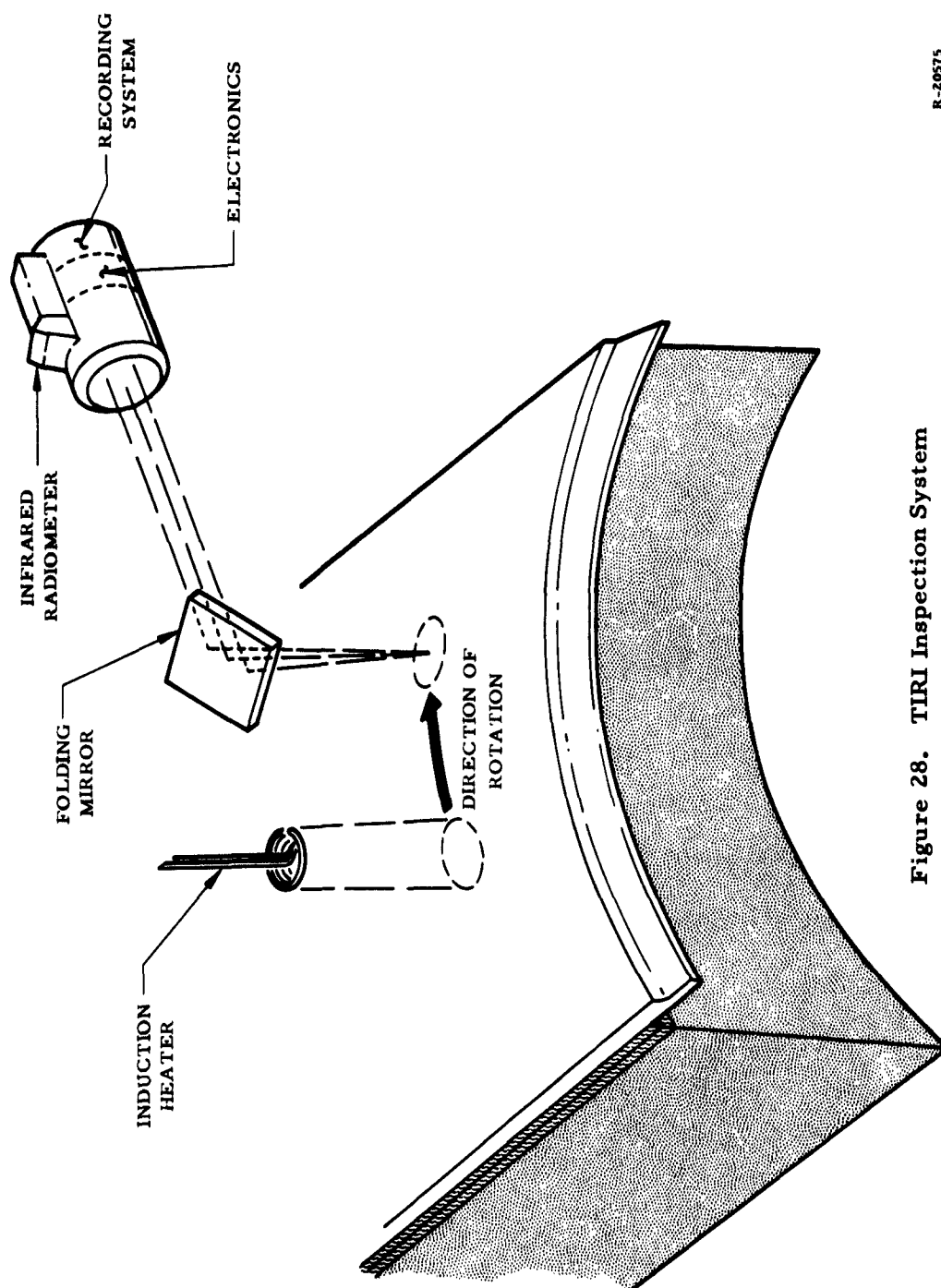
INDUCTION
HEATER

Figure 28. TIRI Inspection System

With a 2.5 kw induction heater and Perkin-Elmer GPR-6 radiometer, an area inspection rate in excess of one sq ft/min is conceivable using a continuous-scan technique. The PE Model GPR-6 radiometer, which uses a thermistor detector, has a spectral band of 7.5 to 14 microns and a field of view 0.17 inch x 0.42 inch at an object distance of 45 inches. Its equivalent temperature sensitivity is $0.05°C$.

In operation, the surface of the rocket casing is moved past the fields of the induction heater and radiometer. Tangential velocity of the casing or the distance between heater and radiometer may be varied to determine exposure time. Each point is scanned four times in the experimental system, the direction changing by $90°$ each time. For each direction an emissograph is plotted on an X-Y recorder. The ordinate scale of the emissograph is proportional to the surface emission along the scan strip and its abscissa proportional to displacement on the specimen in the direction of continuous scan. Each emissograph shows a family of lines produced by scans indexed at 0.250-inch intervals. The degree of departure of the lines (or plateaus on those lines in the case of the six square inch test specimens which show marked end effects) from true flatness is an accurate measure of temperature variations arising from non-uniformities along the line of scan.

The emissographs in turn have been used to create sets of contour plots of dynamic thermal patterns. These contour maps serve primarily as an aid to visualization and interpretation and do not necessarily provide more information than is available on the emissographs. Advanced display techniques are currently being developed to eliminate the intermediate step of manual contour plotting. The flow pattern can be established by evaulating the contour plots.

For the construction and steel thickness (1/8-inch) characterizing the test specimens, a seven second exposure time (delay) has proved about optimum for maximum contrast in first interface bonding flaws. It is significant to note that delayed emissographs taken 15 to 20 seconds after heat injection showed line uniformities essentially the same as those typified by a flawless reference plate. Of even greater interest, however, are the subtle changes observed with delays of the order of 30 seconds, the nominal optimum exposure for penetration to the second interface. No evidence of second-interface flaws appears with a seven-second delay. Preliminary results indicate that a second interface flaw detection is promising and in some cases positive. .

These results have generally verified the predictions of a preliminary study based on electrical analogs. [3] In that study, extension of the principle to the detection of flaws located a short distance into the propellant was predicted. Such a possibility will be investigated in Phase II of the Perkin-Elmer study in which tubular rocket casings about five inches in diameter and 12 inches long will be examined in detail with spiral scans. Loading of the casings and the introduction of simulated flaws are being carried out by ARGMA technicians.

Comparison of the Perkin-Elmer flaw maps and those supplied by ARGMA with the specimens is quite difficult. It was found (by destructive examination) that flaws existed which had not been intentionally introduced, some of those having been created by overheating during experimentation with the induction heating mechanism. The TIRI flaw patterns were compared, however, with data supplied by outside testing laboratories whose technicians subjected the specimens to ultrasonic and X-ray inspections. The TIRI technique proved to be much more sensitive detection method than either of the others.

It should be noted that the cellophane tapes represented very subtle flaws, particularly when both sides of the tape were well bonded to adjacent layers, and X-ray evidence was particularly ineffective.

The Perkin-Elmer technique, when more fully developed to eliminate some of the plotting procedures, should be a very worthwhile approach to the detection of bonding flaws. It presumably cannot be extended to the detection of flaws below the surface of the propellant.

Heat-soak Infrared Technique

A heat-soak technique for use with the Polaris program is under development by Lockheed Missiles and Space Company. The motor is heated uniformly to a moderate temperature, then placed in a lower-temperature environment and scanned with an infrared detector.

Infrared scans have been carried out on a Polaris second stage motor. Infrared and radiological data showed a coincidence on some of the bond defects, but data were not sufficiently detailed to permit a thorough comparison. At the present time infrared scanning can detect the presence of a flaw, but not its depth. Further detail improvements on the infrared scanning sensor are in progress, and a program to determine the capability of this method for NDT of fiberglass motor cases has been initiated.

Evaporograph

The Evaporograph is a thermal imaging device which converts an infrared image into a visible image by differential evaporation

or condensation of oil on a thin membrane. The radiation is focused by a germanium lens onto a nitrocellulose membrane about 4×10^{-6} inch thick with an absorbing layer of gold black. Vaporized oil introduced into the evacuated chamber containing the membrane condenses on the nitrocellulose at a rate dependent on the membrane temperature and eventually forms a film whose thickness varies as the image temperature. Visible light is then reflected from the oil-membrane interface and forms a colored visible image of the infrared image. In laboratory tests, temperature differences of a few tenths of a degree have been resolved. However, under field conditions it is likely that the sensitivity would be more on the order of one degree. Exposure times vary from a few seconds for hot targets to several minutes for very cool targets.

Much of the recent development work on this instrument has been done by Baird-Atomic Corporation where some attention to its application to NDT of solid-propellant rockets has been given. BAC engineers could offer no hope of its use for that purpose. At the temperatures to which the propellant can be safely be raised, several minutes of exposure time would be required for a 3/4-inch diameter test area. Therefore, a test could only be made at steady-state conditions. Establishment of suitable steady-state conditions would require raising the temperature of a spot on the inner surface of the propellant to a relatively high temperature and force-cooling the case. This condition would produce strains which could well damage an already strained propellant.

The most that could be expected from such a system would be a possible indication of case - liner - propellant bonding flaws. Irregularities in the inside-out heat flow through the propellant due to flaws therein might be detectable at the surface if it were not for the presence of the highly conductive case. The case would, however, undoubtedly erase whatever image that might have appeared. Since a more sensitive means of detecting bonding flaws is available in the TIRI system, there is little advantage in considering the Evaporograph at the present stage of its development.

Miscellaneous Infrared Detectors

Infrared detectors generally fall into three categories - thermal, photo-conductive, and photoemissive. Thermal detectors, such as the thermistor radiometer or evaporograph are generally characterized by a wide spectral response band but are slow and less sensitive than either of the other types. Photoconductive detectors are generally quite sensitive and fast, although spectral response varies greatly with different photoconductors and in some cases covers a useful region only at very low temperatures. Photoemissive detectors, are generally very sensistive and fast, but the best photoemissive surfaces have a spectral response extending only slightly beyond the visible region out to about 1.3 microns. At temperatures to which the propellant can be safely raised, the emitted wavelengths are much longer and exist in the 7 to 15 micron range.

The only practical thermal imaging device with the possible exception of IR photography is the Evaporograph, but at the present stage of development its use is questionable. Photoconductive detectors are fast enough to be used as imaging devices when used in complex optical spot-scanning systems, but no fully developed system of direct image conversion is known for IR wavelengths. A proposed device is, however, under development at MIT and might prove to be a useful image converter in the spectral region of 1 to 40 microns.

The image converter tube of the MIT device utilizes a photoconductive layer upon which the IR image is formed. A photoemissive layer deposited on the first layer is uniformly illuminated with visible light. When a potential is applied across the two layers in series, the photoconductive material acts as a variable resistance regulating the emission of electrons from the emissive surface in accordance with the intensity of its IR illumination. The resultant electrons are focused and accelerated before impinging upon a cathode-ray-tube type phosphor where the visible image is formed. Although the pilot model of the tube only simulated spot irradiation by IR, it is possible that further development may result in a converter capable of handling complete IR images. If so, a sensitive imaging system could be developed which would display transient temperature conditions on the case in response to a pulsed heat source in the core area without the mechanical complication of optical scanning.

It must be concluded that at the present state of the art, no IR imaging device is available which would be of use in solid-propellant grain testing. The field should be watched closely, however, because IR detectors are currently receiving a great deal of attention throughout the industry.

2.3.2.3 Ultrasonics

Although the ultrasonic inspection technique serves admirably
for case-liner unbonds, the extension of this method to the de-
tection of other defects has not been so successful. Laboratory
demonstrations have been made of marginally successful detec-
tions of liner-propellant unbonds. Test equipment manufacturers
are confident that liner-propellant unbonds are detectable on a
production basis, but so far have been unable to demonstrate
this capability in the field or provide firm costs for such
equipment.

The detection of interior grain defects with ultrasonics does not
appear feasible.

Most propellants are characterized by a low acoustic impedance,
high attenuation, and low acoustic velocity. In the case of PBAN
propellant the velocity was found to be 800 meters per second and
the attenuation three decibels per centimeter at 10 megacycles. The
severe attenuation losses in such materials make it necessary
to resort to lower and lower test frequencies (20 to 500 kc). At
lower test frequencies, efficient transducers must be large and
large transducers are inherently poor at resolving small defects.
In addition, defects smaller than a wavelength are almost immune
to detection. Consequently, the detection of defects in the size
of interest by ultrasonic techniques cannot be relied upon.

2.3.2.4 Microwave Techniques

Only the microwave technique which was considered in the electro-
magnetic category appears to show theoretical promise of success
with the present propellant formula.

A type of radar system located within the core area which could display a two-dimensional PPI presentation of a section of propellant was considered. The idea was abandoned when it became evident that pulse repetition rates of about 10^{12} cps would be required for adequate resolution.

A much more reasonable system is proposed which depends on a sharply defined microwave beam originating at a transmitting horn in the core area, reflected from the case, and impinging on a directional receiving antenna (such as another horn) displaced a short distance from the transmitting horn. Such a system is depicted in Figure 29. Microwaves are refracted at the interface between two materials having different dielectric constants (such as air and the propellant) much as light waves are refracted at the interface between materials of different density. Consequently, it seems reasonable to assume that sufficient refraction could occur at a void or crack in the propellant to cause the path of the reflected beam to differ from that in a flawless section. The antennas, together with the transmitter and receiver, could be rotated in a helical manner, as in the other two scanning systems which have been described, to scan the entire grain quite rapidly. Unlike the other two systems, however, it should be possible by displacing the horns vertically as well as horizontally from each other and properly interpreting the flaw evidence on successive rotations to derive three-dimensional flaw-location information. (See Figure 30.)

There is some question as to the amount of scattering and absorption which might be caused by the aluminum particles in the

TRANSMITTER
RECEIVER
AND
DETECTOR

RECEIVING
HORN

TRANSMITTING
HORN

R-20576
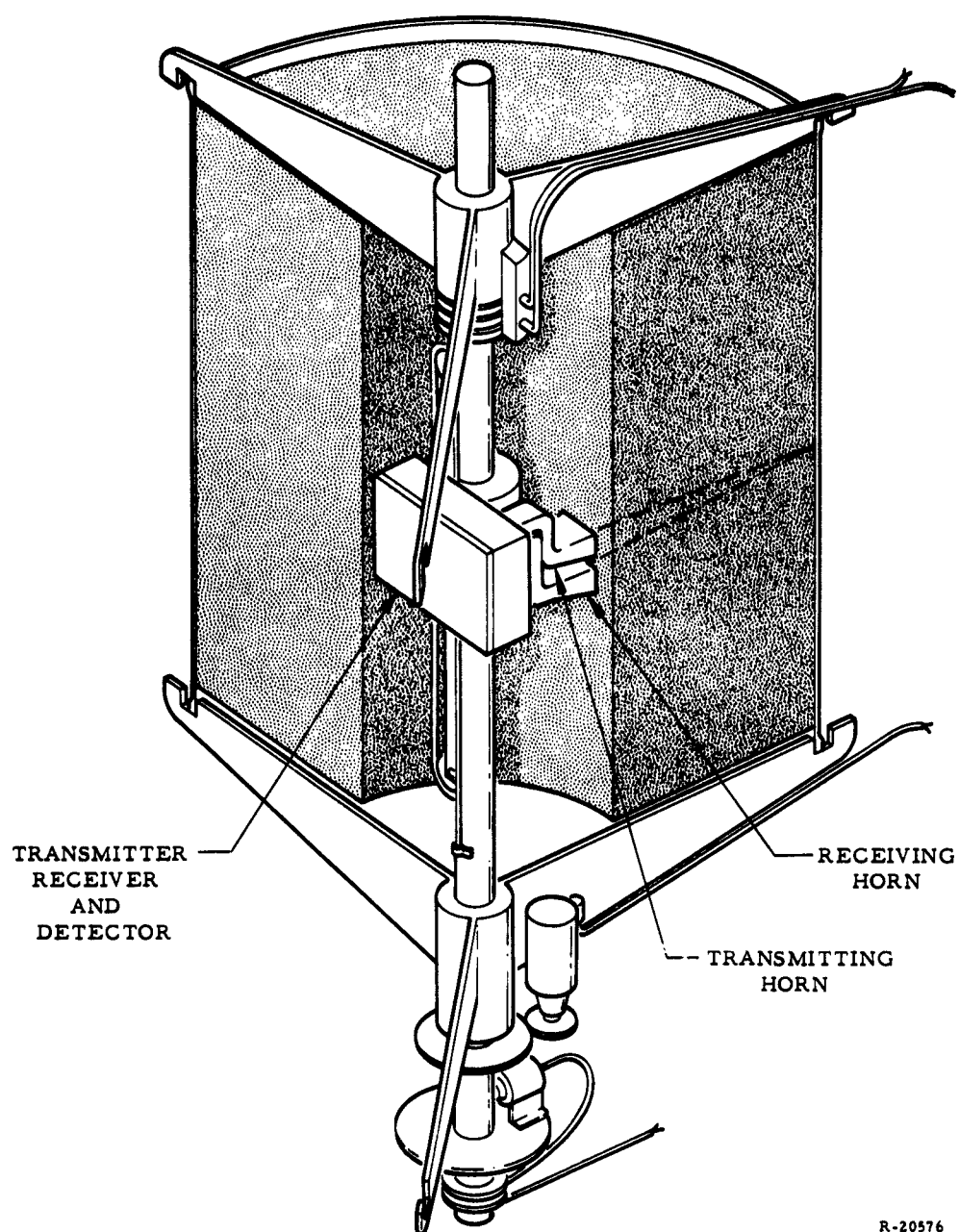
Figure 29. Microwave Scanning System

R-20577

VERTICAL DISTANCE FROM TOP

RADIAL LOCATION

ANGULAR POSITION

A

C

B

RADIAL LOCATION

PROPELLANT

CASE

CROSS SECTION OF GRAIN

T

R

A

B

C

A AND B ARE VOIDS LOCATED AT DIFFERENT ANGULAR POSITIONS (BUT ILLUSTRATED ON SAME CROSS-SECTION TO SHOW RADIAL LOCATION). C IS A CRACK LOCATED AT A THIRD ANGULAR POSITION. THE CRACK IS ROUGHLY SQUARE, EXTENDING INTO THE PLANE OF THE PAPER.

Figure 30. Modified "B-Scan" Recording with Microwave System

Page 93

propellant. The number of conflicting opinions indicate that this question can only be answered experimentally. It would only be necessary for a part of the energy to remain in a defined beam to accomplish the purpose. Void information could then be derived from signal strength measurements at the receiver. Any refraction or change in absorption of the beam would appear as a change in received signal strength.

Such a system would have fewer problems associated with development of a suitable scanning system than any others. Simple recording techniques could be employed or, if desired, a more elaborate data handling system could be developed to facilitate translation of the test data into three-dimensional location indices.

2.3.2.5 Dielectric Flux Scanner

A dielectric flux test has been conceived in the course of these study efforts which seems promising as a candidate for development into an applicable system. In this proposed technique, a section of cylindrical conducting material is placed against or very close to the inside surface of the grain, as shown in Figure 31. A small centrally-located segment of that conducting section is insulated from the rest of the conducting surface but maintained at the same potential as the surrounding surface by electronic means. If a potential is then applied between the case and this inner conductor, those flux lines impinging on the small insulated segment would traverse a straight path

DEMOUNTABLE
UPPER TRIPOD

PROPELLANT

SIGNAL
SLIP-RING
ASSEMBLY

INNER CONDUCTOR
(CYLINDRICAL
SECTION)

DETECTOR
SEGMENT

ANGULAR DRIVE

VERTICAL DRIVE
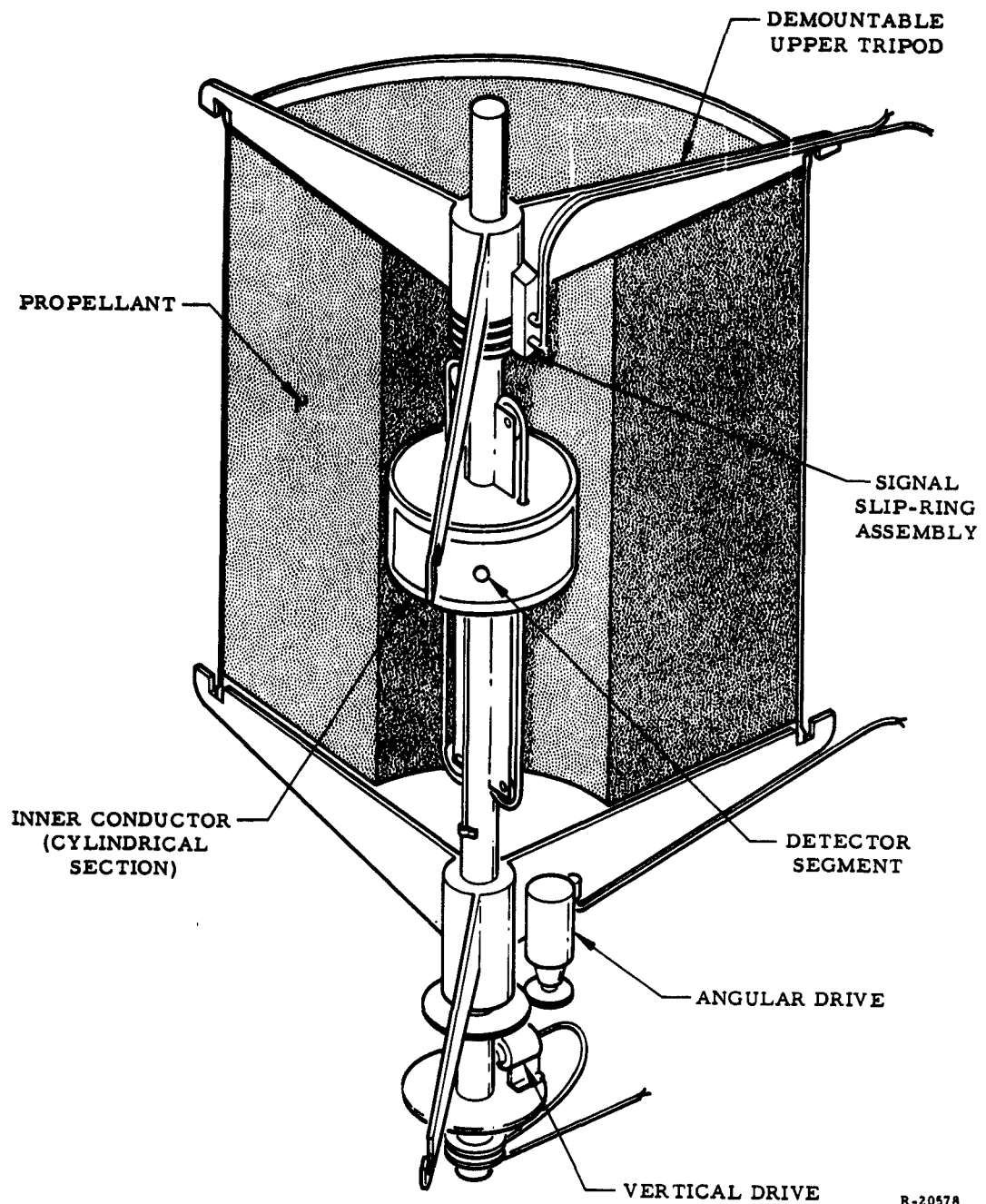
R-20578

Figure 31. Dielectric Flux Scanning System

of small cross-sectional area between the segment and the
case. The volume inspected by the segment would actually be
slightly conical, depending on the dimensions of the large
inner conductor.

If the potential applied between case and inner conductor were
a high-frequency a. c. voltage, the displacement current to
the small segment could be measured with a sensitive a. c.
recording micrometer. The propellant could then be scanned
in a helical pattern coordinated with the recorded trace. The
recording would be a straight line except where the segment
scans a volume containing a flaw and the resulting variation
of the dielectric flux produces a fluctuation in the displacement
current. The capacitance between case and inner conductor
would be 5-6 $\mu\mu$f/ft^2, which gives a capacitance for a 1/2 square
inch segment of about 0. 01$\mu\mu$ f. The current to such a segment
could be detected with only a few volts of signal applied across
the propellant under suitably controlled conditions.

The system development would require close design control.
If the inner conductor did not contact the propellant directly,
for example, nonuniformity of the air gap between the detector
segment and the propellant would result in a disturbing fluctuation
of the recorded trace, though it is possible that such an effect
could be distinguished from flaws. If the inner conductor is in
contact with the propellant, noise might develop during the scan-
ning operation which could interfere with the measurement of
signal. These problems are not insurmountable, and it is felt
that good system development engineering practices can over-
come such details.

This system in the initial development would not present more than rudimentary information (such as in the sharpness of discontinuities) regarding radial distance of a flaw along the flux path. It would, however, provide a quick indication of the existence of a flaw and design refinements could be expected to provide more precise resolution. The speed of scanning would be limited only by such considerations as the amount of heat or electrical noise generated by the mechanical system. Feasibility of the system can easily be determined with a small scale model.

Electro-Magnetic Scanner

The permeability of PBAN propellant does not appear to warrant serious consideration of magnetic techniques at this time. However, the following system was proposed before the permeability was known, and since it might prove to be useful with propellants other than PBAN, it is included here for future reference.

The heart of the detection apparatus would consist of a cruciform iron core mounted in a scanning assembly much like that used with the dielectric flux system. The core, as shown in Figure 32a, would have magnetizing coils wound on two of the arms, diametrically opposed (the A and B arms). Detection coils, electrically opposed, would be wound on the C and D arms. The magnetic circuit would be such that the a. c. magnetizing field would induce equal and opposite voltages in the C and D coils with homogenous propellant. Should there be any slight disturbance of one of the four flux loops such as might occur when a void was present, the balance would be destroyed and a potential would appear at the detection terminals.

Figures 32b and 32c show the resultant potential, rectified by a phase-sensitive demodulator, which would appear as the transducer scanned

32a. COIL CONFIGURATION AND
FLUX PATHS IN FLAW-
LESS PROPELLANT
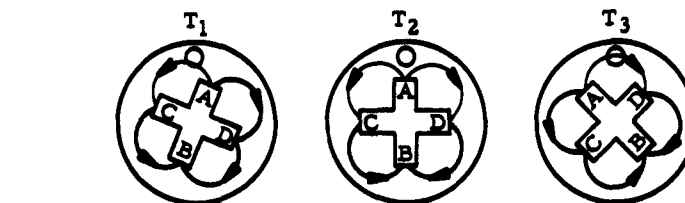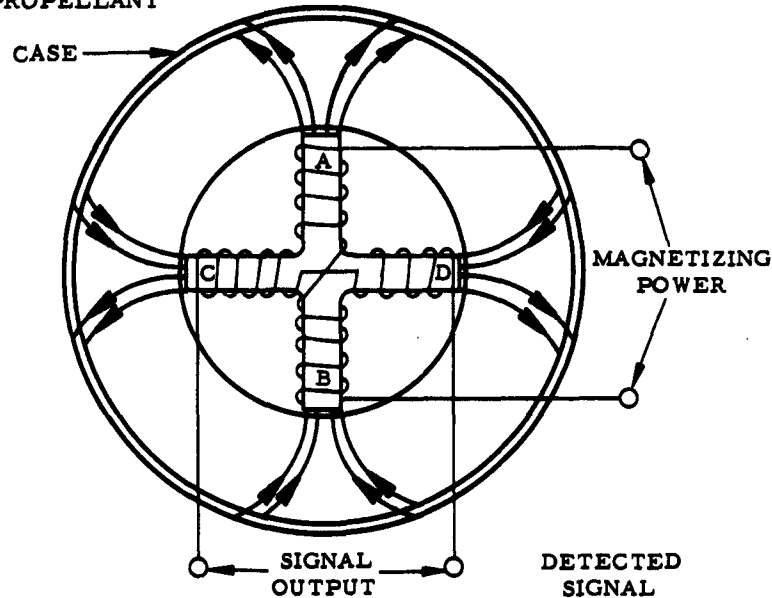
32b. FLAW IN "A" PATH. LIGHT LINES REPRESENT
PATHS OF REDUCED FLUX.
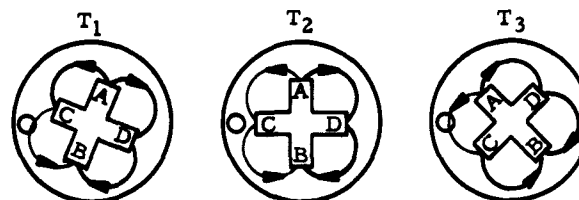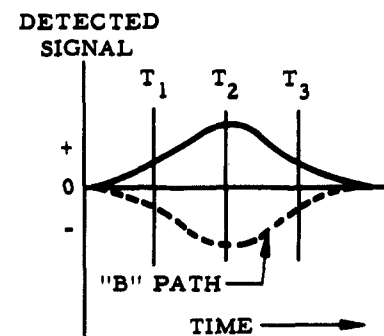
32c. RELATIVE INTENSITY OF FLUX LINES FOR
FLAW IN "C" PATH
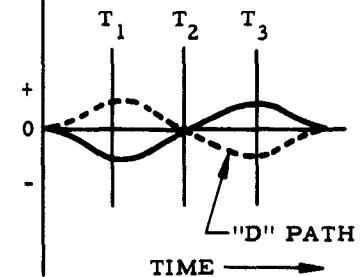
R-20579

Figure 32. Magentic Scanning System

past a flaw. The differences in flux are greatly exaggerated for clarity. Figure 32b shows the effect of the A arm (or, in dotted lines, the B arm), rotating counter-clockwise past a flaw. Figure 32c shows the effect of the C arm (or D arm) scanning the flaw. It can be seen that the angular location of the flaw could be determined with respect to the instantaneous attitude of the core by referring to the shape of the recorded signal fluctuation. No information as to the radial location would be generated by the configuration shown but a double sensing mechanism could be employed for radial flaw location by triangulation.

2.3.2.6 Migratory Tracers

In the category of anomaly intensifiers, only the specific item of migratory tracers could be developed to any extent in the six week time period budgeted for this study. This field was explored in some detail at the Pratt & Whitney Research Laboratories. Consideration was given to substances having large gamma or neutron absorption coefficients which could seem to intensify the anomaly in a radiograph, and to radioactive compounds which, when concentrated in pockets, could be detected by scintillation detectors or similar instruments.

It was conceded at the outset that gases would have the greatest probability of migration to the surfaces of cracks or voids. It was also quite apparent that since the concentration at such anomalies would be slight, detection of gaseous concentrations by X-rays or gamma rays would be highly unlikely. Some gases having high neutron capture probabilities were considered, but since it is likely that the propellant itself has a large neutron cross-section, sufficient contrast again seems doubtful. Gas concentrations of the type considered would cause a density change at such flaw locations in the grain and, therefore, might be detectable by other techniques than radiation. Sufficient time was not available

to carry out such tests. Radioactive gases appeared to show the greatest promise in the migrating tracer area and were investigated.

A new class of substances called Clathrates[4][5] would be useful if the general technique is worth pursuing. The Clathrates are crystalline structures wherein hydroquinine molecules, crystallized from a melt under pressure, form a cage to hold atoms of krypton, xenon, or similar gases. 25.8 atmospheres of krypton can thus be trapped in one mole of the Clathrate and subsequently released by raising the temperature to about 212° F. The quantity of gas released at the curing temperature of 160° F would be negligible. The Clathrate crystals are normally ground into a fine powder and could thus be included in the propellant mix.

There are several questionable aspects of this approach. First, it is possible that the released gas molecules might not migrate to the flaw surfaces rapidly enough. In any event, a portion would also migrate to the surface of the grain itself and escape. Secondly, the released molecules might damage the grain by forming new pockets of gas. Also, as shown in Table XI, those isotopes of xenon which have gamma energies high enough to be useful have short half-lives. None of the isotopes of krypton which emit gammas has a useful half-life. Krypton 85 with a half-life of 10.4 years emits beta particles with an energy of 0.672 mev but such particles would probably be completely absorbed in the propellant. The technique employing such isotopes would, therefore, serve only for an examination shortly after the curing process and would be of little value after sustained periods of storage. Radon or other gases with long half-lives and high-energy emissions would necessitate excessive shielding measures during storage if used in sufficient concentration to provide flaw detection.

In spite of the above listed negative aspects, it is the UTC project opinion that this technique bears further study. It is possible that slight concentrations of even the weakly radioactive isotopes could be detected by sensitive scintillation counters, particularly if the grain were scanned both inside and outside. If so, the exact location of such concentrations could be determined by triangulation. The feasibility of such a system can probably be proven only by preliminary experimental work.

TABLE XI

HIGH-LIFE AND ENERGY VALUES OF XENON ISOTOPES

Isotope	Half-Life	γ Energies (mev)
Xe^{127}	36.4 days	0.056, 0.145, 0.170, 0.203, 0.37
Xe^{129m}	8.0 days	0.040, 0.196 (100%)
Xe^{131m}	12.0 days	0.1639 (100%)
Xe^{133m}	23.0 days	0.233 (100%)
Xe^{133}	5.27 days	0.081 (100%)

2.3.2.7 Radiographic Readout Techniques and Devices

A number of miscellaneous readout techniques and devices have been considered. All are aimed at solving one or more of the problems encountered in conventional radiography.

Direct Viewing

The use of image converters as X-ray readout devices is frequently considered in order to speed up inspection procedures. They seem particularly attractive when used with TV monitoring systems because of the degree of personnel protection offered. However, their use in a system which is not overly endowed with sensitivity is not advisable. In general, high energy generators producing shorter wavelengths produce contrast images in such image formers. Attempting to increase contrast with lower voltage results in decreased brightness. The compromise between low contrast and subvisual light level, together with loss of definition produced by phosphor scattering imposes definite limitations on the image quality. More responsive (sensitive) screens also produce loss of definition over less responsive screens.[6] Fluoroscopy, therefore, cannot provide sufficient resolution and sensitivity in many applications.

A Thiokol installation utilizes a Lumicron in radiographic inspection. The Lumicron is an electronic image intensifying device manufactured by Friese Instrument Division of Bendix Corporation. It is used with a closed circuit TV monitor which utilizes about four percent of the available X-ray intensity to produce a 14 x 18 inch visible display. Where evidence of a defect is indicated, a radiograph is taken to develop more detail. It is believed that this system is not in current use.

The present state of the art in image intensifying devices is such that adequate resolution for large grain testing seems unlikely for some

time to come. An example of such a device is the X-ray panel ampli-
fier developed by RCA under Contract DA-36-034-ORD-2856RD, which
is a PEP type (photoconductive-electroluminescent phosphor). Its
capabilities are outlined in Table XII together with those of the better
known CB-2 fluoroscopic screen.[7]

A variation on the image converters is a direct viewing X-ray system
under development by American Microwave & Television Corporation.
An electron tube whose surface is sensitive to high energy radiation is
incorporated into a high-resolution TV camera. The image is presented
on a monitor screen, which may be placed at any distance from the
inspection room. In its present form, the sensitive area of the tube
is very small (1/2 x 3/8 inches).

It has been successfully used in an X-ray of small parts (diodes, transis-
tors, etc.) with machines up to 100 kv intensity. A solder ball 0.006-
inch in diameter can be discerned with this viewing system. There
are no known problems in enlarging the size of the inspected area or
in operating the equipment with linear accelerators. A prototype
demonstration of this system with a LINAC could not be arranged.

TABLE XII
X-RAY PANEL AMPLIFIER CAPABILITIES

	Performance	1/2 in. Steel	1-in. Steel	2-in. Steel	2-in. Steel	3-in. Steel
Electrolum.	Contrast	2%	4%	2%	4%	Greater than 8%
Panel Amp.	Detail	4%	18%	16%	8%	Greater than 32%
CB-2 Fluor.	Contrast	4%	2%	4%	4%	4%
Screen	Detail	24%	8%	8%	8%	8%

The detail parameter in the above table is penetrameter sensitivity, defined as the thickness, expressed as
the percent of total thickness, that produces a just-visible radiographic image of the pentrameter holes or
slots. Similarly, contrast is the ratio of minimum perceptible abrupt thickness increment to the thickness
of the test object.

Nonvisual Scanning Systems

A system using paired photo multiplier tubes has been the subject of
investigation at the Navy Radiological Defense Laboratory. The motor
is scanned by the paired detectors, and the outputs compared. As the
scanning unit passes over a defect, a difference signal is generated
which indicates the presence of an anomaly. More development is
required before this scheme can be used in production inspection
techniques.

Detail development of suitable sensors is proceeding and holds some
promise.

Scintillation counting equipment of the required sensitivity is not un-
reasonable in price and the new lithium ion drift solid state detectors
are also available for detection of beta-gamma in certain energy regions.
The electronic instrument market is at present glutted with such instru-
mentation of varying reliability. The greatest reliability seems
to be available from those firms that specialize in marketing circuitry
developed by AEC laboratories and similar groups. Examples of such
firms are Hammer Electronics, Cosmic Radiation Laboratories, and
Technical Measurement Corporation. When selected and reliable instru-
mentation is associated with correspondingly reliable power supplies,
a measurement system should be realized which can easily be main-
tained at a high percentage of operating time by a single technician.

Semiconductor detectors have assumed a position of great importance
in the radiation detection field in recent months. [8] [9] Not only
are they sensitive and rugged but they have proved to have excellent
proportional characteristics for spectometry applications. However,
their greatest use to date has been in the detection of charged particles,

for which purpose an insensitivity to gamma radiation is an advantage. Development of gamma detectors has progressed much more slowly and although such detectors exist (the lithium ion-drift detector is an example), they have not yet apparently shown any great advantages over scintillation detectors, except in their proportionality feature and operational reliability outside the laboratory. Likewise, as neutron detectors, their status is still experimental. Much development is being done in this phase of the semiconductor art, however, and undoubtedly the vacuum tube scintillation detector will be super- seded in the same way that ion chambers and proportional gas counters are now virtually outdated.

Color Radiography

The use of color radiography has been investigated with a view toward speeding the interpretation of the radiograph by accentuating the defect by color contrast. Preliminary work has been carried out with com- mercially available color film (Ektachrome and Ektacolor). Though the initial results have been somewhat encouraging, the added costs of both the film and film process make widespread adaptation of this technique doubtful.

Neutron Radiography

Neutron radiography has received a great deal of attention in the NDT field recently, primarily because many elements which are relatively transparent to X-rays have large neutron capture cross-sections. Therefore, details which cannot be resolved with X-rays can often be resolved with neutrons.[10] Photographic detection methods are gen- erally used by secondary irradiation of the film from a bombarded shield material such as gadolinium or gold.[11] Semiconductors have been used successfully as neutron detectors when coated with B^{10},

fissionable nuclides or hydrogen-containing materials, and a matrix of small semiconductor elements can be used to produce a two-dimensional display. [6]

The difference between neutron cross-section of propellant and that of a void should lead to greater contrast than is possible with conventional X-ray techniques which rely on the density difference. Consequently, the development of neutron radiography may lead to increase sensitivity in the inspection of large solid-propellant grains.

Xeroradiography

Another technique which may be available in terms of equipment in the near future employs the higher sensitivity of the Xerox process to X-rays.

2.4 SUBSCALE VERIFICATION OF NDT TECHNIQUES

To verify the capabilities of various nondestructive test techniques, five UTC TM-3 test motor segments containing various defects were fabricated and inspected by visual ultrasonic, radiographic, and profilometric means. These motors were cast with a live propellant, UTP-3001, a leading candidate for the large booster propellants. This has been done for the following two reasons:

1. All properties of a given propellant cannot be tailored into an inert propellant. Since these motors are to be used with a large variety of NDT techniques, and the results of the tests are being heavily relied on as the basis for future work, the best possible results will be obtained by the use of the propellant itself

2. The option of firing these motors to obtain further data on the defect-failure relationship is retained.

2.4.1 Processing of Defective Test Motors

The defects included in the five motors include voids, case-liner unbonds, propellant-liner unbonds, cracks, porosity, and variation in chemical composition. These defects were allotted among the five motors as shown in Figure 33. A brief description of the method of preparation follows.

A. Voids

The voids were incorporated into a separately cured block of propellant. Holes were drilled in this block with a cork borer, then plugged with cylindrical bits of propellant. The block was then bonded to the liner and propellant cast around it in the normal manner.

B. Cracks

Some difficulties were encountered in the preparation of crack-type defects in these motors. The technique used was to incorporate small Teflon forms 0.001-   0.10-, and 0.100-inch thick at various locations in the motor to simulate cracks. These were to be withdrawn after removal of the casting mandrel; however, removal of the forms is not possible owing to migration during the casting process. To provide for realistic radiographic examination of a crack, a slit was made in the web of one motor (Motor No. 208) 0.005 inch in width, 6.00 inches in length, and 1.00 inch in depth.

C. Unbonds

Case-liner unbonds were prepared by cutting appropriate shapes from previously cured liner material about 0.06-inch thick. These shapes were then bonded to the steel case at the edges only. Additionally, several small unbonds were simulated with Teflon tape. It was observed during the casting process, that these forms distended considerably when a vacuum was pulled, showing conclusively that the bonding was at the edges of the shapes only. Propellant-liner unbonds were obtained by coating the surface of the liner with a suitable release agent (in this case, room temperature vulcanizing rubber). Casting then proceeded in the normal manner.

D. Porosity

Attempts to produce porous propellant by chemical means only (such as would be the case in actual practice) proved unsatisfactory in the time

MOTOR No. 206

PARABOLIC CRACK

15 in.

3 in.

0.100 in.

A-A

SECTION A-A
ENLARGED

2 in.

OXIDIZER-RICH
SOLID PROPELLANT
3 in. 3

6 in.   6 in.

FUEL-RICH
SOLID PROPELLANT

90°

MOTOR No. 208

CRACK

15 in.

3 in.

0.010 in.

A-A

3 in.

SECTION A-A
ENLARGED

6 in.   6 in.

90°

10 in.

AREA CONTAINING SCATTERED
NONCONNECTED VOIDS – 1/8-in. dia – 10
1/4-in dia – 3
1/2-in dia – 3

MOTOR No. 209

15 in.

CRACK

0.001 in.

3 in.

90°

PROPELLANT - LINER
UNBOND 3 sq in.

PROPELLANT TO
LINER UNBOND
10 in. EQ. TRIANGLE
(BOTH SIDES)

PROPELLANT -
LINER UNBOND
3 in. 2

R-20457

Figure 33. Defect Locations for TM-3 Motors
(Page 1 of 2 Pages)
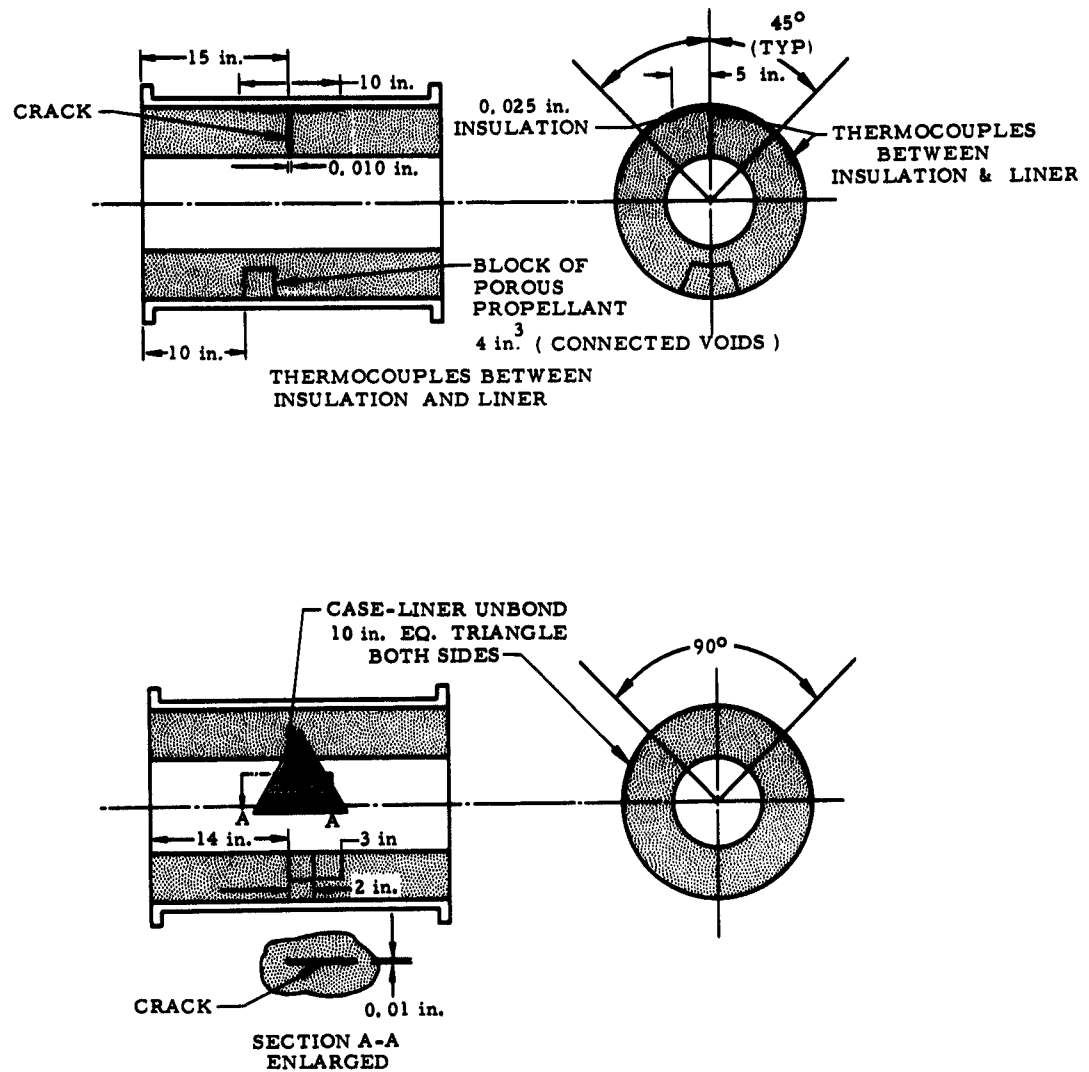
Figure 33. Defect Locations for TM-3 Motors
(Page 2 of 2 Pages)

available. Consequently, a mechanical technique was used in which small propellant shavings were obtained by milling the propellant. The scheme of pressing these shavings together in a hydraulic press to form a solid block was considered unsafe. To contain the loose particles, a box was built of propellant slabs about 0.13-inch thick. Epoxy cement was used to join the edges. The particles of propellant were inserted in the box and compressed by hand. The top of the box, again a slab of propellant, was cemented on and the entire assembly bonded to the liner interior.

Variations in Chemical Composition

To simulate the condition of insufficient mixing actions, blocks of fuel and oxidizer-rich propellant were prepared. The variation chosen was such that the average density (through the web and case) differs from the nominal density by -0.74 percent (oxidizer rich) and -0.58 percent (fuel rich). These blocks were then bonded to the liner.

2.4.2 Visual Inspection

Visual inspection of the defect test motors was carried out at the UTC Development Center. With the exception of the propellant grain cracks and the propellant-lines unbond at the edge of the grain. No visual evidence of the defects was noted.

2.4.3 Ultrasonic Inspection

The ultrasonic inspection of the defect test motors was also carried out at the UTC facility. The equipment used consisted of a Sperry UM 700 Reflectoscope fitted with a 1.00-inch diameter barium sulphate transducer operated at 2.25 and 5.0 megacycles.

It will be recalled that two equilateral triangles of case-liner unbond were incorporated into one motor. In addition, a narrower triangular unbond 10 inches long by 1 3/8 inches wide was also prepared. All known unbond areas were positioned in exact accordance with sketches and measurements taken during processing. The unbonded area corresponding to the equilateral triangles measured nine inches on a side, and the narrower triangle could be traced for eight inches of its length, corresponding to an

unbond width of 0.27 inch. These results were in accordance with the actual size of the prepared defects except that the epoxy resin used in the defect preparation had extended further under the edges of the defects than had been expected. This condition reduced the bonded area and sharpness of the boundary definition.

It may be concluded that unbonded areas are detectable somewhat dependent on the degree of unbond rather than as a function of size. When sharply defined unbonded areas are produced in test samples, it is possible to detect accurately circular areas of unbond as small as 3/8-inch in diameter. Long narrow areas can be detected when only 0.27-inch wide.

2.4.4 Radiographic Inspection

The detailed radiographic reports from Naval Ammunition Depot, Concord, California are included on the following pages. An ultrasonic inspection was also carried out at that activity. The following points should be kept in mind.

A. The crack-type defects axially oriented at the ends of the grain are splices in the motor insulation structure.

B. The unbonds reported at the ends of the segment should be regarded with suspicion. The high degree of unbond reported is even more puzzling in view of the epoxy adhesive used to bond in the insulators. The properties of this adhesive is such that even a thin layer of adhesive alone will result in sufficient signal attenuation to imply a good bond. A retesting of these suspected unbonds failed to confirm their existence.

C. The rubber insulation for all motors consists of two strips 5 inches wide and 0.37 inch thick, arranged circumferentially at each end of the motor. Motor No. 209 has, in addition to the above,

a 10 x 13 inch patch of rubber located under the crack. This condition was correctly diagnosed in Motor No. 206 only.

2.4.4.1 Defect Test Motor TM-3A 206 Nondestructive Test Results

A. Inserts three inches square of low density material were observed radiographically in the propellant at 0°, centered approximately eight inches from the forward and aft ends of the motor at the case. The locations of the inserts are shown (Figure 34). A 1/4 x 1 inch void was observed at 0°, 16 inches forward of the aft roll ring.

B. Three longitudinal propellant cracks were radiographically shown at 0°. One was observed to extend four inches forward from the aft roll ring; the second began 15 inches forward of the aft roll ring and extended four inches forward; and the third began 16 inches forward of the aft roll ring and extended one inch forward. A fourth crack, which was observed to extend four inches aft from the forward roll ring, was radiographically identified at 180°. The positions of the cracks are ploted in Figure 34.

C. The rubber insulation-adhesive liner configuration of the motor was radiographically observed to terminate five inches forward from the aft end of the motor and five inches aft of the forward end of the motor. In the interval between, the propellant body was apparently bonded to the case. No liner-propellant separation was detected.

D. Case-insulation separation extending from 80° to 120° was radiographically detected. Since this area could not be located by the technique, its longitudinal location could not be determined.

UTC ,TM-3A DEFECT TEST MOTOR CASE LAYOUT
S/N 206

RADIOGRAPHIC INDICATION OF CRACK OR CRACK-LIKE LINE
RADIOGRAPHIC INDICATION OF PROPELLANT VOID
RADIOGRAPHIC INDICATION OF PROPELLANT CUT
RADIOGRAPHIC INDICATION OF HIGH DENSITY AREA IN PROPELLANT
RADIOGRAPHIC INDICATION OF LOW DENSITY AREA IN PROPELLANT
ULTRASONIC INDICATION OF CASE/INSULATION SEPARATION
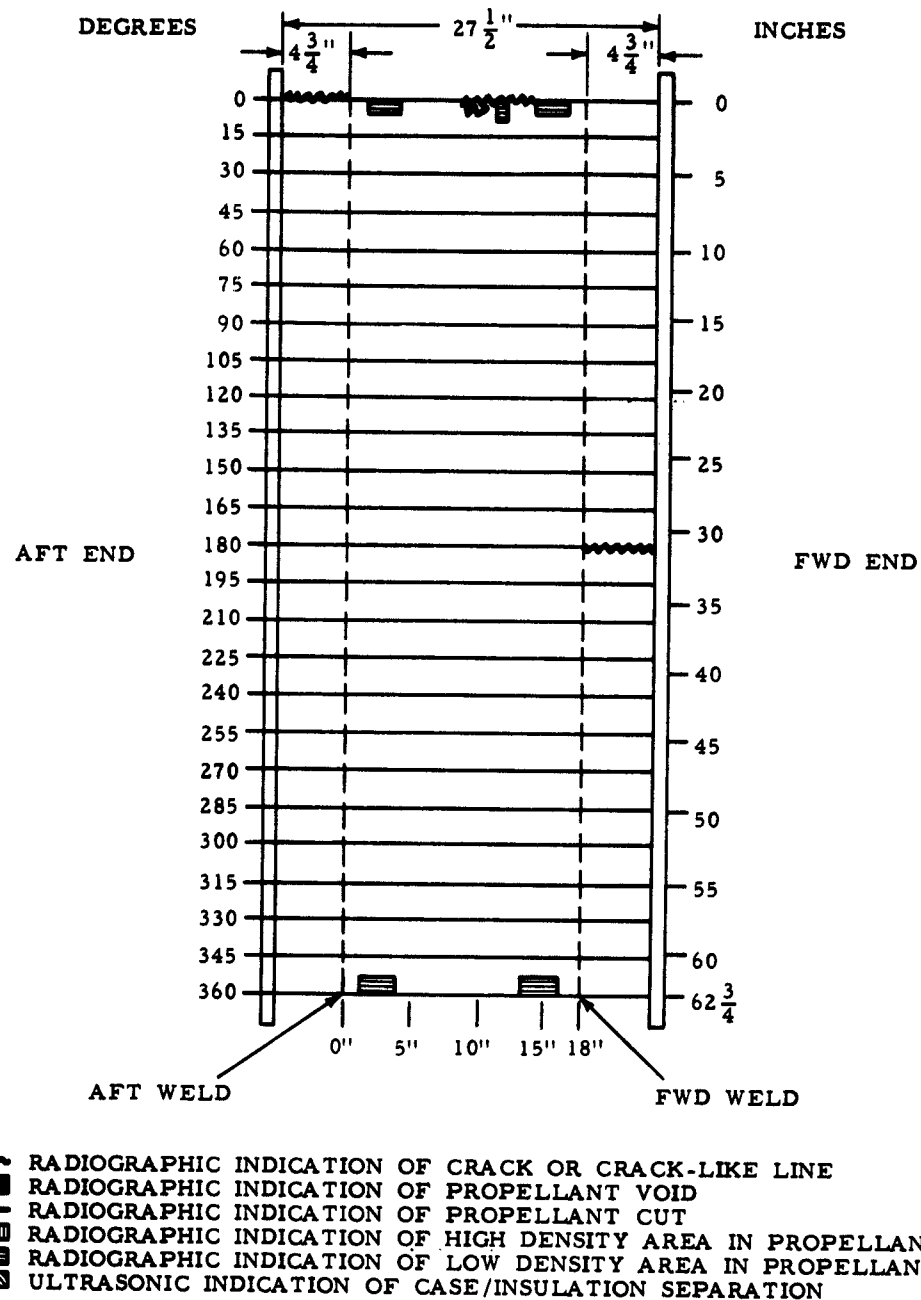
R-20888

Figure 34. Radiographic Identification of Defects in
Motor Case (TM-3A 206)

E. Ultrasonic examination revealed case-insulation separation in the areas shown (Figure 35).

2.4.4.2 Defect Test Motor TM-3A 207 Nondestructive Test Results

A. Numerous voids of 1/8 to 1/4 inch were radiographically observed in a propellant area bounded by 0° and 60° and planes four inches forward of the aft roll ring and four inches aft of the forward roll ring. A 3/4 x 1 inch void was observed at 110°, and two 1/2 inch voids were observed at 120° in a propellent area centered approximately three inches aft of the forward roll ring. An area of propellant containing numerous 1/4 inch voids was radiographically shown to extend from five inches aft of the forward roll ring to five inches forward of the aft roll ring at 320°. Void locations are plotted in Figure 36.

B. Four circumferentially oriented crack-like lines, extending approximately from 15° -45°, 20° -30°, 105° -130° and 300° -345°, were radiographically observed five inches aft of the forward roll ring. A fifth crack-like extended approximately from 320° - 335°, five inches forward of the aft roll ring. An area of high density material which extended five inches aft from the forward roll ring lines of low density material was observed to extend from 15° -40° and from 28° -31°. At 240° a propellant crack was observed to extend four inches forward from the aft roll ring. The locations of the crack, crack-like lines, low density and high density lines are shown in Figure 36.

C. TM-3A 207 contained a rubber insulation-adhesive liner configuration which extended the entire length and circumference of the motor. No liner-propellant separation was detected.

UTC TM-3A DEFECT TEST MOTOR CASE LAYOUT
S/N 206
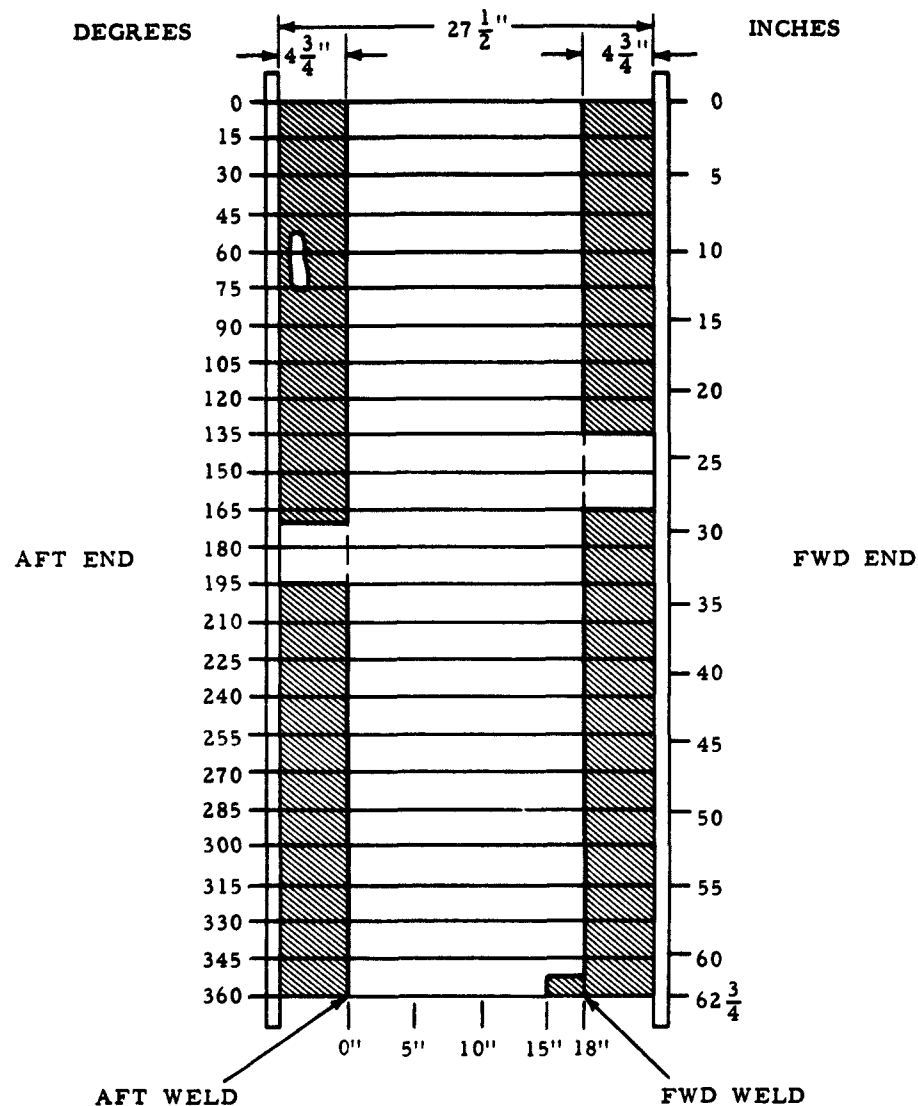
RADIOGRAPHIC INDICATION OF CRACK OR CRACK-LIKE LINE
RADIOGRAPHIC INDICATION OF PROPELLANT VOID
RADIOGRAPHIC INDICATION OF PROPELLANT CUT
RADIOGRAPHIC INDICATION OF HIGH DENSITY AREA IN PROPELLANT
RADIOGRAPHIC INDICATION OF LOW DENSITY AREA IN PROPELLANT
ULTRASONIC INDICATION OF CASE/INSULATION SEPARATION

R-20889

Figure 35. Ultrasonic Identification of Case/Insulation
Separation (TM-3A 206)

UTC TM-3A DEFECT TEST MOTOR CASE LAYOUT
S/N 207

DEGREES   INCHES

AFT END   180   FWD END

AFT WELD   FWD WELD

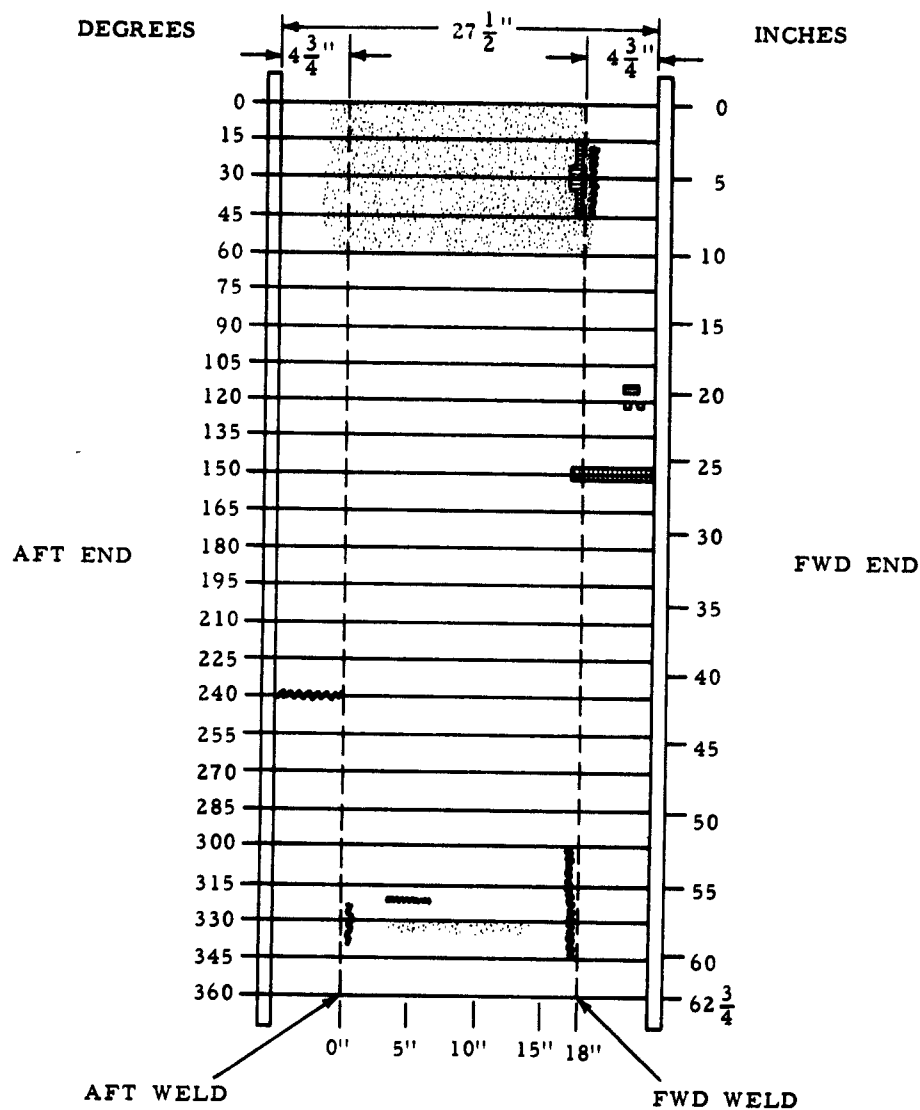〜〜〜 RADIOGRAPHIC INDICATION OF CRACK OR CRACK-LIKE LINE
▇▇ RADIOGRAPHIC INDICATION OF PROPELLANT VOID
━━ RADIOGRAPHIC INDICATION OF PROPELLANT CUT
▥▥ RADIOGRAPHIC INDICATION OF HIGH DENSITY AREA IN PROPELLANT
▤▤ RADIOGRAPHIC INDICATION OF LOW DENSITY AREA IN PROPELLANT
▨▨ ULTRASONIC INDICATION OF CASE/INSULATION SEPARATION

R-20890

Figure 36. Radiographic Identification of Void Locations (TM-3A 207)

D. Ultrasonic examination revealed areas of case-insulation separation as shown in Figure 37.

2.4.4.3 Defect Test Motor TM-3A 208 Nondestructive Test Results

A. A circumferentially oriented cut in the propellant was both visually and radiographically observed six inches forward of the aft roll ring to extend from 140° to 200°. A crack in the propellant was observed to extend five inches aft from the forward roll ring at 60°. The locations of the cut and crack are shown in Figure 38.

B. Areas of rubber insulation appeared to have been removed from 240° -250°, 290° -300° and 190° -200°, such that voids were formed between the case and the propellant. From 330° to 30° the radial thickness of the insulation appeared to have been reduced to 1/16 of an inch in such a manner that a void lay between the case and the insulation. Case-insulation separation was also radiographically detected from 330° to 30° at a different longitudinal location. The longitudinal locations of these areas also cannot be determined because they were only revealed through the longitudinal over-all radiographic technique.

C. The rubber insulation-adhesive liner configuration of TM-3A 208 extended the entire length and circumference of the motor. No liner-propellant separation was detected.

D. The areas of case-insulation separation revealed by ultrasonic examination are shown in Figure 39.

UTC TM-3A DEFECT TEST MOTOR CASE LAYOUT
S/N 207
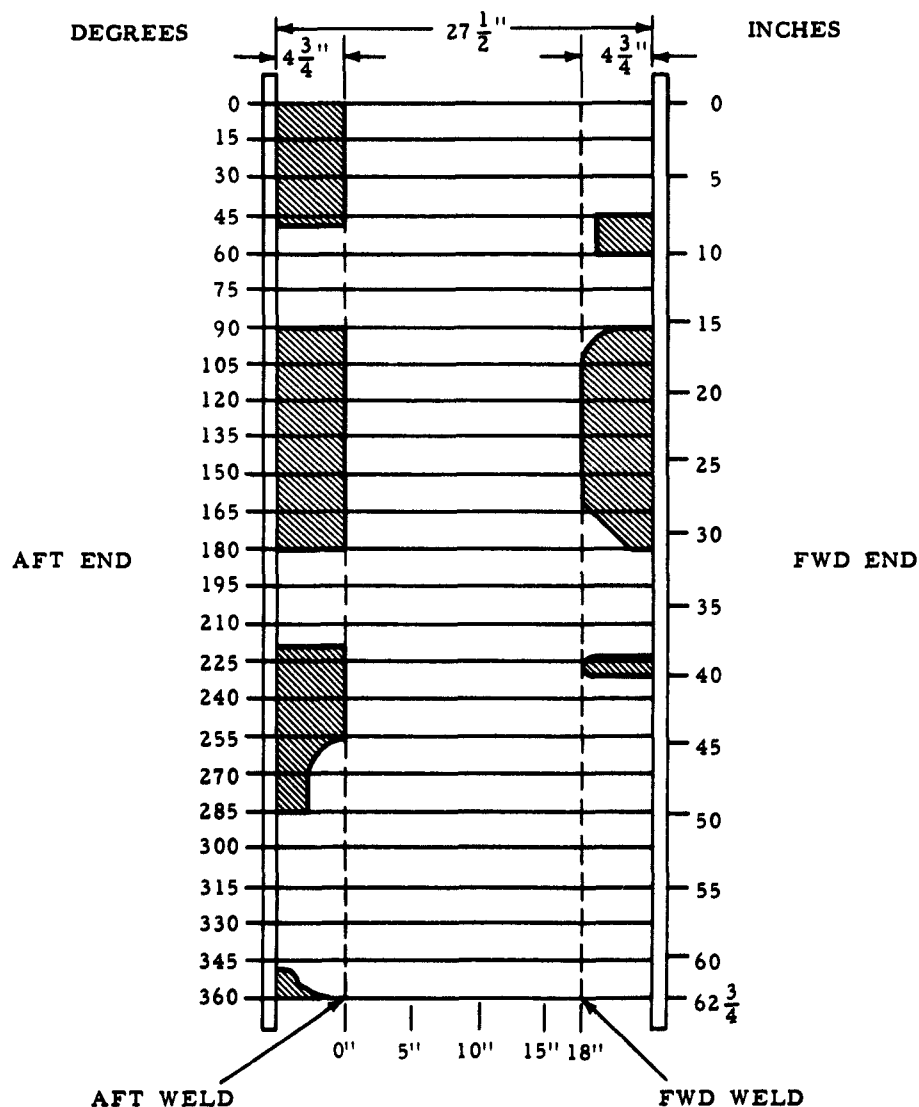
RADIOGRAPHIC INDICATION OF CRACK OR CRACK-LIKE LINE
RADIOGRAPHIC INDICATION OF PROPELLANT VOID
RADIOGRAPHIC INDICATION OF PROPELLANT CUT
RADIOGRAPHIC INDICATION OF HIGH DENSITY AREA IN PROPELLANT
RADIOGRAPHIC INDICATION OF LOW DENSITY AREA IN PROPELLANT
ULTRASONIC INDICATION OF CASE/INSULATION SEPARATION

R-20891

Figure 37.   Ultrasonic Identification of Case/Insulation
Separation (TM-3A 207)

UTC TM-3A DEFECT TEST MOTOR CASE LAYOUT
S/N 208

Figure 38. Locations of Cut and Crack Visually and
Radiographically Observed (TM-3A 208)

UTC TM-3A DEFECT TEST MOTOR CASE LAYOUT
S/N 208

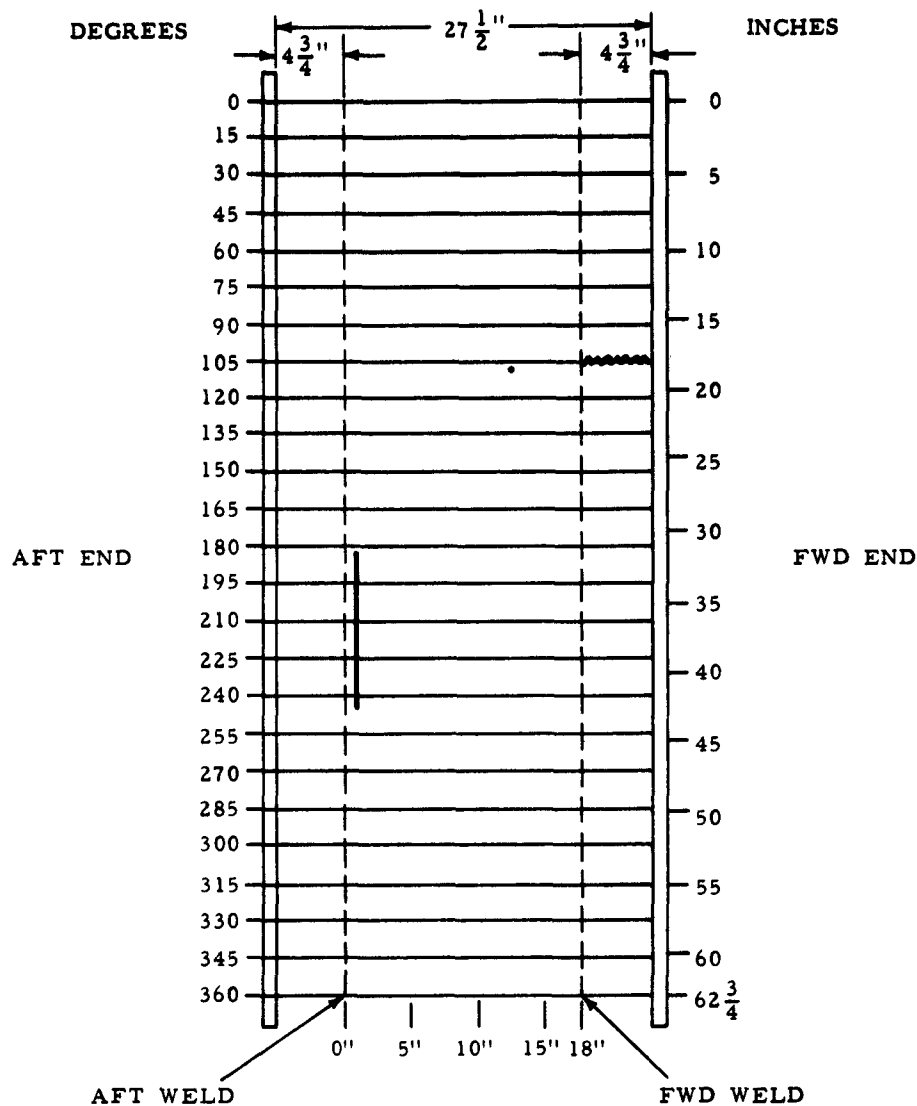RADIOGRAPHIC INDICATION OF CRACK OR CRACK-LIKE LINE
RADIOGRAPHIC INDICATION OF PROPELLANT VOID
RADIOGRAPHIC INDICATION OF PROPELLANT CUT
RADIOGRAPHIC INDICATION OF HIGH DENSITY AREA IN PROPELLANT
RADIOGRAPHIC INDICATION OF LOW DENSITY AREA IN PROPELLANT
ULTRASONIC INDICATION OF CASE/INSULATION SEPARATION   R-20893

Figure 39.   Ultrasonic Identification of Case/Insulation
Separation (TM-3A 208)

2.4.4.4 Defect Test Motor TM-32 209 Nondestructive Test Results

A. Two blocks, approximately five inches square, of high density material were observed to be inserted in the propellant at 0° at the case of the motor such that they were separated by a thin line of low density material at the longitudinal center of the motor.

B. A block, approximately five inches square, of a density closely approximating that of the surrounding propellant, was radiographically observed at the case at 180° extending aft from 10 1/2 inches aft of the forward roll ring. In the center of the block was a quadrangular star-shaped void. The shape, size and location of the block with the void is shown in Figure 40.

C. A longitudinally oriented crack was observed to extend five inches aft from the forward roll ring at 270°. A circumferentially oriented crack-like line was detected from 255° to 290°, five inches aft of the forward roll ring. A 2 1/2 inch diameter hole was both visually and radiographically observed in the propellant at the surface of the bore between 5° and 20°. A crack extended forward from the aft roll ring at 10° for four inches. Six inches forward of the aft roll ring a circumferentially oriented crack was observed to extend from 30° to 60°. The locations of the hole, the cracks, and the crack-like lines are plotted in Figure 40.

D. The rubber insulation-adhesive liner configuration of TM-3A 209 extended the entire length and circumference of the motor. No liner-propellant separation was detected.

E. The areas of case-insulation separation which were ultrasonically detected are shown in Figure 41.

F. The wires of the thermocouple inserted in the propellant at 60° in the forward end of the motor appeared to terminate between the high density blocks.

UTC TM-3A DEFECT TEST MOTOR CASE LAYOUT
S/N 209

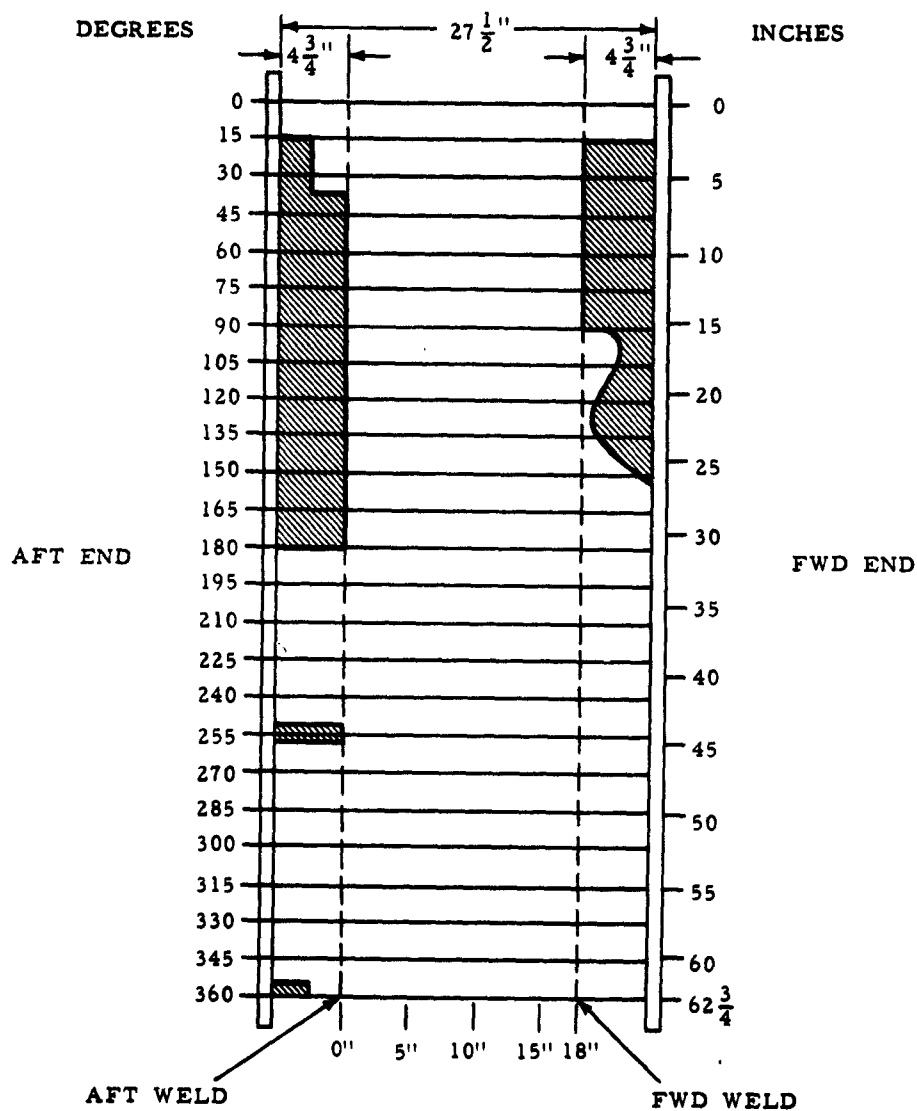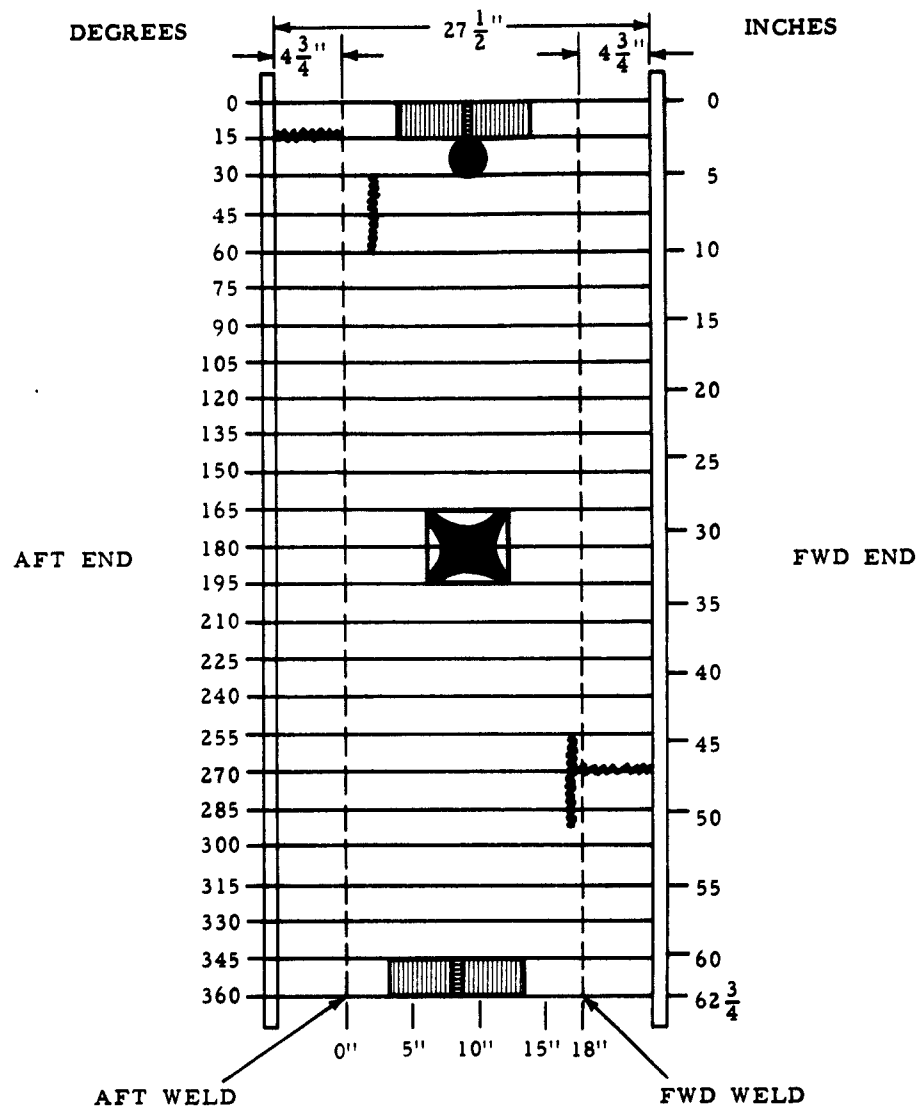
Figure 40. Radiographic Identification of
Void Location (TM-3A 209)

RADIOGRAPHIC INDICATION OF CRACK OR CRACK-LIKE LINE
RADIOGRAPHIC INDICATION OF PROPELLANT VOID
RADIOGRAPHIC INDICATION OF PROPELLANT CUT
RADIOGRAPHIC INDICATION OF HIGH DENSITY AREA IN PROPELLANT
RADIOGRAPHIC INDICATION OF LOW DENSITY AREA IN PROPELLANT
ULTRASONIC INDICATION OF CASE/INSULATION SEPARATION

R-20894

UTC TM-3A DEFECT TEST MOTOR CASE LAYOUT
S/N 209

RADIOGRAPHIC INDICATION OF CRACK OR CRACK-LIKE LINE
RADIOGRAPHIC INDICATION OF PROPELLANT VOID
RADIOGRAPHIC INDICATION OF PROPELLANT CUT
RADIOGRAPHIC INDICATION OF HIGH DENSITY AREA IN PROPELLANT
RADIOGRAPHIC INDICATION OF LOW DENSITY AREA IN PROPELLANT
ULTRASONIC INDICATION OF CASE/INSULATION SEPARATION   R-20895

Figure 41. Ultrasonic Identification of Case/Insulation
Separation (TM-3A 209)

2.4.4.5 Detect Test Motor TM-3A 210 Nondestructive Test Results

1. A longitudinal crack-like line was radiographically observed to extend 5 1/2 inches forward from the aft roll ring at 240°. A six inch long crack, obliquely oriented to the longitudinal axis, was observed to begin 12 inches aft of the forward roll ring and extend aft, with its midpoint located approximately at 60°. A crack also was observed to extend five inches forward from the aft roll ring at 100°. The locations of the cracks in the propellant are plotted in Figure 42.

2. A 1 1/2 x 1/2 x 1 inch void was observed to be located in the propellant at a radial depth of one inch from the case, five inches aft of the forward roll ring at 210°. The location of the void is shown in Figure 42.

3. Implementation of the radiographic technique revealed case-insulation separation extending from 345°-30°, 60°-120°, and 240°-300°, at indeterminate longitudinal locations.

4. The areas of case-insulation separation detected ultrasonically are shown in Figure 43.

5. This motor contained a rubber insulation-adhesive liner configuration which extended the entire length and circumference. No liner-propellant separation was detected.
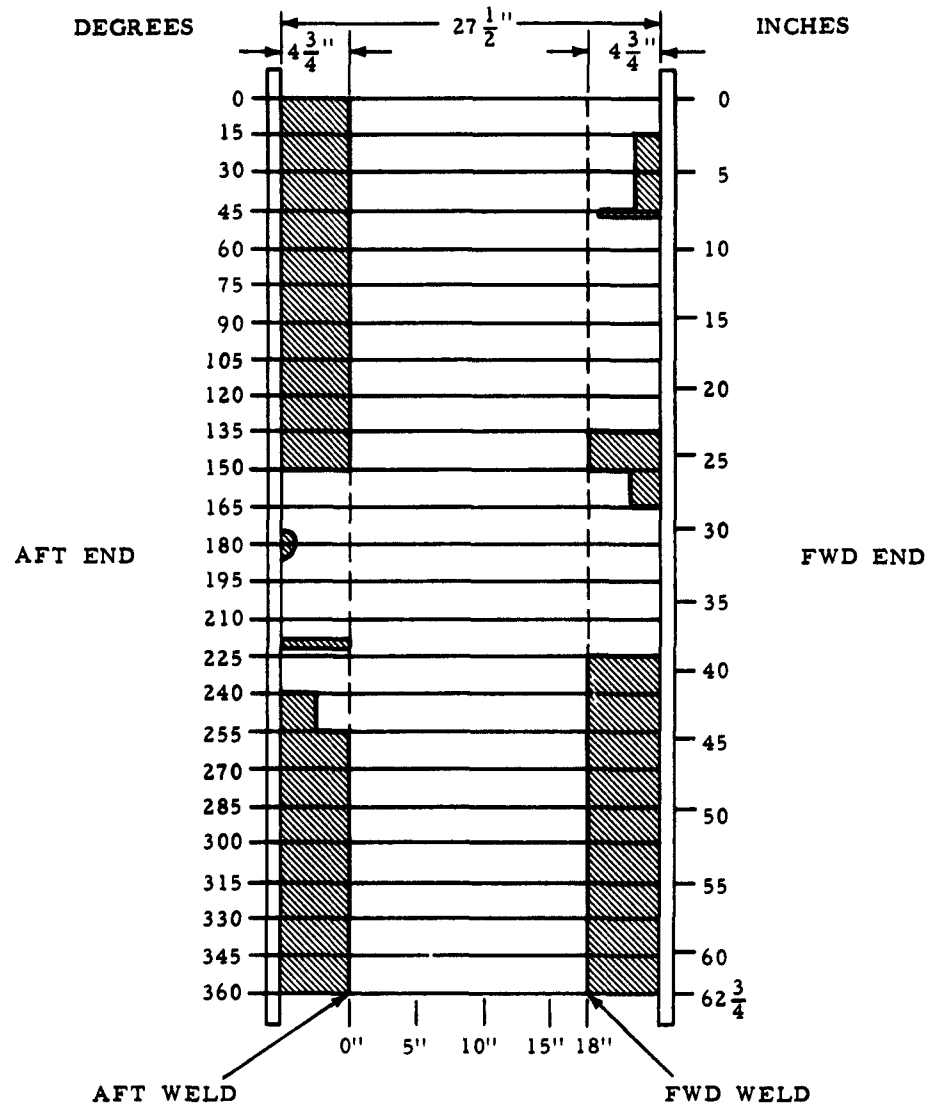
UTC TM-3A DEFECT TEST MOTOR CASE LAYOUT
S/N 210

RADIOGRAPHIC INDICATION OF CRACK OR CRACK-LIKE LINE
RADIOGRAPHIC INDICATION OF PROPELLANT VOID
RADIOGRAPHIC INDICATION OF PROPELLANT CUT
RADIOGRAPHIC INDICATION OF HIGH DENSITY AREA IN PROPELLANT
RADIOGRAPHIC INDICATION OF LOW DENSITY AREA IN PROPELLANT
ULTRASONIC INDICATION OF CASE/INSULATION SEPARATION

R-20896

Figure 42. Radiographic Identification of
Propellant Cracks (TM-3A 210)

UTC TM-3A DEFECT TEST MOTOR CASE LAYOUT
S/N 210
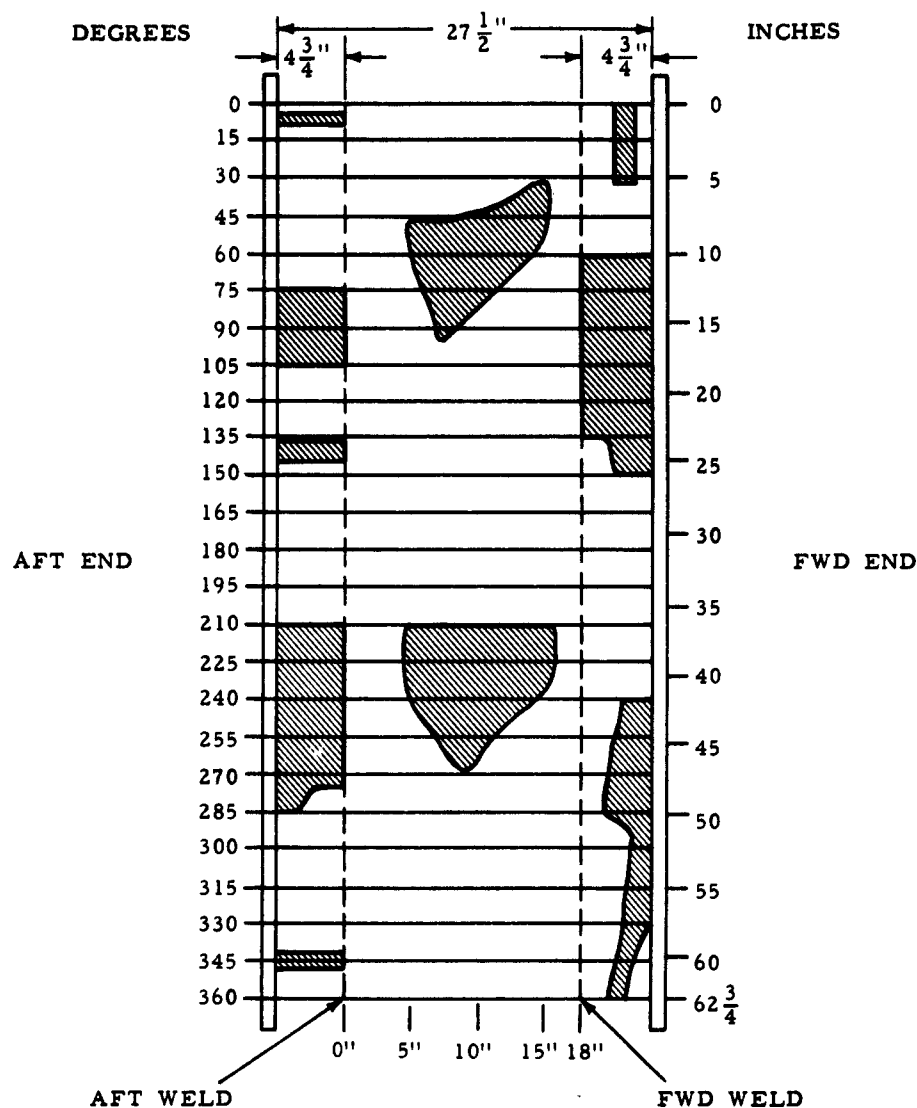
RADIOGRAPHIC INDICATION OF CRACK OR CRACK-LIKE LINE
RADIOGRAPHIC INDICATION OF PROPELLANT VOID
RADIOGRAPHIC INDICATION OF PROPELLANT CUT
RADIOGRAPHIC INDICATION OF HIGH DENSITY AREA IN PROPELLANT
RADIOGRAPHIC INDICATION OF LOW DENSITY AREA IN PROPELLANT
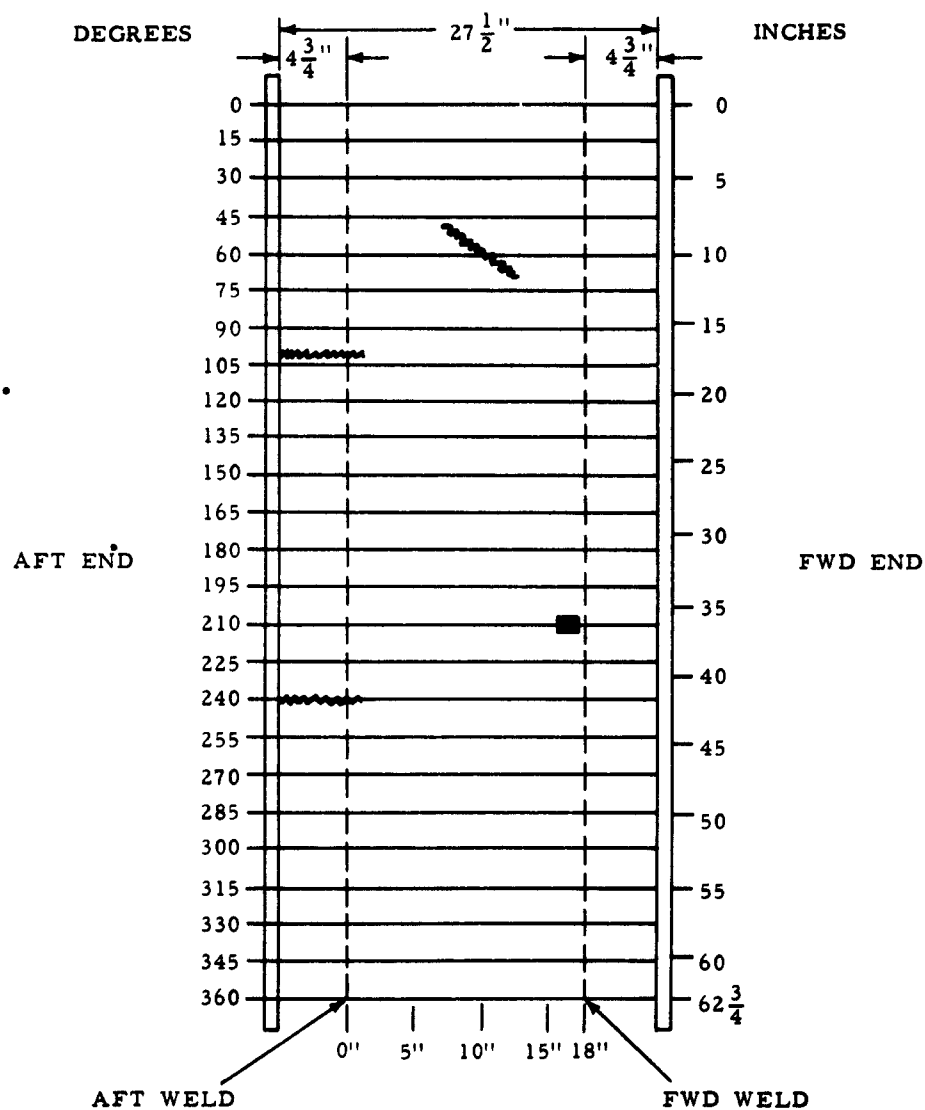ULTRASONIC INDICATION OF CASE/INSULATION SEPARATION   R-20897

Figure 43.   Ultrasonic Identification of Case/Insulation
Separation (TM-3A 210)

2.4.5 Profilimetric Inspection

Profilimetry of the defect test motors was also done in the UTC facilities. The equipment used is shown in Figure 44. A long bar of square cross-section is mounted in the center of the segment to be inspected. Affixed to the bar is a linear sliding potentiometer with a nylon roller, to which the demonstrator is pointing, which bears on the inner surface of the propellant grain core. When a low direct current voltage is supplied, the potentiometer output signal varies with the position of the roller. In the setup employed, this voltage was read with aid of a Cubic Corporation Model VR-45 digital voltmeter. The accuracy and resolution of this equipment is such that the position of the roller can be read to 0.0001 of an inch. In operation, the bar is traversed the length of the segment, and readings are recorded every half inch. After a traverse is completed, the bar is rotated 15 degrees and another traverse begun. In this manner the entire contour of the inner bore is surveyed.

Figure 44. Profilimetry Equipment

A vertical segment orientation is shown in Figure 45. Equipment flexibility is such than any orientation may be employed.

The inspection of large numbers of segments could be greatly facilitated by a minor change in the instrumentation employed. An x-y plotter could be used, with the x-axis corresponding to the distance from the forward end of the grain. This signal could be supplied by another linear potentiometer which is linked to the bar. The y-axis would be the distance from the centerline of the segment to the bore contour, as before. This scheme would eliminate the tedious **readout** and replotting employed for these experiments.

The results of the profilimetric inspection are quite interesting. Profilimetric contours from TM-3 motor segment No. 208 are shown in Figure 46. The ordinates are the axial distance measured from the aft end. The abscissas are the radial distance from the centerline of the segment to the surface of the bore. The contour for various rotational stations are shown and are displaced for clarity. The maximum variation in any one of the contours is about 0.23 inch. The characteristic shape of the contours is easily seen. The shrinkage upon cure and cooldown causes the ends to decrease in diameter more than the center, and is visible on the figure as the turning down of both ends of the contour. The slight taper of the bore is shown by the gentle slope of the contours.

It will be recalled that this motor incorporated a triangular shaped propellant-liner unbond. This is superimposed over the contour with dotted lines. The basic outline of the triangle can be discerned. Although it is obvious that considerable work remains to reduce this technique to routine use, the ability to find this unbond, which was undetectable by radiographic means, is intriguing.

Figure 45. Vertical Segment Orientation
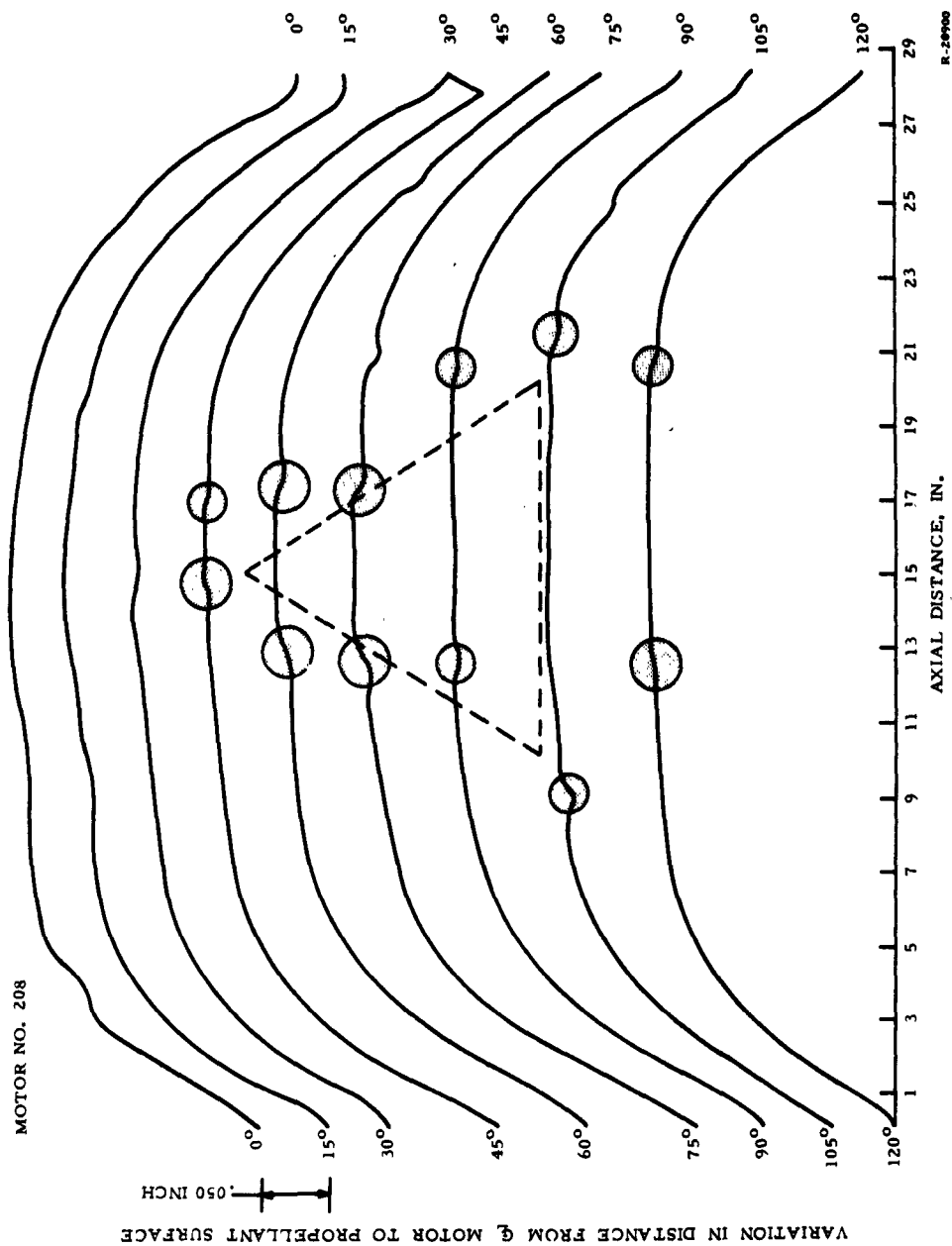
Figure 46. Profilimetric Contours

2.4.6 Conclusions

The general adequacy of visual, ultrasonic, and radiographic techniques was demonstrated. Several differences of opinion were noted in the ultrasonic investigations. The regions of disagreement were confined to the ends of the motor case, where the case itself is tapered. Standardization of individual techniques in this area will be required before consistent results are obtained.

The failure of the radiographic technique to detect the large propellant-liner unbond is largely a matter of geometry. This inspection relies on the detection of a measureable separation between the propellant and liner. A deliberate attempt was made in preparation of these defects to insure the minimum possible separation. This small separation was not accentuated by gravity forces as would occur in a large motor.

The necessity for complete familiarity with motor construction in interpreting NDT information was confirmed by these evaluations.

2.5 FULL-SCALE VERIFICATION OF NDT TECHNIQUES

To demonstrate the ability of NDT techniques to detect defects in large solid rocket motors, a 120-inch diameter inert-loaded segment was fabricated containing known critical defects.

The defects incorporated in the motor segment consists of voids, cracks, unbonds, porous propellant, and propellant inhomogeneities. These defects are shown in Figure 47. (Detailed location information is purposely omitted, so that the segment may be used for other NDT investigations in an objective manner.) The gray areas indicate those anomalies discovered by NAD Concord. The inert propellant selected was UTP-2015, whose composition and physical properties are summarized in Table XIII.

TABLE XIII

PROPERTIES OF UTP-2105 INERT PROPELLANT,
Percent by Weight

Composition

	PBAN	10.683
	MNA	0.577
	DOA	2.655
	Fe_2O_3	0.300
	Al H-322	15.97
	FeAA	0.030
	NaCl	44.00
	$(NH_4)_2SO_4$	22.00
	DER-322	3.785
		100.00

Physical Properties

	UTP-2105 (Samples cured with motor)	UTP-3001 (Typical PBAN Live Propellant)
Density, gm/cc	1.754	1.747
Sm, psi	79	159
Em,%	50.4	51
Peel Strength from Liner	4.0	10
Modulus	159	300
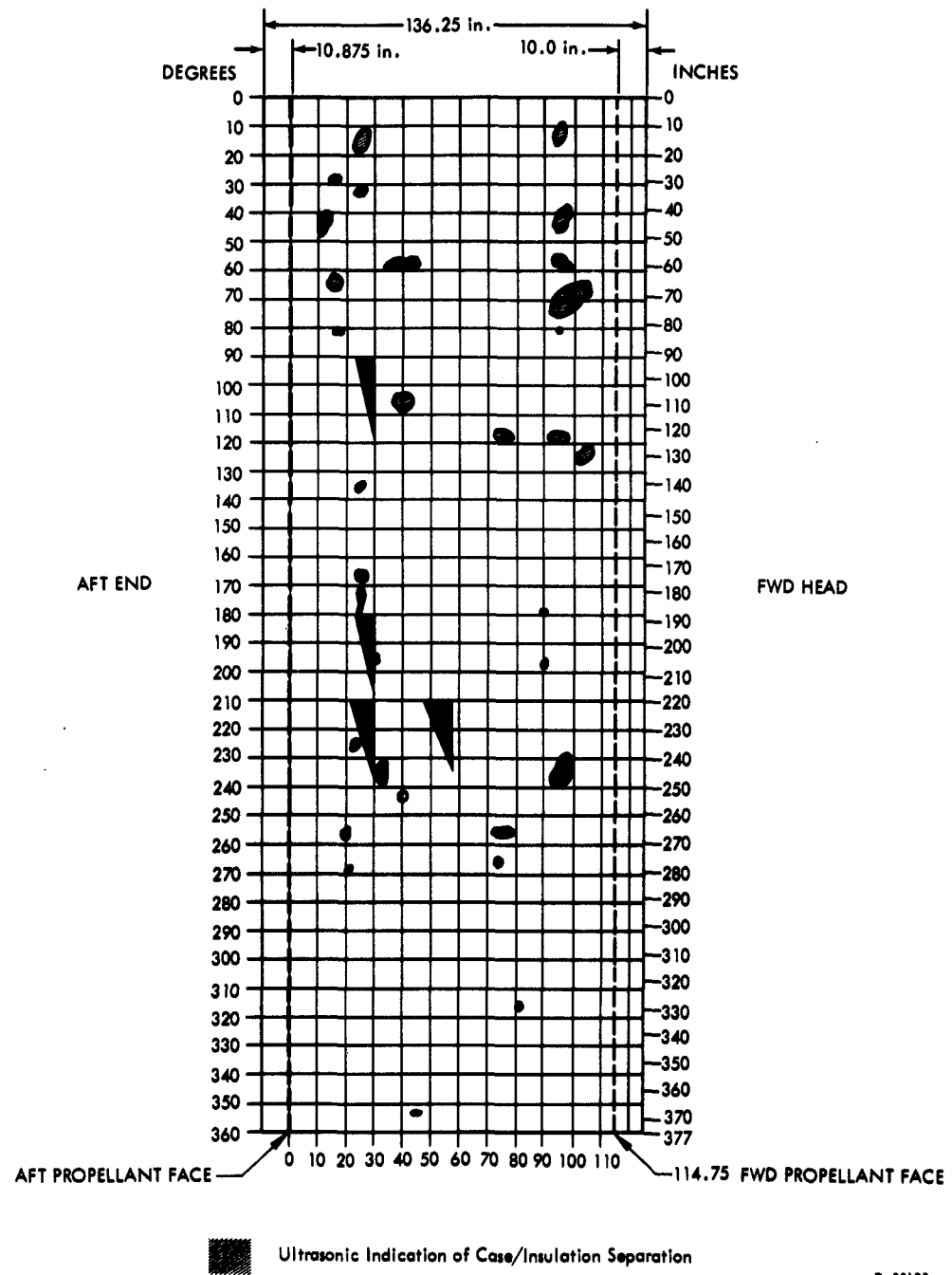
Figure 47. Propellant Grain Defects for 120-Inch
Diameter Inert-Loaded Segment

2.5.1 Visual Inspection

Visual inspection of the basic propellant grain was easily carried out
due to the excellent access offered. The simulated cracks were
readily visible. Visual inspection of the core with the naked eye
revealed no surface indication of other defects. Inspection of the
bond system at the edge of the grain requires removal of the segment
rounding rings, but is easily carried out when this is done.

2.5.2 Ultrasonic Inspection

The ultrasonic inspection on this segment was conducted in the same
manner as for the subscale verifications. Detection of the case-liner
and case-insulation unbonds was a routine matter.

Following completion of these inspections at the Contractor facility, the
segment was sent to NAD, Concord for radiographic inspection and
ultrasonic inspection. The report of that examination is reproduced
as Section 2.5.3. A discussion of the results is found in Section 2.5.4.

2.5.3 Inspection at NAD Concord

TM-120, a United Technology Center 120-inch diameter inert loaded
defect-test rocket motor segment, was received at NAD Concord on
5 November 1962 for the nondestructive testing requested in UTC
Purchase Order No. 25031. The segment is similar in configuration
to the 20-inch motor segments nondestructive testing of which was
reported during the contract period.* As in those examinations, the
primary concern of the nondestructive testing conducted in this exam-
ination was to determine the effectiveness of test techniques in

---

* QE/CO Reports 62-UTC-1 through 5, Figures 52 through 56 of NAD
Concord ltr 2730:HTG:mn 3960.6 of 8 Sep 1962.

detecting the various types and extents of discontinuities and anomalies fabricated into the peripheral insulation area and inert load of the motor.

The segment is a 120-inch diameter cylinder, approximately ten feet long, with a perforation diameter of 46 inches and inert load web of 36.5 inches. Its steel case is 0.5-inch thick in the center of the motor, and tapers to approximately 1.5 inches at both ends. Figure 48 shows the segment mounted on rollers on a truck trailer outside of the NAD Concord 10-mev X-ray facility.

Radiographic investigation of the inert load was performed in accordance with the requirements listed in Table XIV and Figures 49 and 50. Figure 51 shows the attitude of the film cassettes in the perforation and position of the linac for a typical grain exposure. The 34 x 42 inch lucite vacuum film cassette holder, specially fabricated by NAD Concord for the simultaneous exposure of six 14 x 7 inch radiographs of the TM-120, is shown within the segment, in Figure 52. A tabulation of the discontinuities and anomalies found in the inert load is contained in Table XV.

Tangential radiography was conducted in accordance with the exposure plan and technique sheet contained in Table XVI and Figures 53 and 54. Figure 55 shows the arrangement of shielding, film cassette holder, and the position of the 10-mev linac for a typical tangential exposure. The film support and shielding, which consisted of 32 sheets of lead, each 1/4 inch thick, is shown in Figure 56. Both wire and slit-type penetrameters, fabricated to demonstrate system sensitivity of 1%, were used in these procedures. A tabulation of the discontinuities and anomalies detected in the peripheral area of the segment by tangential radiography is contained in Table XVII.

Figure 48.   Photograph of TM-120 at NAD Concord X-ray Facility

TABLE XIV

UTC TM-120 10-MEV INERT LOAD
RADIOGRAPHIC EXPOSURE PLAN

Motor Attitude	Horizontal
Coverage	Eighteen exposures, at 20° intervals from 0° through 340° for each longitudinal section
Tube Position	Directed at the centerline of the motor at an angle of 35° to the horizontal
Tube Filter	None
Collimator	30° cone
Focal-Film Distance	16 feet
Penetrameter	Two lucite plaque-type penetrameters (T = 0.280, 0.5 percent sensitivity, , placed on the motor case to project on the center of the middle-left and middle-right film
Shielding	None
Film Position	Within the bore and perpendicular to the central ray
Cassette Filter	None
Film	Six 14 x 17 inch Kodak Type AA film per exposure, double loaded
Screens	Lead, 30 mils thick, front and back
Film Identification	Section and degree
Exposure	2000 rads for an average film density of 2.0
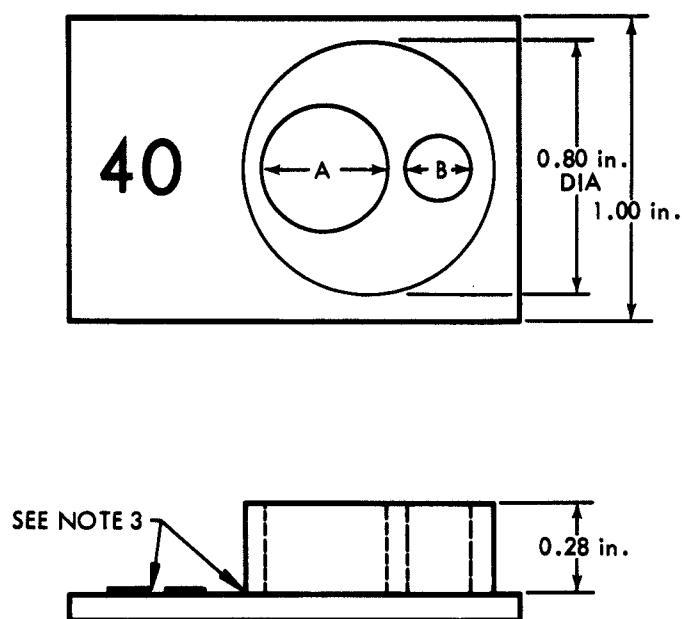
NOTES: 1. Material - Lucite (Density 1.1 to 1.2 gm/cm^3)

2. Use for Path Length Which Consists of the Equivalent Thickness
of 40 inches of Propellant to Demonstrate 0.5 % System Sensitivity

3. Lead Numerals and the Penetrameter Adhere to a Plastic Strip

4. Dimensions were Determined as Follows:

Thickness   = $40 \times 0.5\% \times (\frac{1.7}{1.2})$

Diameter   = $40 \times 2\%$

Diameter A   = 40×170

Diameter B   = $40 \times 0.5\%$

R-30195

Figure 49.   Penetrameter for Inert Load Radiography (TM-120)

SIDE VIEW

105 in.

74 in.

46 in.

15 in.

CR

CR

CR

CR

FWD

SIX – 14 in. x 17 in. FILM CASSETTES

ROLL RING

R-30196

END VIEW

VERTICAL

HORIZONTAL

33°

X-RAY BEAM
F.F.D. = 16 FEET
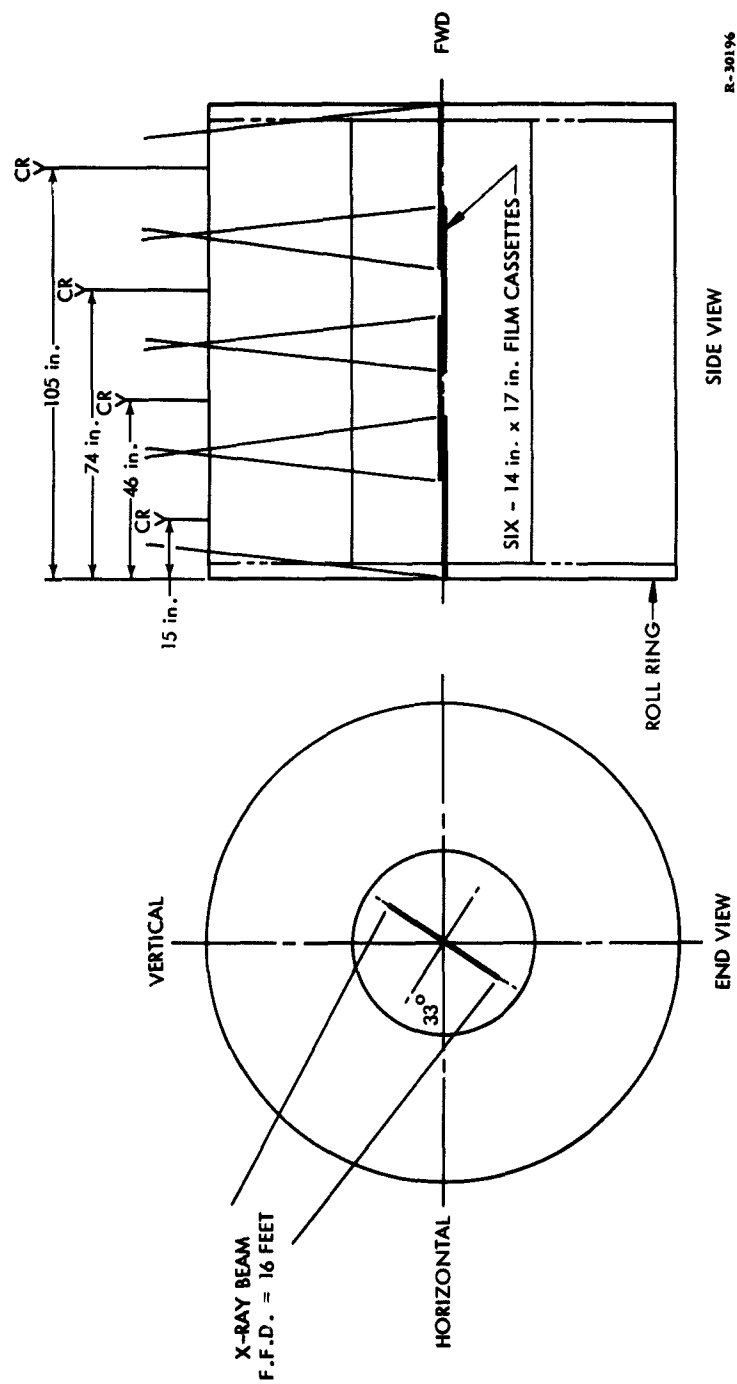
Figure 50. TM-120 10-mev Inert Load Radiographic Exposure Plan

Figure 51. Equipment Composition for Inert Load Radiography
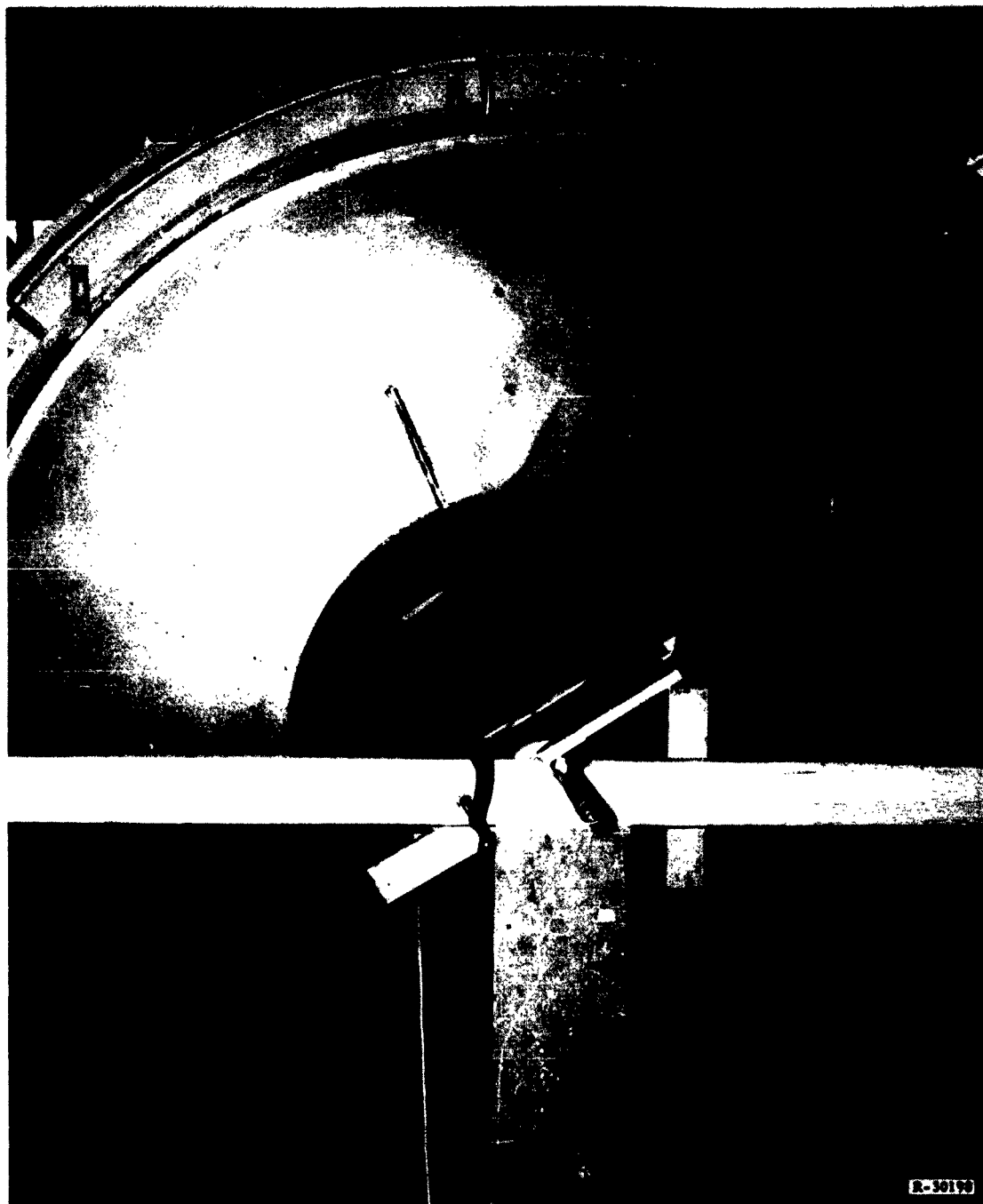
Figure 52. Lucite Vacuum Film Cassette Holder
in the Perforation of TM-120

TABLE XV

UTC TM-120

RADIOGRAPHIC INDICATIONS OF INERT LOAD ANOMALIES AND DISCONTINUITIES

Type	°Location	Radial Limits (measured in inches from I.D. of case)		Longitudinal Limits (measured in inches from the aft propellant face)	
		Outboard	Inboard	Aft	Forward
Material of lesser density than the inert load	9°	3	13	0	30
Material of higher density than the inert load	140° 160° 320° 340°	Triangulation for radial extent was precluded because these indications did not appear in other radiographs		8 26 70 92	16 34 78 100
Material of approximately the same density as that of the inert load					
(a) Containing 3 crack-like lines	290°	0 +	8	36	42
(b) Containing 3 radial and 2 longitudinal crack-like lines	290°	3	9	54	62
(c) Containing no anomalies or discontinuities	310°	7	15	46	60
Material of a spongy, porous appearance	315°	12-1/2	22-1/2	0	10
A crack-like line	290°	Could not be triangulated		106	110

TABLE XV

UTC TM-120

RADIOGRAPHIC INDICATIONS OF INERT LOAD ANOMALIES AND DISCONTINUITIES (continued)

Type	°Location	Radial Limits (measured in inches from I.D. of case)		Longitudinal Limits (measured in inches from the aft propellant face)	
		Outboard	Inboard	Aft	Forward
Voids					
(a) 1/8" to 1/4" dia. (numerous)	7°	24	30	4	10
(b) 3" dia.	166°	14	17	44	47
(c) 2" dia.	167°	15-1/2	17-1/2	50	52
(d) 3/4" x 1/2"	166°	15-1/2	16	46	46-3/4
(e) 3/8" x 3/4"	165°	27	27-3/8	81	81-3/4
(f) (2) 3/4" dia.	170°	28-1/4	29	86	86-3/4
(g) 1" dia.	170°	6	7	96	97
(h) 3/8" dia.	172°	9-1/2	9-7/8	3	3-3/8
(i) 2" dia.	170°	13-1/2	15-1/2	31	33
(j) 3" dia.	168°	5-1/2	8-1/2	26	29
(k) 1/4" x 2"	170°	13-1/2	13-3/4	35	37
(l) 3" dia.	170°	13	16	37	40
(m) 2" dia.	168°	14	16	26	28
(n) 3" dia.	169°	5-1/2	8-1/2	41	44
Wires	350°	12	12 +	0	58
	350°	20	20 +	0	58
	350°	27	27 +	0	58
Wooden Board 1/4" x 12" x 24"	10°	40	55	89	113

TABLE XVI

UTC TM-120 10-MEV TANGENTIAL
RADIOGRAPHIC EXPOSURE PLAN

Motor Attitude	Horizontal
Coverage	Twenty exposures per motor section, at 18° intervals from 0° through 342°
Tube Position	Vertical, directed at a point 60 inches outboard from the centerline of the segment and the applicable longitudinal location
Tube Filter	None
Collimator	15° cone
Focal-Film Distance	12 feet
Penetrameter	One lucite slit-type (shown on page) and one wire penetrameter, to demonstrate system sensitivity of one percent
Shielding	32 sheets of 1/4 inch thick lead
Film Position	Position A — 42 inches beyond the tangent from the X-ray source Position B-H — 24 inches beyond the tangent from the X-ray source
Film Filter	Brass, 1/4 inch thick
Film	Position A — One 14 x 17 inch Kodak Type KK Position B-H — 7 x 17 inch Kodak Type AA
Screens	Position A — Lead, 120 mils thick front, 30 mils back Position B-H — Lead, 30 mils thick front and back
Identification	Section and degree
Exposure	Position A — 5000 rads Position B-H — 3300 rads, for an average film density of approximately 2.0 at the liner/propellant interface

Page 144

DRILL 1/8 in. DIA THRU,
PARALLEL TO SLIT

0.010 in. SLIT WIDTH

1.00 in.

1.00 in.

0.64 in. (SEE NOTE 2)

2.00 in.

1.00 in.
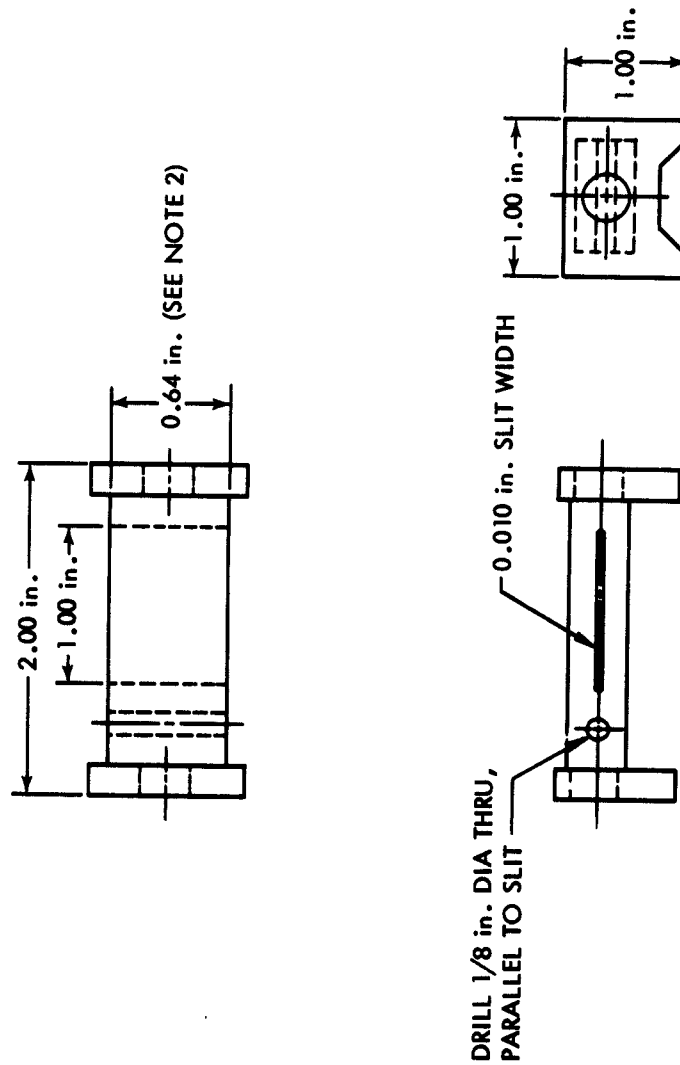
R-30199

NOTES: 1. Material – Lucite (1.2 gm/cm^3)

2. Penetrameter Thickness Based on:

$$T = (1\%) \; (Propellant \; Thickness) \; \frac{(Propellant \; Thickness)}{(Lucite \; Density)}$$

Figure 53. Penetrameter for Tangential Radiography

CR

114-7/8 in.

CR

78-7/8 in.

CR

52-7/8 in.

CR

21 in.

CR

9-7/8 in.

SEVEN - 7 in. x 7 in.
FILM
TYPE AA

ONE - 14 in. x 17 in.
FILM
TYPE KK

136-1/4 in.
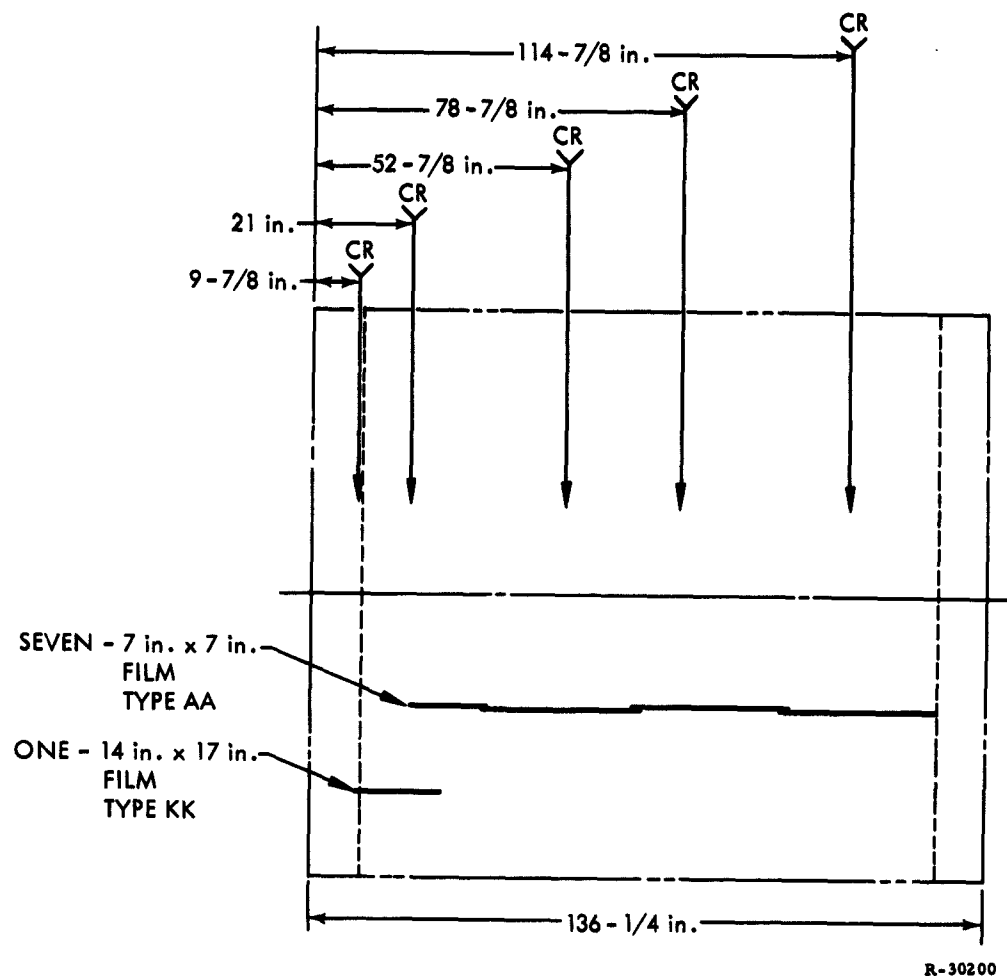
R-30200

Figure 54.   Exposure Plan for Tangential Radiography

Figure 55. Equipment Composition for Tangential Radiography

Figure 56. Shielding and Film Support in Position
for Tangential Radiography

TABLE XVII

UTC TM-120 RADIOGRAPHIC INDICATIONS OF PERIPHERAL ANOMALIES AND DISCONTINUITIES

Type	Circumferential Limits, degrees	Longitudinal Limits (measured in inches from the aft propellant face)	
		Aft	Forward
Material of higher density than the inert load			
a. At the liner/propellant interface	350 clockwise to 2	0	14
b. In the aft boot gap	36	0	14
c. At the liner/propellant interface	36	0	14
d. At the liner/propellant interface, 1/4 inch thick radially	270	0	114-3/4
e. In the forward boot gap, tapering from 4 to 8 inches forward to aft	160 clockwise to 220	103	114-3/4
Material of lower density than the inert load, or possible cuts in the insulation			
a. In the insulation boot	216	105	107+
b. In the insulator	330 to 310, very pronounced at 324	14	16
Distorted floating insulation boot			
a. Of lesser radial thickness than otherwise observed	230 clockwise to 310	14	16
b. Of approximately same radial thickness as observed elsewhere	160 to 220	103	114-3/4
A cut in the floating insulation boot	36	105	107+
Apparent liner/propellant separation	240 clockwise to 300	100	106+

Ultrasonic examination was made with a Brenson Sonoray Unit, utilizing a 2.25 mc/sec transducer. A chamber layout showing the location of ultrasonic indications of case-insulation separation is shown in Figure 57. A tabulation of visible discontinuities and anomalies is contained in Table XVIII.

The 10-mev LINAC proved effective in obtaining radiographs of good quality of the entire body of the inert load and the peripheral areas from 11-3/4 inches forward of the aft propellant face to 8-1/2 inches aft of the forward propellant face. Satisfactory radiographs could not be obtained at the extreme forward and aft ends because of the extraordinarily heavy wall thickness of the case in these areas.

Radiography was completed 16 November 1962 at which time the segment was removed from the NAD Concord X-ray facility for return to United Technology Center. A set of the radiographs made in the examination of TM-120 has been supplied to the addressee.

2.5.4 Discussion of NAD Inspection Results
The detection of the various types of defects in the inert motor segment is discussed separately below.

2.5.4.1 Voids
Voids were simulated in the propellant grain with polystyrene spherical shapes. Balls of 1.25-inch diameter, 2.40-inch diameter, and 2.95-inch diameter were used. These shapes were strung on nylon fishing line and positioned in the motor segment.
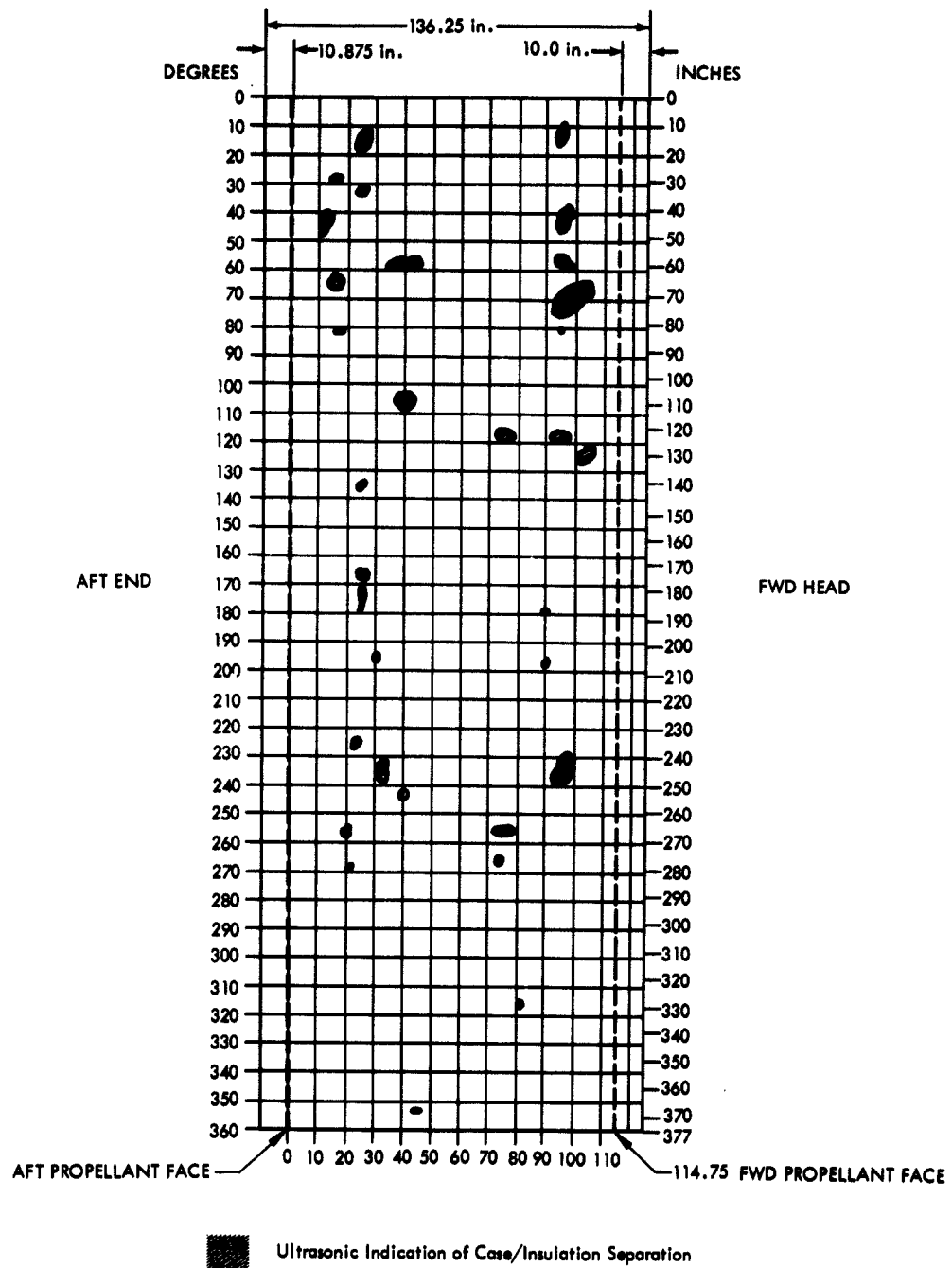
Figure 57. TM-120 Chamber Layout Showing Areas of Ultrasonic
Indication of Case-Insulation Separation

TABLE XVIII

UTC TM-120 VISUAL OBSERVATION OF ANOMALIES AND DISCONTINUITIES

Type	Circumferential Limits (measured in degrees)	Radial Limits (measured in inches from the case I. D.)		Longitudinal Limits (measured in inches from the aft propellant face)	
		Outboard	Inboard	Aft	Forward
Liner/propellant separation	280 clockwise to 315	1-1/2	1-1/2+	0	12
	340 clockwise to 345	1-1/2	1-1/2+	0	4
	160 clockwise to 180	1-1/2	1-1/2+	0	15
	60 clockwise to 90	1-1/2	1-1/2+	0	10
Holes in the inert load (of less than 1/8 inch diameter)					
a. Three holes	350 to 350+	—	—	—	114-3/4
b. Three holes	170 to 170+	—	—	—	114-3/4
c. Four holes	310 to 310+	—	—	0	—
Patches in the inert load					
a. Three patches	0 to 10	—	—	—	—
b. One patch	170 to 180	—	—	—	—
Wires	350	12	12+	0	—
	350	20	20+	0	—
	350	27	27+	0	—
Wooden Board	10	40	55	90	114-3/4

Thirteen voids were reported in the approximate area containing the shape. Several of the voids were reported in locations differing widely from the original position. During the casting and curing of the propellant grain, the shapes may have come adrift and gravitated to the reported position. Continuous surveillance during the casting operation disclosed no evidence of shape migration however. The sizes of voids reported differed from the size of the polystyrene ball incorporated in some cases. The maximum error was 25 percent.

2.5.4.2 Propellant Density Anomalies

Included in this classification are propellant blocks simulating oxidizer-rich, fuel-rich, and porous propellant. These blocks were processed, cast, and cured separate, then epoxied to the the case wall. The porous propellant was simulated by placing small particles of inert propellant in a box made of slabs of propellant. This box was also cemented to the case wall, but came adrift as the rising propellants engulfed it during the casting process. It was subsequently recovered and buried seven inches below the surface of the aft end.

The fuel-rich and oxidizer-rich blocks were disclosed by NAD, Concord, in the correct location except that both were reported approximately 10 inches nearer the aft end. The block of porous propellant was not reported; NAD indicated that the increased case wall thickness in this area rendered radiographic coverage more difficult.

Case-Liner Unbonds

Four right triangular case-liner unbonds 8 inches by 24 inches were placed on the interior of the case wall.

These defects were readily seen by ultrasonic investigation at UTC immediately after processing, and although the size indicated by the inspection was reduced to seven by 20 inches, the shape and location was easily discernible. A complete scan of the outer case wall indicated no other separations larger than four square inches.

2.5.4.3 Propellant-Liner Unbonds

A total of 17 liner-propellant unbonds were incorporated in the inert test segment. By far the most prevelant cause of this defect is contamination of the liner surface. Therefore, this condition was simulated by painting selected areas with RTV-60 (a compound used extensively as a release agent for tooling used with solid propellant). In this manner a definite unbond was assured. After curing the inert load, two additional separations were noted between 130° and 170° on the aft end. These apparently occurred when the insulation boot flap failed to follow the propellant grain shrinkage.

Of the 17 unbonds incorporated into the segment, only one was reported by the inspecting activity. This was one at the aft end between 42 and 70°, and was detected visually. The unintentional unbonds mentioned above were also disclosed by a visual inspection. None of the remaining 16 propellant-liner unbonds was detected radiographically. The largest of these undetected unbonds was 24 by 48 inches.

Radiographic detection of a propellant-liner unbond requres a physical separation between the two. In the analysis presented by NAD, Concord detection of a separation of less than one thousandth of an inch is predicted with the radiographic technique employed. Examination of the radiographs by both NAD and UTC personnel revealed no evidence of any physical separation. It is interesting to recall that the same technique was used to prepare small thickness unbonds in the small scale motor studies. It was noticed that when the unbond was allowed to extend to the end of the grain, physical separation of approximately 0.006 inch occurred on curing and cooling the motors. On two of the motors, the unbonded area terminated approximately 0.1 inch below the surface of the propellant. No burning in these unbonds occurred during the firing.

From these considerations, it may be tentatively concluded that an isolated propellant-liner unbond will not have a physical separation under curing and cooling deformations of the grain. The detection of such an unbond is not possible unless some separation is present. It is possible that the probability of detection could be enhanced if the motor could be oriented in such a manner that the gravity force propellant grain would accentuate or cause a separation. (See Figure 58.) This method was discussed with NAD personnel, but was not considered feasible in view of the problem of shifting the heavy shielding between segment rotations with the tooling available.
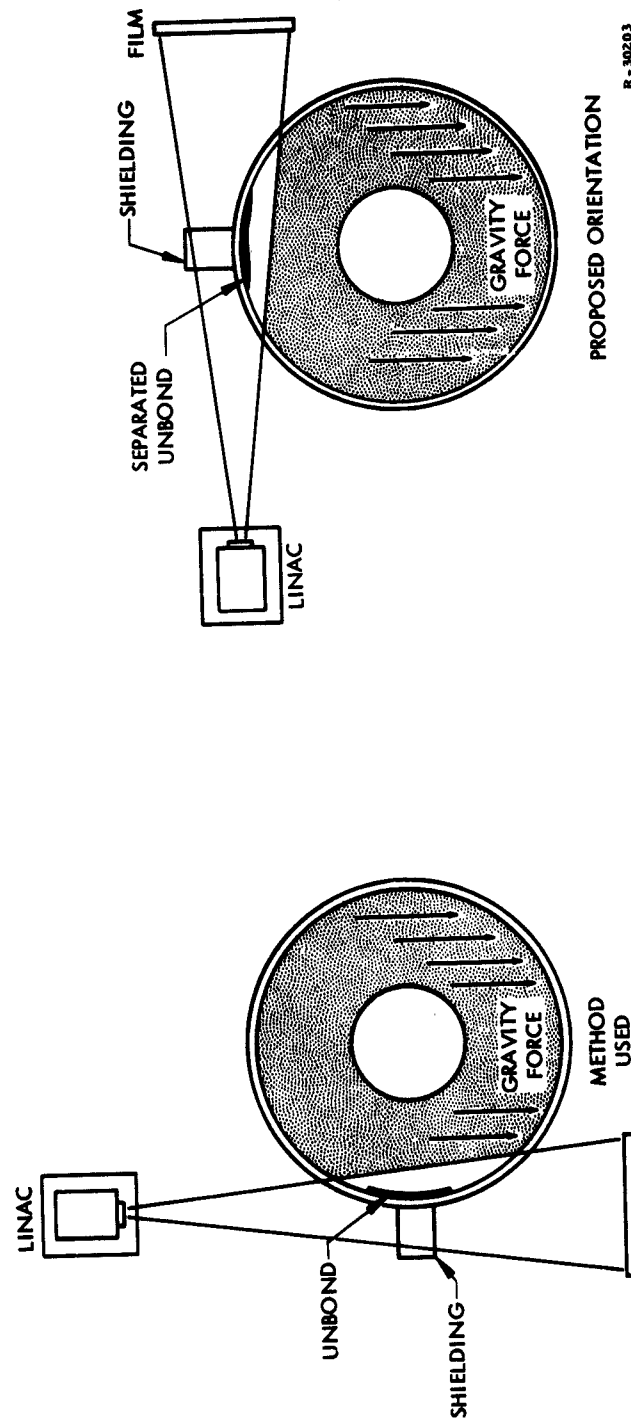
Figure 58. Actual and Proposed Orientation for TM-120 Motor

CONCLUSIONS

The importance of nonpropagating defects may be judged by predicting their effects on motor performance and comparing the results with mission requirements. It is not possible to make this comparison without detailed information of both the solid rocket motor and the mission. However, assuming that large solid motors are to be used in a multistage booster, the following general conclusions may be drawn:

A. Voids are unlikely to have any perceptible effect on motor performance

B. Cracks are not critical unless their surface area contributes excessively to motor thrust or their depth to motor case burnthrough

C. Case-liner unbonds occurring at the edge of the grain are critical. The same unbonds occurring elsewhere have no effect unless their combined areas are sufficient to compromise the structural support of the grain

D. Propellant-liner unbonds must be judged on the escess area contributed to the burning surface, and on excessive exposure of insulation to propellant gases. The unbonded area from two to five inches in length is lit within 10 milliseconds

E. Propellant porosity (interconnected pores) must be evaluated for excessive burning area. Porosity has never been encountered with PBAN propellant at the contractor facility

F. Variations in chemical composition of propellant appear extremely remote in view of modern processing techniques.

Techniques for quantitative evaluation of the effects of defects on motor performance are summarized in the body of the report.

The following NDT techniques are available:

A. Radiography of the grain will detect and locate voids but, in view of the minor effect of this defect, it is not recommended.

B. Analytical studies and experience suggest that cracks always begin at the surface of the grain perforation. Hence, if present, they may be detected by visual inspection

C. Case-liner unbonds or case insulation unbonds may be detected by ultrasonic techniques

D. Propellant-liner unbonds may be detected at some finite probability level with tangential radiography. In view of the expense and inherent uncertainty of this technique, it is recommended that development of alternate techniques be pursued. Candidate methods are infrared, extensions of sonic techniques, and microwave reflection

E. Propellant porosity may be detected with propellant grain radiography. For PBAN propellants, this inspection is not required because porosity has not been encountered

F. Variations in chemical composition may be detected by grain radiography. In view of the extremely low probability of this defect occurring, this inspection is not recommended.

RECOMMENDATIONS

It is recommended that new methods of detecting liner propellant unbonds be sought. The most promising are extensions of sonic, infrared, and microwave techniques. In view of the renewed interest in very large solid rockets (260 inches in diameter and over), emphasis should be given to those techniques which could be employed after motor assembly. Ideally these detection techniques would be best employed while the motor is positioned on the launch pad.

LIST OF REFERENCES

1. Thiokol Chemical Corporation Report. E70-62 Annual Summary Report, "A Research Study to Advance the State of the Art of Solid-Propellant Grain Design".

2. "Development of Nondestructive Testing Techniques for Large Solid-Propellant Rocket Motors", Second Quarterly Progress Report, No. 2015-QP2, Contract AF 04(611)-8018, United Technology Corporation, 14 September 1962.

3. "Phase I Summary Report: Feasibility Study of a Nondestructive Testing Infrared Inspection System for Bonding Flaw Detection, Interim Report No. 2", R. Gorman, H. L. Sachs, P. Yettito, Perkin-Elmer Corp. Report No. PD-TR-5959, April 1961.

4. "Krypton in a Cage — Clathrate Beta Sources", D. J. Chleck and C. A. Ziegler, Nucleonics, Sept. 1959.

5. "Development of Radiochemical Analysis for Non-radioactive Gases and Study of Radioactive Clathrates", AEC Report No. AECF-4493, July, 1959.

6. "Practical Image Formation in Industrial Fluoroscopy", Donald W. Bowman and Raymond A. Pulk, Nondestructive Testing, July-Aug., 1961.

7. "High Energy X-Ray Fluoroscopy with Solid State Panel Intensifier", Nondestructive Testing, Sept.-Oct., 1961.

8. "Tiny Semiconductor is Fast Linear Detector", Stephen S. Friedland and James W. Mayer (Nuclear Electronics Lab., Hughes Aircraft, Culver City, California) and John S. Wiggins (Semiconductor Div., Hughes Aircraft, Newport Beach, California) Nucleonics, Feb. 1960.

9. "Semiconductor Nuclear Particle Detectors", Edited by J. W. T. Dobbs and I. H. Walte, National Academy of Sciences - National Research Council Publication No. 871.

10. "Watch for These New Nondestructive Testing Tools", Steel, Jan. 22, 1962.

11. "A Discussion of Neutron Radiography", Harold Berger, Nondestructive Testing, May-June 1962.